HOLISTIC WATERSHED MANAGEMENT FOR EXISTING AND FUTURE LAND USE DEVELOPMENT ACTIVITIES: OPPORTUNITIES FOR ACTION FOR LOCAL DECISION MAKERS: PHASE 1 – MODELING AND DEVELOPMENT OF FLOW DURATION CURVES (FDC 1 PROJECT)

SUPPORT FOR SOUTHEAST NEW ENGLAND PROGRAM (SNEP) COMMUNICATIONS STRATEGY AND TECHNICAL ASSISTANCE

TASK 5 TECHNICAL MEMO

FINAL DRAFT APRIL 30, 2021

Prepared for:

U.S. EPA Region 1

Prepared by:

Paradigm Environmental

Great Lakes Environmental Center

Blanket Purchase Agreement: BPA-68HE0118A0001-0003
Requisition Number: PR-R1-20-00322
Order: 68HE0121F0001

Table of Contents

Figures

Tables

1 INTRODUCTION

The purpose of this technical memo is to assemble, review and develop information to define the specific scope of modeling work to be conducted and to provide an initial quantification of the magnitude of change to watershed functions associated with landscape conversion to impervious cover. Available hydrological, meteorological, and geospatial data for the Wading River watershed and the larger Taunton basin are summarized and analyzed. This includes identifying trends in streamflow, precipitation, and land use/land cover. The configuration of the existing Hydrological Simulation Program – FORTRAN (HSPF) model is also discussed. Candidate sub-watersheds, representing a range of imperviousness, are identified for the development of flow duration curves to occur in subsequent tasks. Two major results of this memo are an analysis of past, current, and future climate data, including a proposed method for downscaling General Circulation Model (GCM) output for use in the EPA Region 1's Stormwater Management Optimization Tool (Opti-Tool), and the development of Hydrological Response Units (HRUs). Additionally, a modeling approach for the candidate sub-watersheds is proposed that accounts for the full water balance associated with precipitation, runoff, evapotranspiration, runoff, groundwater interflow, and deep groundwater recharge. The unit-area modeling analysis at the HRU level will be performed under Task 6 when the hydrological model, Loading Simulation Program – C++ (LSPC) is calibrated to the Wading River watershed. This memo identifies a representative historic period, which has precipitation that is statistically similar to the current conditions period (Section 3). Section 5 of this memo presents flow metrics for historical and current conditions in the Wading River watershed. Comparing flow for those two periods helps isolate and understand how impervious surfaces impact the flow duration curve in the Wading River. Plots of potential evapotranspiration, dew point temperature, wind speed shortwave solar radiation, and cloud cover used for review and quality assurance are presented in Appendix A.

The technical steering committee (TSC) provided comments on the draft memo submitted on April 7, 2021. Those comments were received during the second TSC meeting through group discussion as well as through email. Where appropriate, this document has been updated to address those comments, the full set of comments and responses is available in Appendix B.

2 TASK 5A. DATA/INFORMATION ASSESSMENT

Readily available data that could facilitate the Flow Duration Curve Phase 1 (FDC1) project were collected, reviewed, and assessed. Data were obtained from online repositories as well as from employees at the United States Environmental Protection Agency (EPA), the United States Geological Survey (USGS), and the Massachusetts Department of Conservation & Recreation (DCR). While data were collected at the Taunton basin scale, most data in this memo is presented for the Wading River watershed (Figure 1). As discussed in later sections, the Wading River has a long-term USGS gage that will facilitate the watershed model calibration.

2.1 Data Review

2.1.1 *Landscape Data*

Several land-use/land-cover layers were downloaded and assessed (Table 1). Land use data sources included Multi-Resolution Land Characteristics (MRLC) Consortium, National Atmospheric and Oceanic Administration (NOAA), the United States Department of Agriculture National Agricultural Statistics Service (USDA NASS), and the Massachusetts Bureau of Geographic Information (MassGIS). Elevation data were acquired from the United States Geological Survey 3D Elevation Program (USGS 3DEP), surficial materials data were acquired from the USGS Scientific Investigations Map 3402 – Surficial Materials of Massachusetts (USGS SIM 3402) and MassGIS.

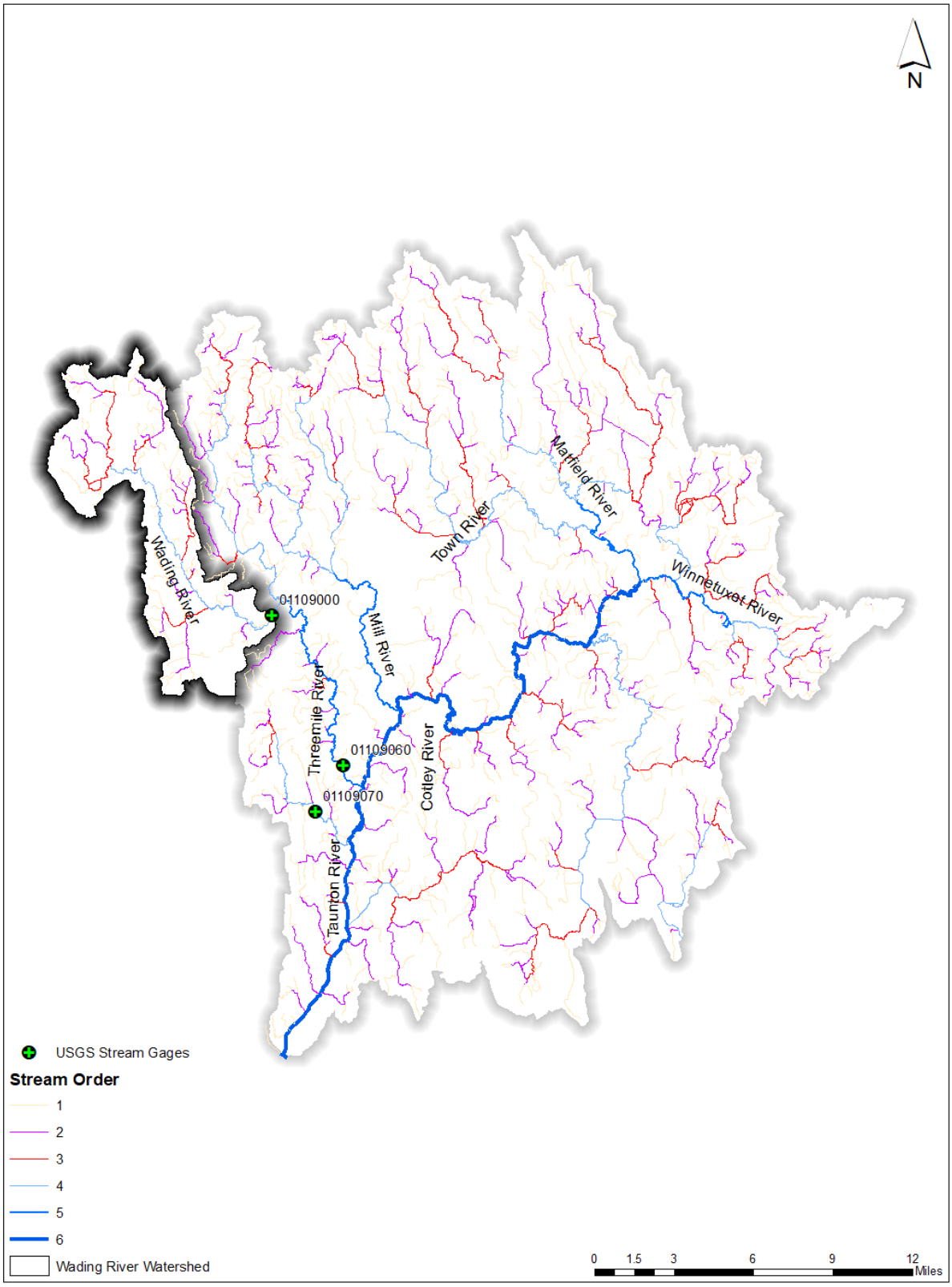

Figure 1. Wading River watershed location within Taunton basin.

Table 1. Landscape GIS data

Description	Dataset	Data type	Time period	Resolution	Source
Land Use/Cover	CCAP16_C	raster	2016	1m	NOAA
	CDL16_Taunton	raster	2016	30m	USDA NASS
	NLCD_2001	raster	2001	30m	MRLC Consortium
	NLCD_2001_Imp	raster	2001	30m	MRLC Consortium
	NLCD_2004	raster	2004	30m	MRLC Consortium
	NLCD_2006	raster	2006	30m	MRLC Consortium
	NLCD_2006_Imp	raster	2006	30m	MRLC Consortium
	NLCD_2008	raster	2008	30m	MRLC Consortium
	NLCD_2011	raster	2011	30m	MRLC Consortium
	NLCD_2011_Imp	raster	2011	30m	MRLC Consortium
	NLCD_2013	raster	2013	30m	MRLC Consortium
	NLCD_2016	raster	2016	30m	MRLC Consortium
	NLCD_2016_Imp	raster	2016	30m	MRLC Consortium
	NLCD_Land_Cover_Change_Index_C	raster	2016	30m	MRLC Consortium
	Impervious_2005	raster	2005	1m	Mass GIS
	Landuse_Poly_History	polygon	N/A	N/A	Mass GIS
	LCLU_2016	polygon	2016	1:40,000	Mass GIS
	LU_1971_21_Class	polygon	1971	1:40,000	Mass GIS
	LU_1985_21_Class	polygon	1985	1:40,000	Mass GIS
	LU_1985_37_Class	polygon	1985	1:40,000	Mass GIS
	LU_1999_21_Class	polygon	1999	1:40,000	Mass GIS
	LU_1999_21_Class_Transparent	polygon	1999	1:40,000	Mass GIS
	LU_1999_37_Class	polygon	1999	1:40,000	Mass GIS
	LU_2005	polygon	2005	1 acre	Mass GIS
	LUchange_1971_1985	polygon	1971-1985	1:40,000	Mass GIS
	LUchange_1971_1999	polygon	1971-1999	1:40,000	Mass GIS
	LUchange_1985_1999	polygon	1985-1999	1:40,000	Mass GIS
Elevation/Slope	Slope_13_TauntonB	raster	N/A	10m	Processed
	USGS_13_TauntonB	raster	N/A	10m	USGS 3DEP

Description	Dataset	Data type	Time period	Resolution	Source
Soils	SSURGO_Taunton	Polygon	N/A	30m	USDA NRCS through ESRI
	STATSGO2	Polygon	N/A	1:250,000	USDA NRCS
Surficial Geology	GM_DataSourcePolys	polygon	N/A	1:24,000	USGS SIM 3402
	GM_MapUnitPolys	polygon	N/A	1:24,000	USGS SIM 3402
	Bedrock_Outcrops_and_Thin_Till_CP	polygon	N/A	1:24,000	Mass GIS
	Glacial_Stratified_Deposits_CP	polygon	N/A	1:24,000	Mass GIS
	Postglacial_Deposits_CP	polygon	N/A	1:24,000	Mass GIS
	Shallow_Bedrock_CP	polygon	N/A	1:24,000	Mass GIS
	Thick_Till_and_Moraine_CP	polygon	N/A	1:24,000	Mass GIS

The soil data were acquired from the Natural Resources Conservation Service (USDA NRCS). Historical land use was available for the Taunton basin for 1971, 1985, 1999, and 2005 (Figure 2). These dates represent historical land use and not land cover (i.e., impervious vs pervious surfaces). For mapping purposes, the original mapping categories were revised and combined into fewer classifications (Table 2). Additionally, the precision of the historical data changed over the datasets. Figure 3 highlights an example area in the Taunton basin where the amount of residential land cover appears to decrease, although this is simply due to more precise mapping. The most recent land use data available was for 2016. However, this data did not conform to the land use classification scheme used in the historical datasets. This data also includes land cover classifications that identify impervious surfaces. Additional impervious surface data were available for the years 2001, 2006, 2011, and 2016 (Figure 4).

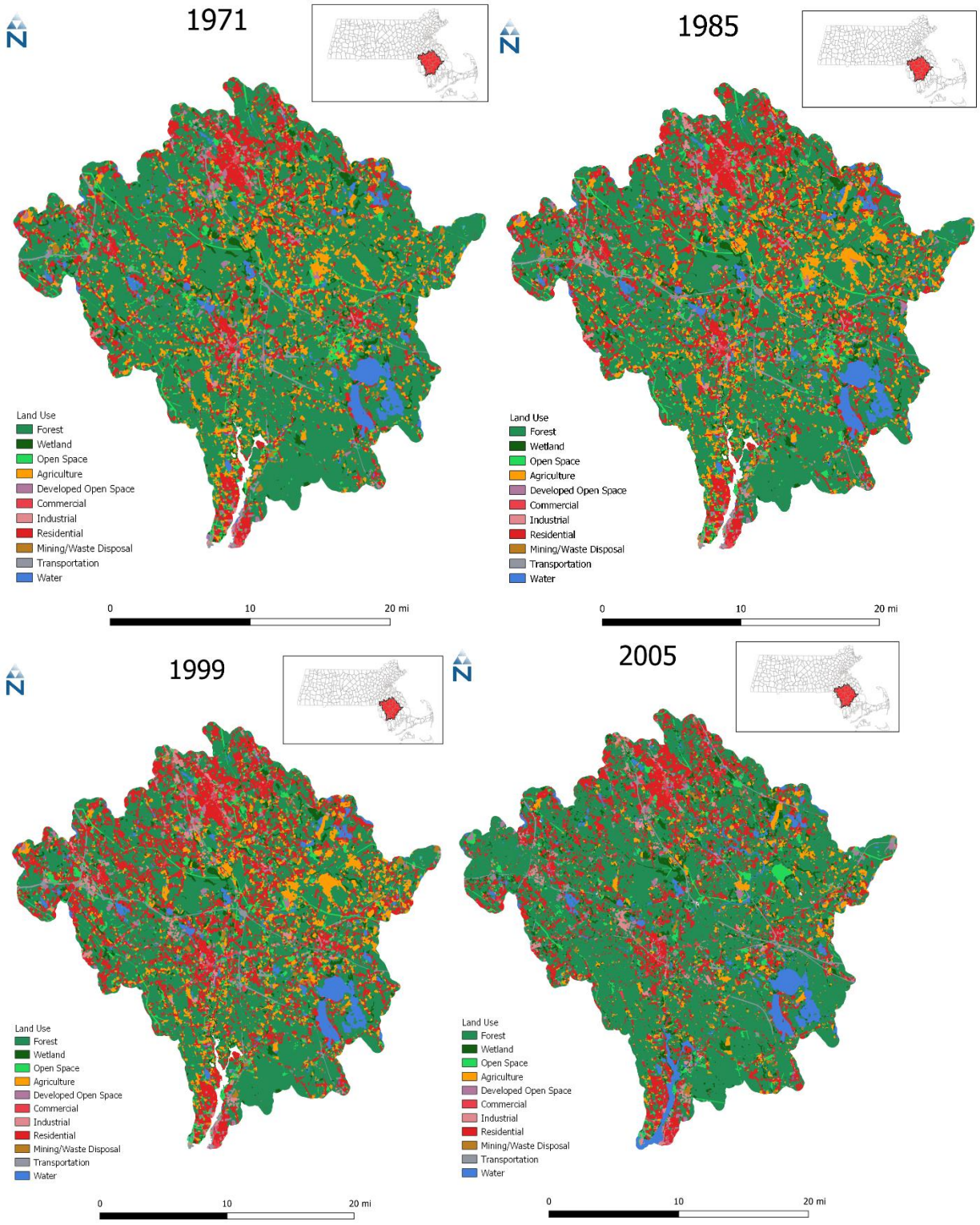

Figure 2. Historical land use for the Taunton basin, Massachusetts.

Table 2. Land use types for 1971-2005 datasets and revised categories

MASS GIS Category	MASS GIS Description	Revised Category for Mapping
Cropland	Intensive agriculture	Agriculture
Pasture	Extensive agriculture	
Woody Perennial	Orchard; nursery; cranberry bog	
Forest	Forest	Forest
Wetland	Nonforested freshwater wetland	Wetland
Salt Wetland	Salt marsh	
Open Land	Abandoned agriculture; power lines; areas of no vegetation	Open Space
Participation Recreation	Golf; tennis; Playgrounds; skiing	
Spectator Recreation	Stadiums; racetracks; Fairgrounds; drive-ins	Developed Open Space
Urban Open	Parks; cemeteries; public & institutional greenspace; also vacant undeveloped land	
Residential	Multi-family	Residential
Residential	Smaller than 1/4 acre lots	
Residential	1/4 - 1/2 acre lots	
Residential	Larger than 1/2 acre lots	
Commercial	General urban; shopping center	Commercial
Industrial	Light & heavy industry	Industrial
Transportation	Airports; docks; divided highway; freight; storage; railroads	Transportation
Mining	Sand; gravel & rock	Mining/Waste Disposal
Waste Disposal	Landfills; sewage lagoons	
Water	Fresh water; coastal embayment	Water
Water-Based Recreation	Beaches; marinas; Swimming pools	

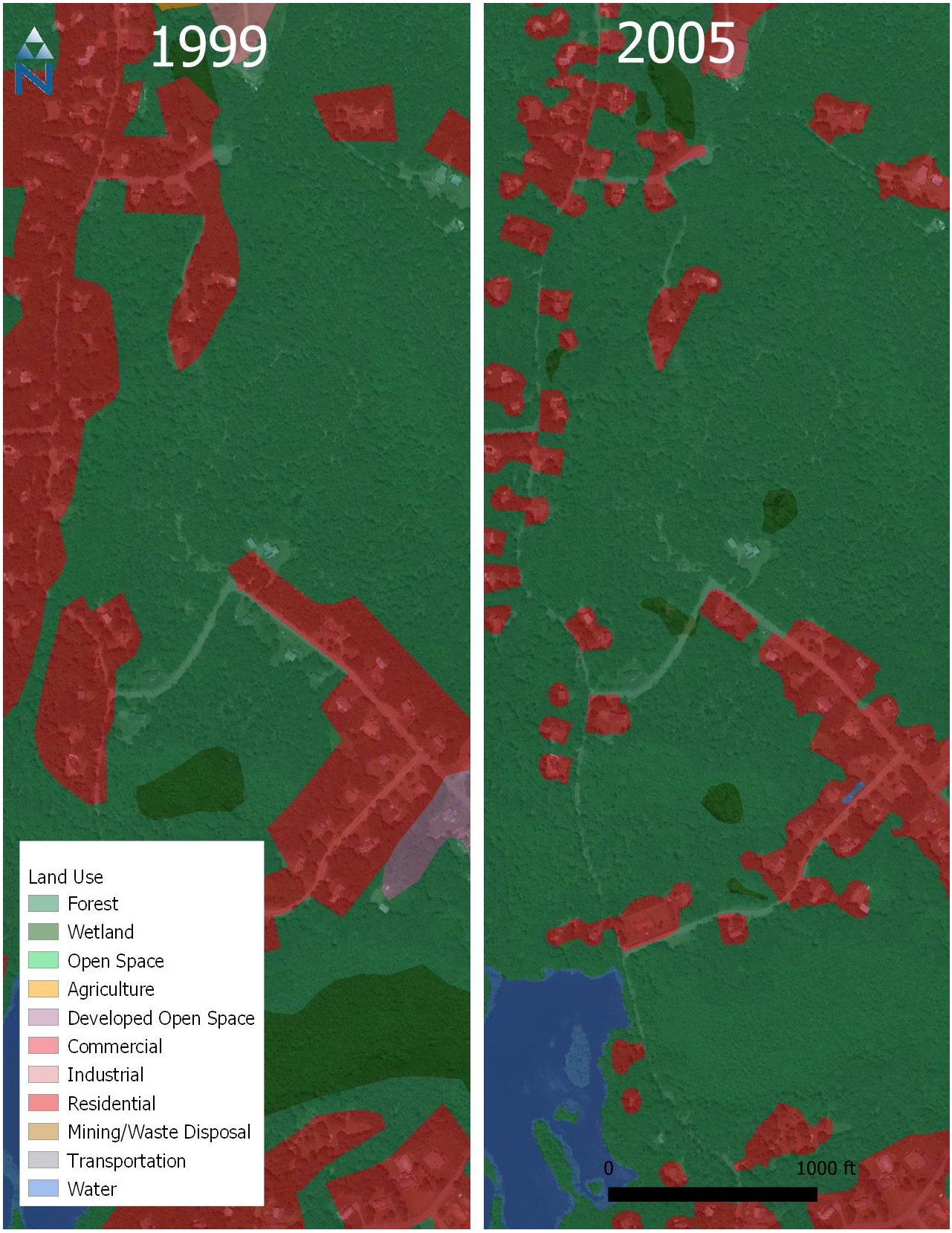

Figure 3. Changes in land use mapping precision.

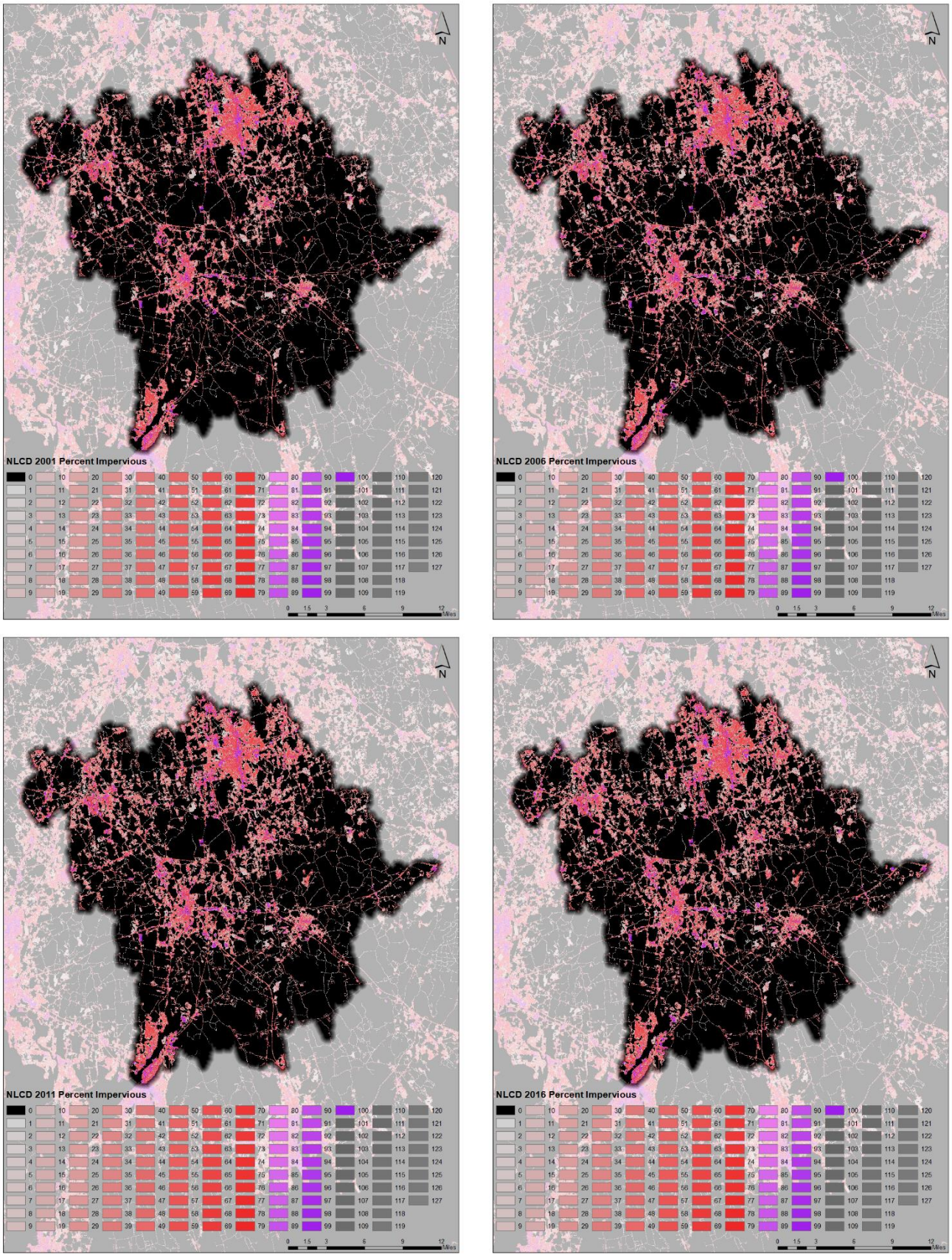

Figure 4. NLCD impervious surface data for the Taunton basin, 2001, 2006, 2011, and 2016.

2.1.2 *Dams and Reservoirs*

There are several small dams within the Wading River watershed. Dam locations were acquired from the Dams_Pt shapefile available from MassGIS. Many of these were built in the 17th and 18th centuries to support industry in the area (Norton Conservation Commission, 2010) and appear to be generally small structures. Figure 5 presents dam locations in the watershed and highlights those associated with water withdrawals (Section 2.1.3). These dams are not explicitly represented in the existing HSPF model, the reaches in the Wading River are simulated using an open-channel flow equation (Section 2.2.1). The largest impoundment in the Wading River watershed is the Lake Mirimichi dam. A 1730 map shows a pond existing in the current location of Lake Mirimichi. Between 1925 and 1927, the larger dam was built to supply drinking water (Friends of Lake Mirimichi, 2020). During this time, a USGS gage (Wading River 01109000) was also installed downstream.

2.1.3 *Water Use*

Water use information, including public water supply (PWS) and non-PWS data, were obtained from the provided by the eASR and eARF databases, respectively, provided by Massachusetts DCR. The facilities located within the Wading River watershed are presented in Table 3. Figure 6 presents withdrawal locations from both surface and subsurface sources. The only major surface water withdrawal is from Blakes Pond, for which consumptive use data were available between 2009 and 2019 (Figure 7). The existing Taunton HSPF model accounted for both water withdrawals and wastewater-return flows. This data and methodology are further discussed in Section 2.2.1.

Agriculture land use comprises a relatively small percentage of the watershed (Section 4.1) and no data were available concerning agricultural water use or hydrological modifications such as tile-drainage and ditch systems. However, these may play an important role in the FDCs of more agriculturally-dominated watersheds and should be considered in these areas.

2.1.4 *Meteorology Data*

One meteorology gage was located within the Taunton basin, another meteorology gage was located at T.F. Green International Airport in Providence Rhode Island, approximately 15 miles southwest of the watershed (Figure 8).

2.1.4.1 Precipitation

Both daily and hourly precipitation data were available as part of historical climate data from the NCDC Global Historic Climate Network (GHCN) and Local Climate Data (LCD) gauge located at the Taunton Municipal Airport (WBAN 54777). A coincident set of records was available from the Providence, RI Airport (WBAN 14765) and was used for comparison purposes and for filling gaps in the observed time series at the Taunton Municipal Airport location. While these two locations are only 25 miles apart, they do have different orientations to the coast making the observed climate patterns slightly different. The Providence Airport gauge sits on the western edge of the Providence River approximately three miles from the mouth where it meets Narragansett Bay while the Taunton Municipal Airport gauge sits approximately 20 miles inland northwest of Narragansett Bay and approximately 20 miles west of Cape Cod. The setting of these two gages and orientation to the coast may result in some differences in the climate patterns. Table 4 summarizes station metadata for these gauges.

The records for the Taunton Municipal Airport and a second Taunton gage (WBAN 98367) gages were ultimately combined during data processing as their periods of record were complimentary with only a short definition of overlap during 2005 (Table 4). Between the combined Taunton records and the Providence Airport a common 73-year period beginning January 1, 1948, was available. Limited data gaps (missing records) were found during the data review for the most recent 40-year period (1981-2020) at both the Providence and combined Taunton gauges, with intervals flagged as suspect accounting for less than 1% of

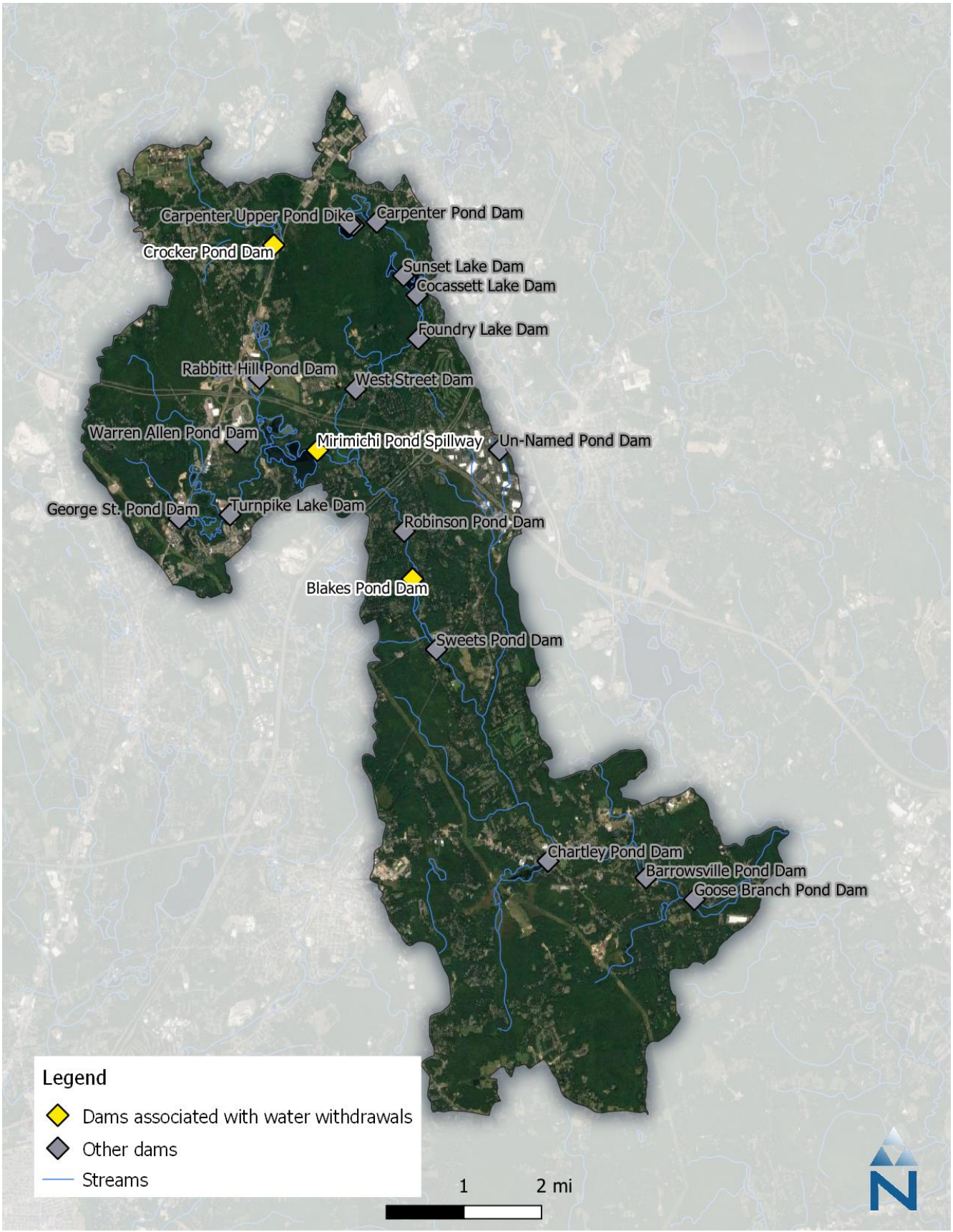

Figure 5. Dam locations in the Wading River watershed

Table 3. Water supply facilities in the Wading River

Type	Name/User	Source Name	Town
Public Water Supply	PLAINVILLE WATER DEPARTMENT	LAKE MIRIMICHI WELL #1	PLAINVILLE
		LAKE MIRIMICHI WELL #2	
		LAKE MIRIMICHI WELL #3	
		WELL 1 AND 1A	
		WELL 2 AND 2A	
		WELL 5	
	PLAINVILLE ATHLETIC LEAGUE	WELL 1	
	ATTLEBORO WATER DEPT	WADING RIVER (BLAKES POND)	ATTLEBORO
	MANSFIELD WATER DIVISION	WALSH PROPERTY WELLFIELD	MANSFIELD
	WRENTHAM WATER DIVISION	CROCKER POND WELL6	WRENTHAM
		WELL 4	
	FOXBORO WATER DEPARTMENT	WELL 4	FOXBOROUGH
	FOXBORO WATER DEPARTMENT	WELL 5	
	FOXBORO WATER DEPARTMENT	WELL 6	
Non-public water supply	Golf	WELL #1(IRRIGATION)	FOXBOROUGH
		WELL #2(#16 Well)	
		WELL #3(#15 Well)	
		PUMP #4 @ 7 TEE PONDS	
	Manufacturing	WRENTHAM BOG	WRENTHAM
		WELL #11	ATTLEBORO
		WELL #1	
		WELL #3	
		WELL #7	

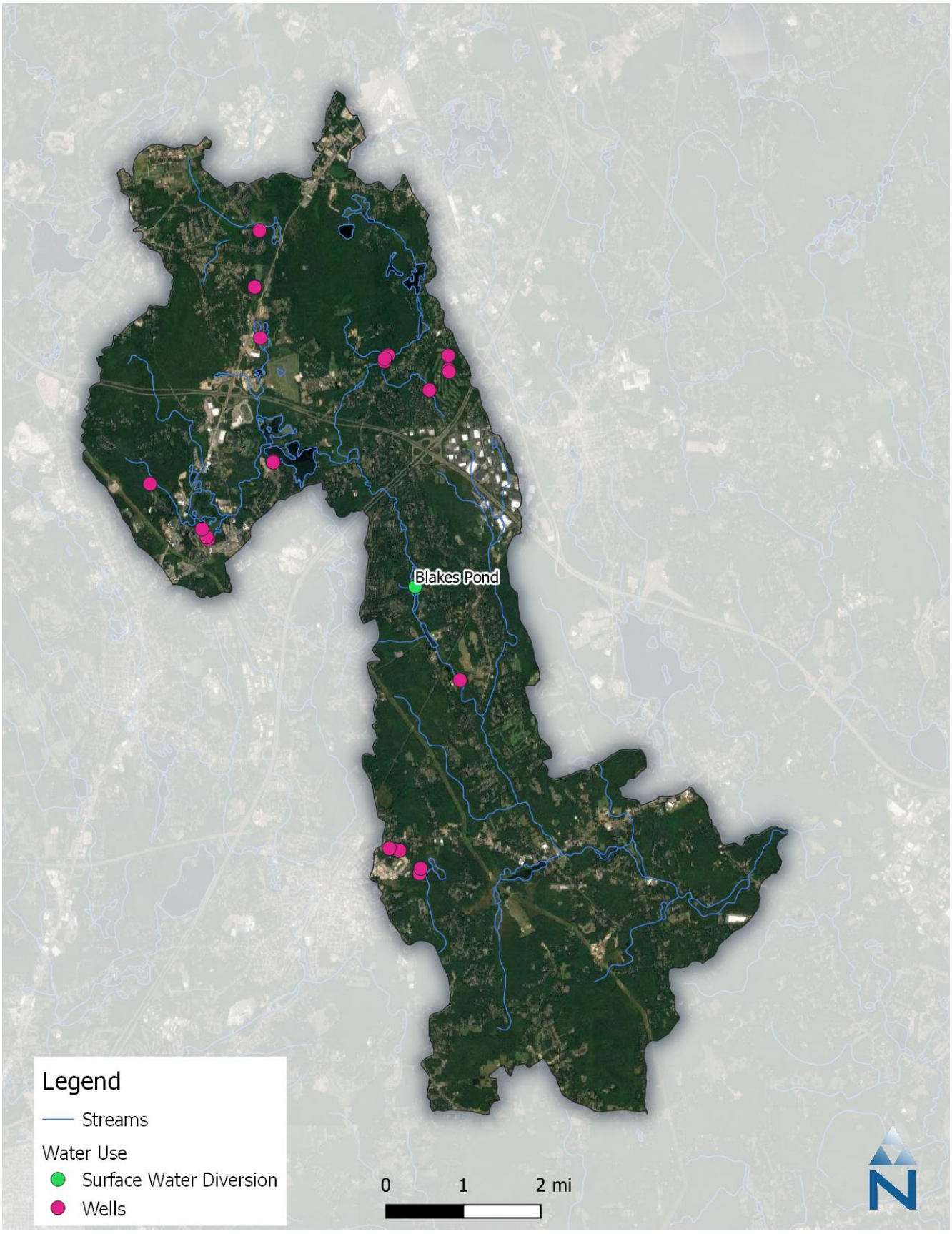

Figure 6. Water use in the Wading River watershed

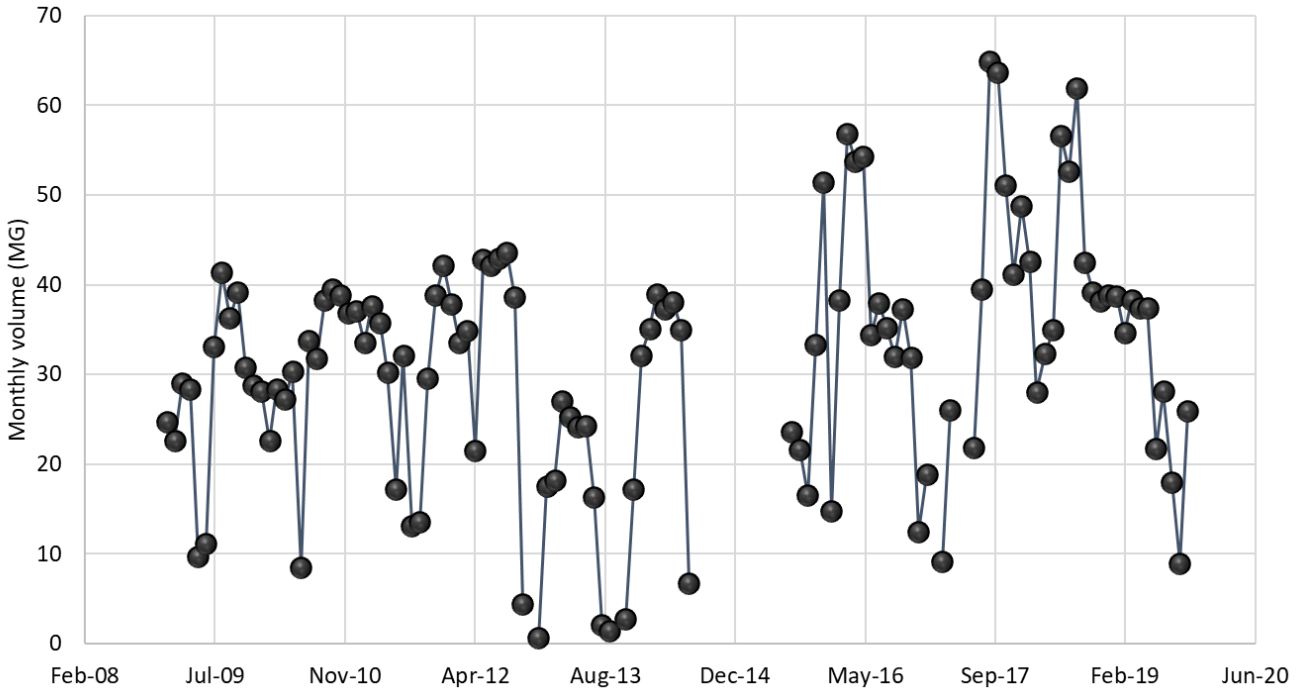

Figure 7. Water withdrawals from Blakes Pond by the Attleboro Water Department.

Table 4. Summary of NCDC gauge location metadata

Station Name	Station ID	Data Period	Latitude	Longitude	Elevation (ft.)
PROVIDENCE, RI US	14765	1942-2021	41.7225	-71.4325	16.8
TAUNTON MUNICIPAL AIRPORT, MA US	54777	2005-2021	41.87556	-71.0211	13.1
TAUNTON, MA US	98367	1942-2005	41.90028	-71.0658	Not Available

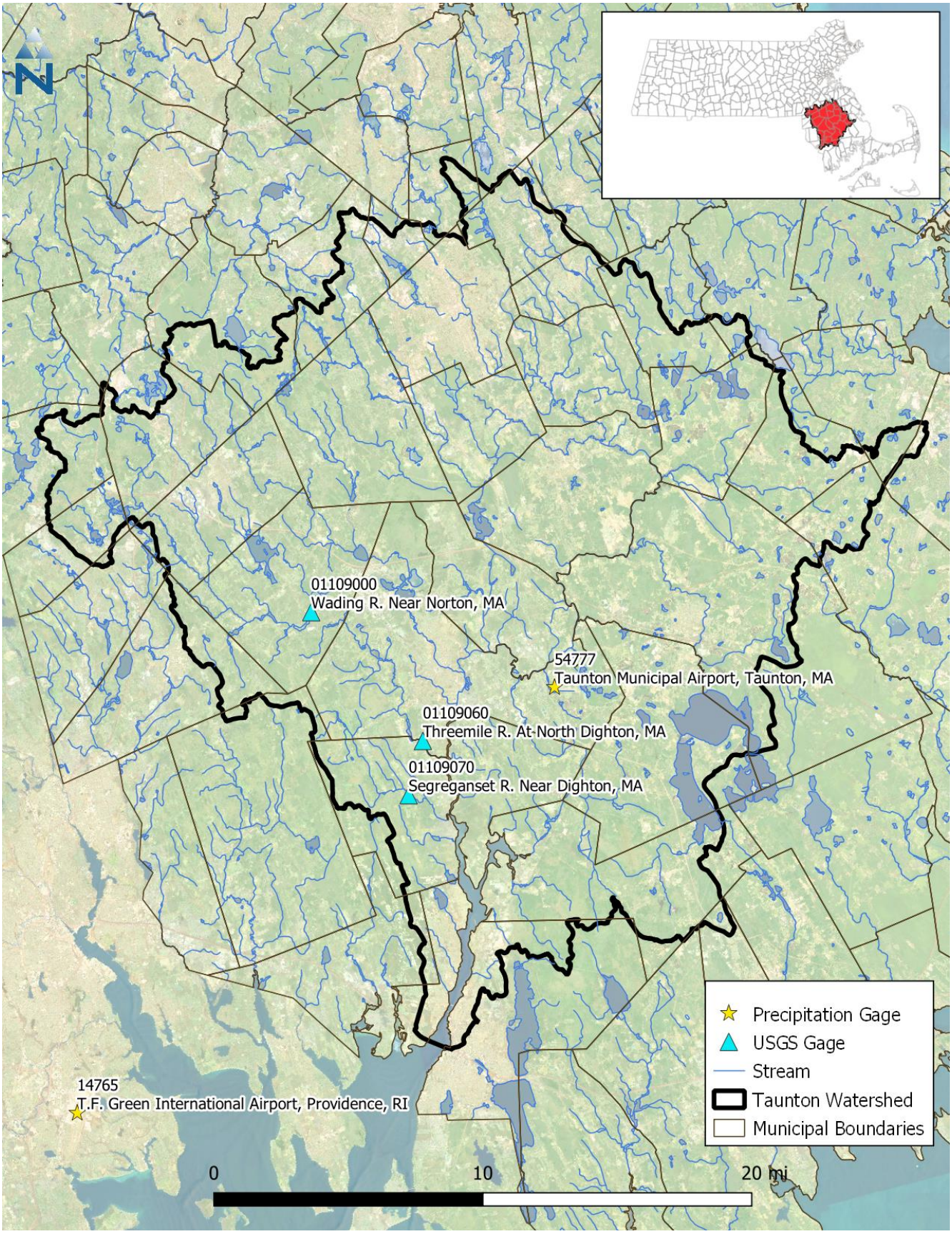

Figure 8. Meteorology and streamflow gage locations.

the long-term time series. More significant data gaps during the pre-1981 period of record were filled at the respective gage using the normal-ratio method with data from the other gauge. Table 5 presents annual precipitation totals for the entire period of record for the T.F. Green Airport, comparing each year against long-term precipitation trends. Table 6 presents a summary of rainfall trends from the most recent 21-year period (2000-2020) compared to the long-term 73-year period (1948-2020) comparing the total annual average precipitation and distribution of storm events by depth. This table shows the most recent 21-year period compares favorably to the trends of the long-term 73-year period in terms of replicating annual depth and storm frequency. Figure 9 presents annual counts by four precipitation depth thresholds from 1948 through 2020. This plot highlights the variability from year to year in frequency of each depth with the highest variability at the lower depth thresholds. No discernable trend over time is present.

Table 5. Precipitation analysis for T.F. Green Airport. Red to blue shading indicates years below and above median values, respectively with darker shading representing larger magnitudes

T.F. Green Airport - Providence, RI								
Year	Rainfall (in)	Percentile 10th % Average 90th %	Difference (in)		Number of Rain Days per Year:			
			Last 20 Years	All Years	>= 0.1in	>= 0.5in	>= 1.0in	>=1.5in
1949	35.65	4%	-10.49	-13.16	72	26	4	2
1950	39.51	18%	-6.63	-9.30	81	25	8	3
1951	45.6	51%	-0.54	-3.21	79	34	11	5
1952	41.54	32%	-4.60	-7.27	75	25	12	5
1953	57.01	90%	10.87	8.20	76	39	21	10
1954	51.53	77%	5.39	2.72	82	34	13	8
1955	51.71	79%	5.57	2.90	74	29	13	10
1956	42.67	37%	-3.47	-6.14	84	33	7	1
1957	30.08	3%	-16.06	-18.73	65	19	6	2
1958	51.54	78%	5.40	2.73	89	33	16	5
1959	43.14	40%	-3.00	-5.67	80	29	11	4
1960	40.08	21%	-6.06	-8.73	64	28	13	5
1961	49.56	71%	3.42	0.75	75	31	13	7
1962	50.33	74%	4.19	1.52	66	33	14	8
1963	39.5	16%	-6.64	-9.31	71	26	13	3
1964	38.41	11%	-7.73	-10.40	69	27	11	3
1965	25.44	1%	-20.70	-23.37	59	19	3	1
1966	38.68	15%	-7.46	-10.13	64	23	13	6
1967	46.5	58%	0.36	-2.31	83	32	10	5
1968	41.36	30%	-4.78	-7.45	71	24	12	5
1969	44.59	41%	-1.55	-4.22	72	28	14	7
1970	45.42	48%	-0.72	-3.39	68	29	12	7
1971	38.42	12%	-7.72	-10.39	71	25	10	5
1972	65.06	97%	18.92	16.25	95	42	21	11
1973	48.24	64%	2.10	-0.57	73	34	12	6
1974	40.66	25%	-5.48	-8.15	76	27	10	5
1975	50.83	75%	4.69	2.02	79	33	19	7

T.F. Green Airport - Providence, RI								
Year	Rainfall (in)	Percentile 10th % Average 90th %	Difference (in)		Number of Rain Days per Year:			
			Last 20 Years	All Years	>= 0.1in	>= 0.5in	>= 1.0in	>=1.5in
1976	46.32	56%	0.18	-2.49	71	26	11	5
1977	48.84	67%	2.70	0.03	84	30	14	8
1978	47.01	60%	0.87	-1.80	72	32	14	8
1979	58.19	95%	12.05	9.38	88	32	17	9
1980	36.11	5%	-10.03	-12.70	67	20	10	4
1981	36.37	7%	-9.77	-12.44	81	25	7	4
1982	49.26	70%	3.12	0.45	77	29	13	9
1983	67.52	99%	21.38	18.71	88	46	20	11
1984	48.74	66%	2.60	-0.07	84	33	10	3
1985	40.42	23%	-5.72	-8.39	74	25	8	6
1986	46.13	55%	-0.01	-2.68	77	31	12	5
1987	40.67	26%	-5.47	-8.14	77	28	8	4
1988	38.37	10%	-7.77	-10.44	66	23	11	6
1989	56.06	88%	9.92	7.25	89	42	19	6
1990	44.78	45%	-1.36	-4.03	83	29	13	3
1991	45.69	52%	-0.45	-3.12	81	32	10	6
1992	47.48	62%	1.34	-1.33	78	31	12	6
1993	42.16	33%	-3.98	-6.65	77	30	9	4
1994	44.69	42%	-1.45	-4.12	73	31	14	7
1995	38.58	14%	-7.56	-10.23	69	28	8	2
1996	48.06	63%	1.92	-0.75	84	27	12	5
1997	37.97	8%	-8.17	-10.84	74	29	9	1
1998	52.7	82%	6.56	3.89	86	33	14	8
1999	42.26	34%	-3.88	-6.55	68	26	12	7
2000	46	53%	-0.14	-2.81	74	29	12	6
2001	40.19	22%	-5.95	-8.62	61	26	11	9
2002	42.34	36%	-3.80	-6.47	76	33	11	1
2003	50.27	73%	4.13	1.46	91	34	18	5
2004	45.33	47%	-0.81	-3.48	76	32	12	7
2005	57.92	93%	11.78	9.11	86	38	14	9
2006	54.3	85%	8.16	5.49	86	32	13	6
2007	42.81	38%	-3.33	-6.00	70	26	13	7
2008	57.12	92%	10.98	8.31	88	32	15	10
2009	54.85	86%	8.71	6.04	85	41	18	6
2010	53.54	84%	7.40	4.73	66	31	15	6
2011	56.72	89%	10.58	7.91	92	39	17	11
2012	41.19	29%	-4.95	-7.62	75	29	10	6
2013	45.46	49%	-0.68	-3.35	75	30	10	4

T.F. Green Airport - Providence, RI								
Year	Rainfall (in)	Percentile 10th % Average 90th %	Difference (in)		Number of Rain Days per Year:			
			Last 20 Years	All Years	>= 0.1in	>= 0.5in	>= 1.0in	>=1.5in
2014	46.94	59%	0.80	-1.87	73	26	16	7
2015	40.83	27%	-5.31	-7.98	75	26	9	4
2016	40	19%	-6.14	-8.81	77	30	8	3
2017	49	68%	2.86	0.19	82	35	16	6
2018	63.49	96%	17.35	14.68	91	46	22	8
2019	51.97	81%	5.83	3.16	101	34	13	4
2020	44.71	44%	-1.43	-4.10	74	25	10	5

Table 6. Precipitation summary for T.F. Green Airport

T.F. Green Airport - Providence, RI					
Period	Average Rainfall (in)	Average Number of Rain Days per Year			
		>= 0.1in	>= 0.5in	>= 1.0in	>=1.5in
(1948-2020)	46.14	77	30	12	6
(2000-2020)	48.81	80	32	13	6

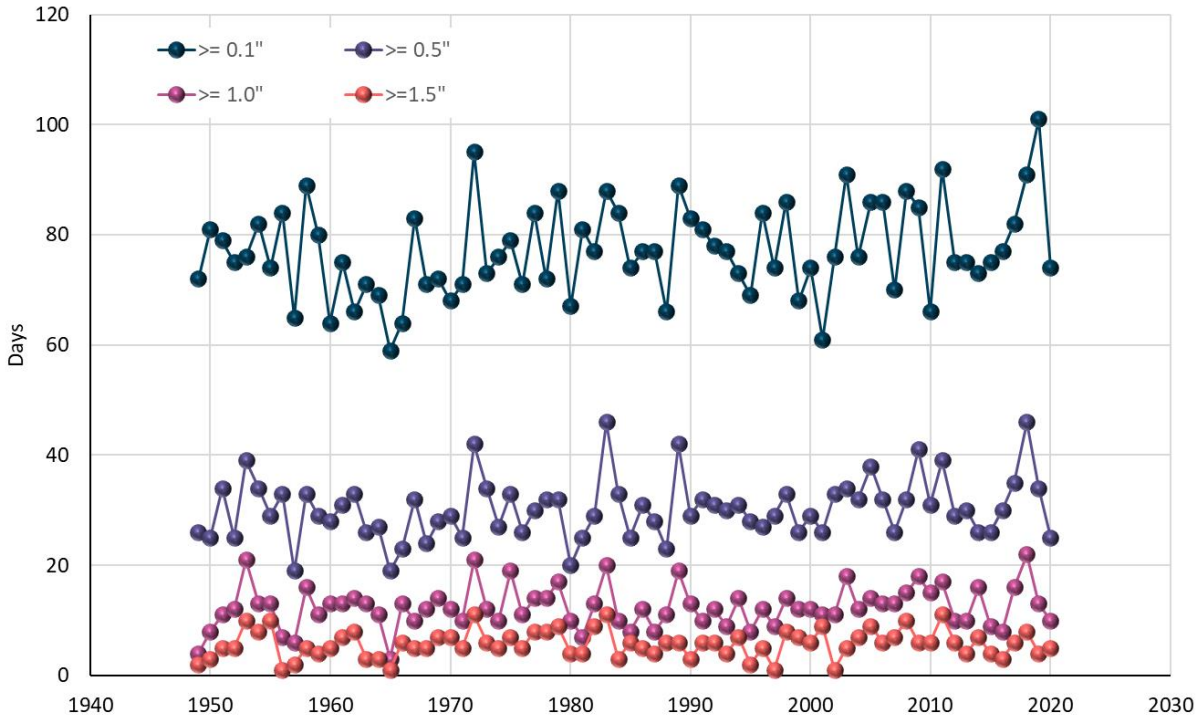

Figure 9. Number of rain days per year by depth (T.F. Greene Airport, Providence, RI).

2.1.4.2 Temperature

Daily and hourly air temperature data were available as part of the same data sets (GHNC and LCD) used for obtaining the precipitation data which was presented in the previous section. The hourly air temperature data were assessed for data gaps by reviewing the quality flags provided with the raw data and reviewing summary statistics. An example of the hourly temperatures obtained for the Providence Airport gauge record is presented below in Figure 10.

Data quality was assessed using NCDC-supplied flagging like the precipitation data presented in the previous section. Values were filled forward to patch short-term data gaps. One outlier maximum temperature value of 148 degrees Fahrenheit was found in the Providence Airport gauge (72506814765) daily records on January 26, 1962, but was not present in the hourly records. This outlier was replaced by the maximum temperature of 43 degrees Fahrenheit found in the corresponding hourly data set. Daily maximum and minimum temperatures were derived from hourly temperature data by searching the 24 hours between midnight and midnight of each day for the highest and lowest temperatures. Missing values were filled with the maximum/minimum daily temperature found in the corresponding hourly data sets, and any remaining missing values without coincident hourly data were filled by linear interpolation of the time series. Large gaps were filled using the more complete daily records which were disaggregated using a typical 24-hour diurnal based on the hourly observations.

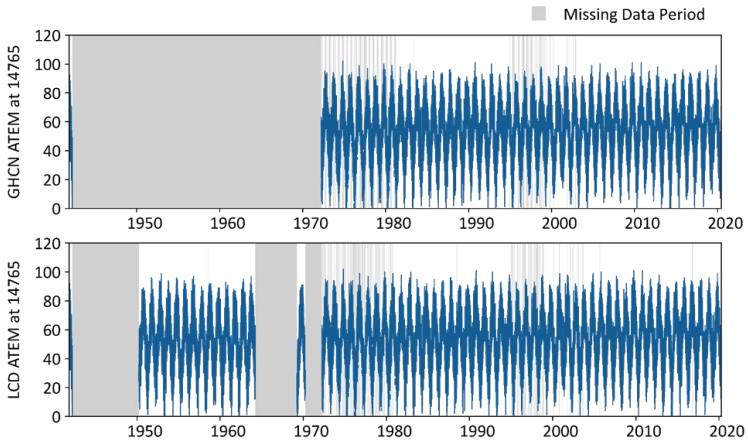

Figure 10. The original hourly temperature data at the Providence Airport gauge (72506814765).

2.1.4.3 Other Climate Data

Other climate data parameters are required to run both hydrology and snow simulation modules in LSPC which include potential evapotranspiration, dew point temperature, wind speed shortwave solar radiation, and cloud cover. Observed values were obtained for these parameters from both the GHCN and LCD data sets used to compile precipitation the temperature data. Some records were available for both the Taunton and Providence airports but monitoring of these secondary parameters is more limited so records at the two gauges were combined to build a complete data set covering the full period of record. Short data gaps were filled using fill-forward techniques while longer data gaps were filled with the long-term daily average by month calculated from the available data. An assessment of the data gaps at the longer Providence Airport gauge record is presented in Figure 11. Observed potential evapotranspiration was not available and was therefore calculated from other parameters using the Penman-Monteith method available in the BASINS WDM Utility (EPA, 2020).

Plots of potential evapotranspiration, dew point temperature, wind speed shortwave solar radiation, and cloud cover used for review and quality assurance are presented in Appendix A.

Figure 11. Data gaps for meteorological information obtained for T.F. Green International Airport, Providence Rhode Island (Gage 1476).

2.1.5 *Streamflow Data*

Three United States Geological Survey (USGS) streamflow gages were located within the Taunton basin (Figure 8).downward trend for low flows. As an example, the 1-day minimum flows (Figure 19) appear to begin a relatively steep decline around the year 2000 although the trend may go back to the 1980s. Similar trends can be seen in the other minimum flow graphs, though the timing of when the trend starts depends on the fit of the polynomial curve.

Table 7 presents a summary of the gages and their datasets. Based on its location and the period of record (1925-present) the Wading River gage was identified as well suited for this study. Figure 12 presents a time series of total discharge for the period of record for the Wading River. The gage drains a 43.3 square mile area and has a very high (98.4%) percentage of complete data. The rating curve for the Wading river was also acquired from the USGS and is presented in Figure 13. A previous study identified the bankfull discharge to be 295 ft^3/s with a recurrence interval of 1.15 years (Table 8).

Figure 14 presents the flow duration curve (FDC) for the Wading River for the entire period of record (1925-2020). Figure 15 presents FDCs for each decade of data available. Each of the nine FDCs represents all the flow data recorded for the associated decade. Figure 16 highlights the right-hand side of Figure 15, focusing on the low flows. While consistent trends are difficult to assess from the graph, data from the 1990s and the 2010s show a portion of low flows becoming even lower. The figure may also suggest increasing variability in flows. Figure 17 highlights the left-hand side of Figure 15, focusing on the high flows. Similar to low flows, while consistent trends are difficult to assess from the graph, it appears that high flows have somewhat increased over the past several decades. However, the highest flows appear to have been in the 1980s.

To further analyze characteristics of the FDC over time, several metrics were calculated using the Wading River gage data and the Indicators of Hydrologic Alteration (IHA) parameters in Table 9. The IHA parameters are a suite of 33 parameters that provide an ecologically meaningful assessment of flow data to provide indicators of anthropogenic impacts to riverine systems (Richter et al., 1996; Swanson, 2002). The IHA parameters are categorized into five groups of metrics that provide information on the magnitude and timing (Group 1), magnitude and duration (Group 2), timing (Group 3), frequency and duration (Group 4), and the rate of change and frequency (Group 5) of flows. Table 10 presents additional metrics that were considered. Several of the associated figures were produced using the USGS Exploration and Graphics for RivEr Trends (EGRET) R-package (Hirsch and De Cicco, 2015). This section provides metric results for the entire period of record for the Wading River, most of the results are calculated for each water year and are presented in graphical time series. This approach is intended to provide an intuitive, visual understanding of how the metrics may change over time as well as to help identify those metrics which may be most beneficial to use in subsequent tasks. In Section 3, two separate time-periods are identified whose differences in observed streamflow may be attributed to changes in impervious surfaces in the watershed. Section 5 presents a comparison of selected metrics between these two periods. The results provide a framework in which baseline and optimized model scenarios may be compared in future tasks.

Figure 18 presents the average monthly flow of the Wading River. The figure presents information on the magnitude and timing of flows (Group 1 IHA parameters). Unsurprisingly, the lowest flows occur during summer when evapotranspiration (ET) is highest. Additionally, increased groundwater pumping likely occurs in the watershed during this time to meet public water supply demands and private irrigation needs for areas such as golf courses. The highest flows occur in late winter/early spring when winter snowpack is likely to be melting, pervious grounds may be frozen and there is little ET demand.

Information on the magnitude and duration of flows (Group 2 IHA parameters) are presented in Figure 19 through Figure 24. Figure 19, Figure 20, Figure 21, Figure 22, and Figure 23 present the 1-day, 3-day, 7-day, 30-day, and 90-day minimum and maximum flows, respectively. The 1-day flow values are calculated from the entire 365 days of mean daily flow observations while multi-day metrics are calculated as rolling averages

of the previous 3, 7, 30, or 90 days. The minimum and maximum values of these averages are then plotted on the graphs. Maximum flows are computed based on water year while low flows are calculated based on climate year (April 1 through March 31). Climate year is used rather than water year for low flows to minimize the probability that individual drought events will span multiple years (Hirsch and De Cicco, 2015). While there does not seem to be a trend associated with maximum flows, there does appear to be a downward trend for low flows. As an example, the 1-day minimum flows (Figure 19) appear to begin a relatively steep decline around the year 2000 although the trend may go back to the 1980s. Similar trends can be seen in the other minimum flow graphs, though the timing of when the trend starts depends on the fit of the polynomial curve.

Table 7. Summary of active, long-term USGS gages located in the Taunton River basin

Location	USGS-ID	Drainage Area (mi^2)	Start Date	End Date	Percent Complete[2]	Percent Estimated
Segreganset River near Dighton, MA[1]	01109070	10.6	7/1/1966	Present	96.2%	3.0%
Wading River near Norton, MA	01109000	43.3	6/1/1925	Present	98.4%	1.6%
Threemile River at North Dighton, MA	01109060	84.3	7/1/1966	Present	97.0%	3.0%

1. The Segreganset River location is missing approximately five months of data in 1992.
2. Records flagged as provisional ("P") and revised ("A:R") are considered complete for this summary.

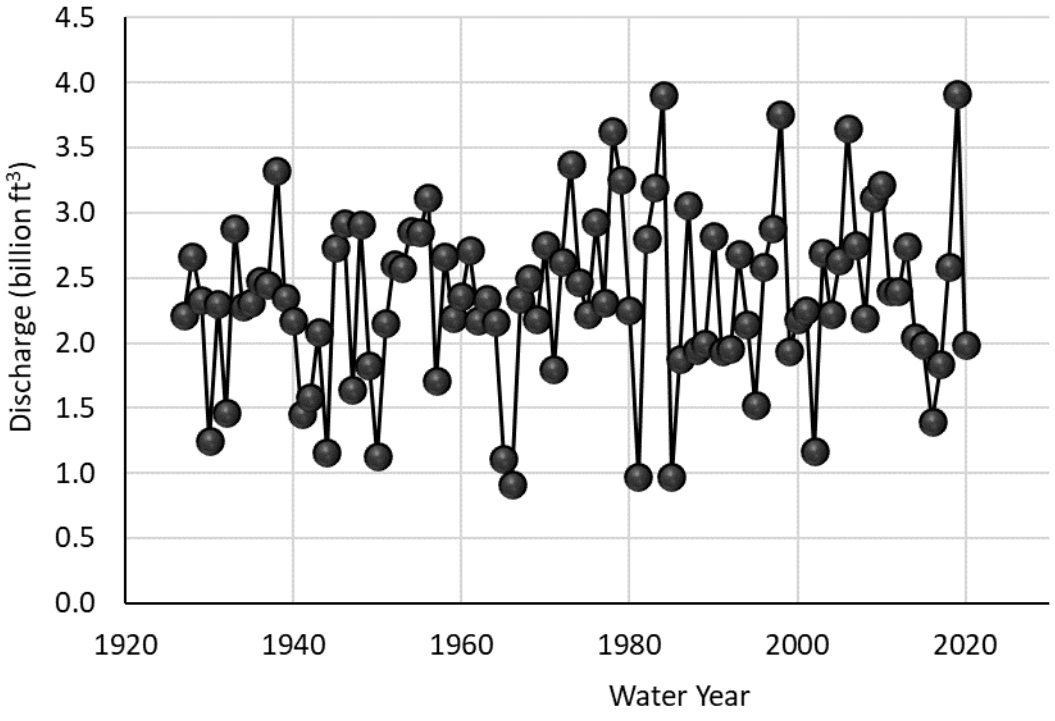

Figure 12. Total discharge by water year based on daily mean discharge at the Wading River (01109000).

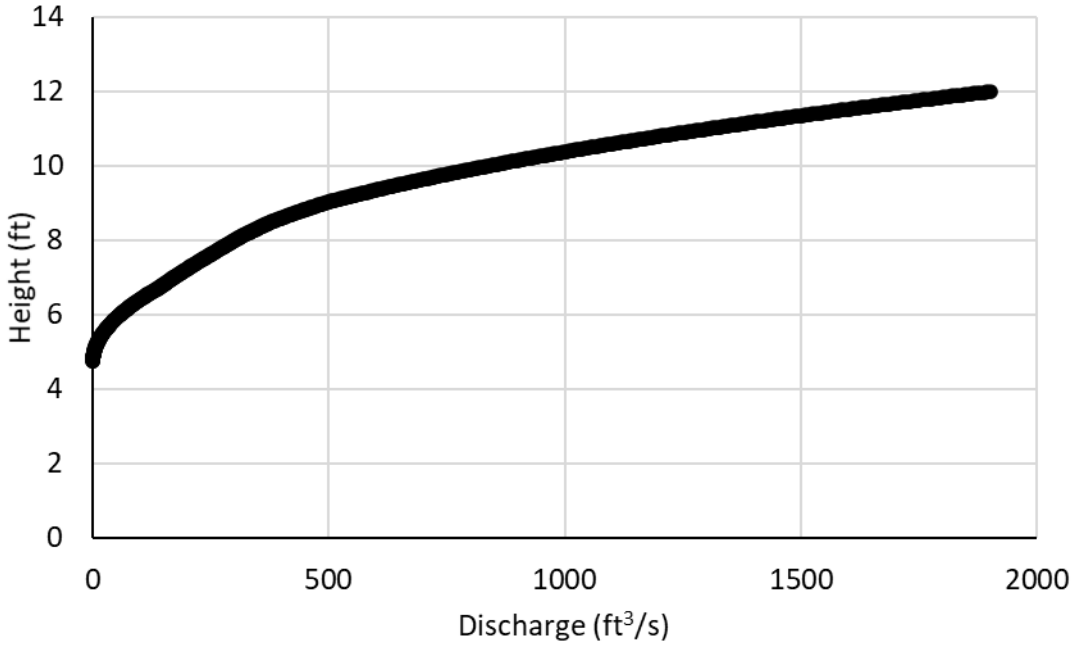

Figure 13. Rating curve for Wading River (01109000).

Table 8. Wading River gage characteristics (Bent and Waite, 2013)

Station	Bankfull Discharge (ft^3/s)	Discharge Recurrence Interval (yr)
01109000 – Wading River near Norton, MA	295	1.15

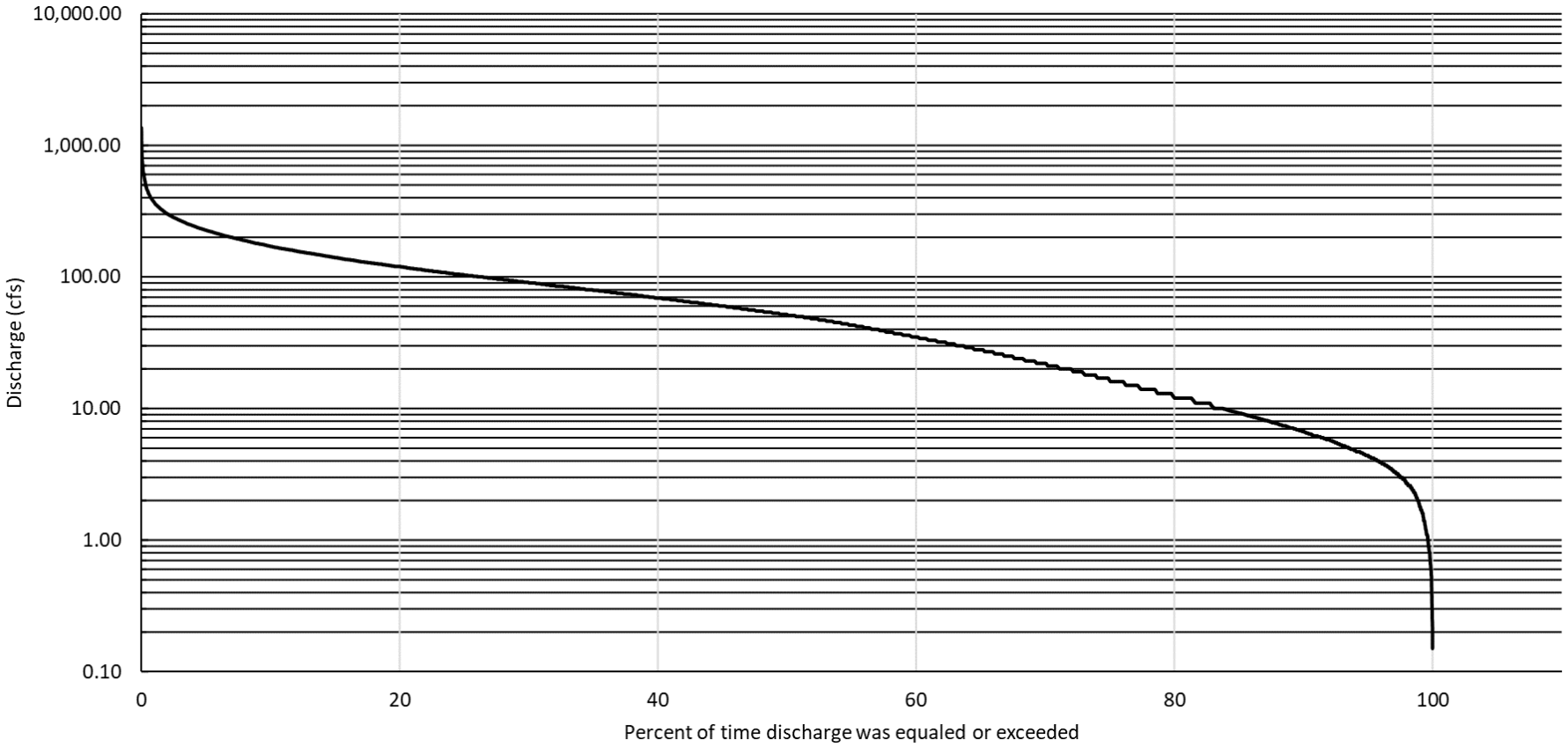

Figure 14. Flow duration curve 1925-2020. Wading River.

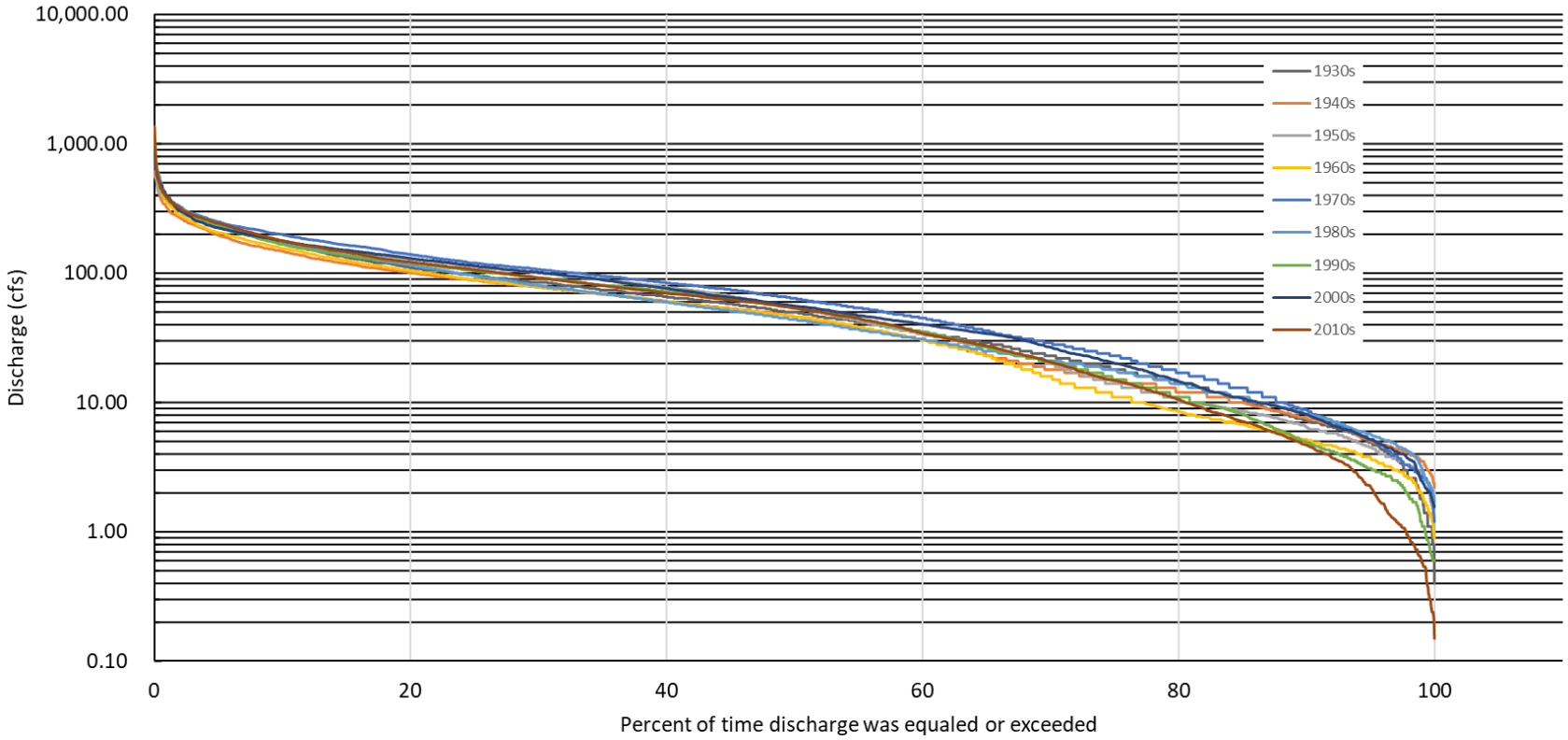

Figure 15. Flow duration curves by decade. Wading River.

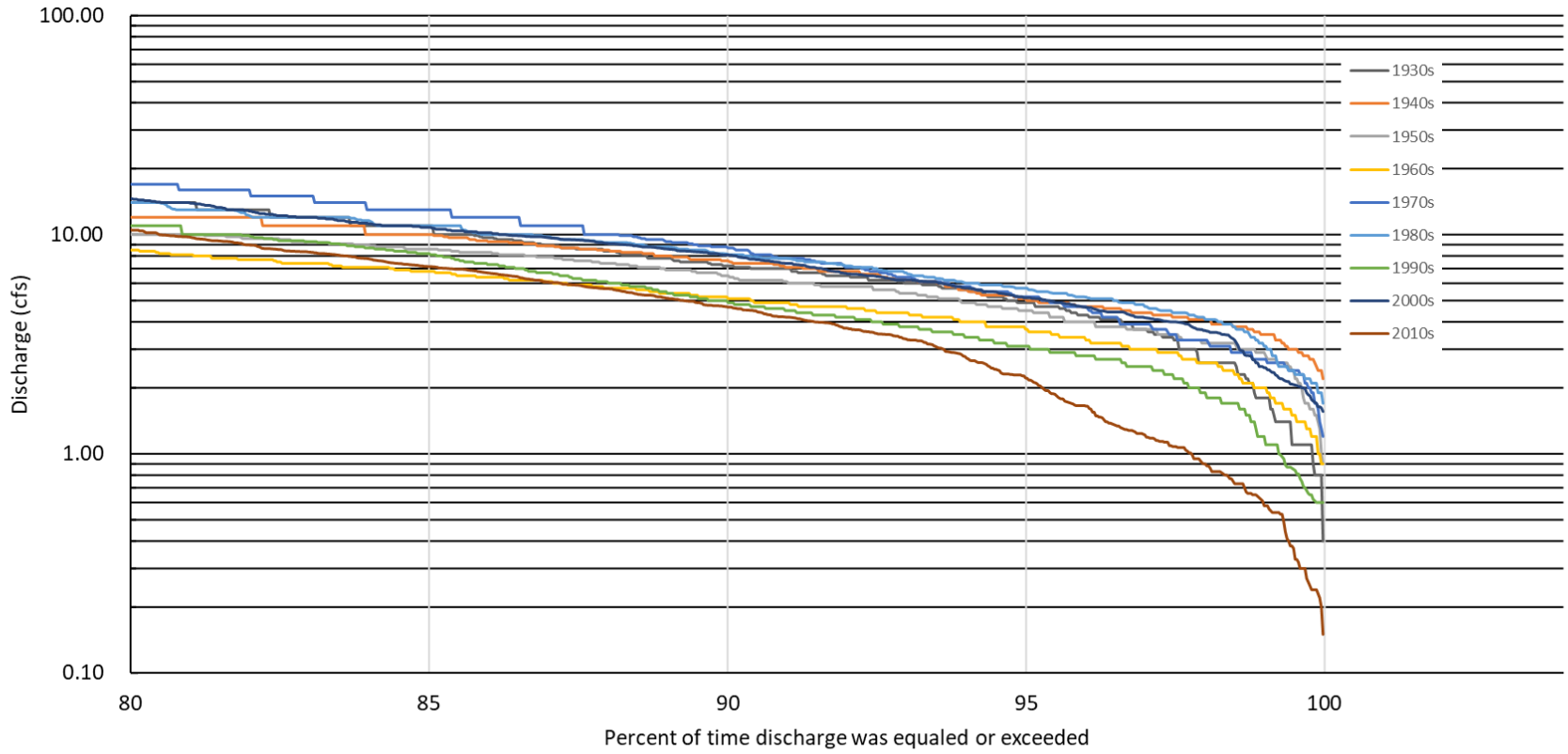

Figure 16. Enlarged section of Figure 15 showing the low flow portion of flow duration curves by decade. Wading River.

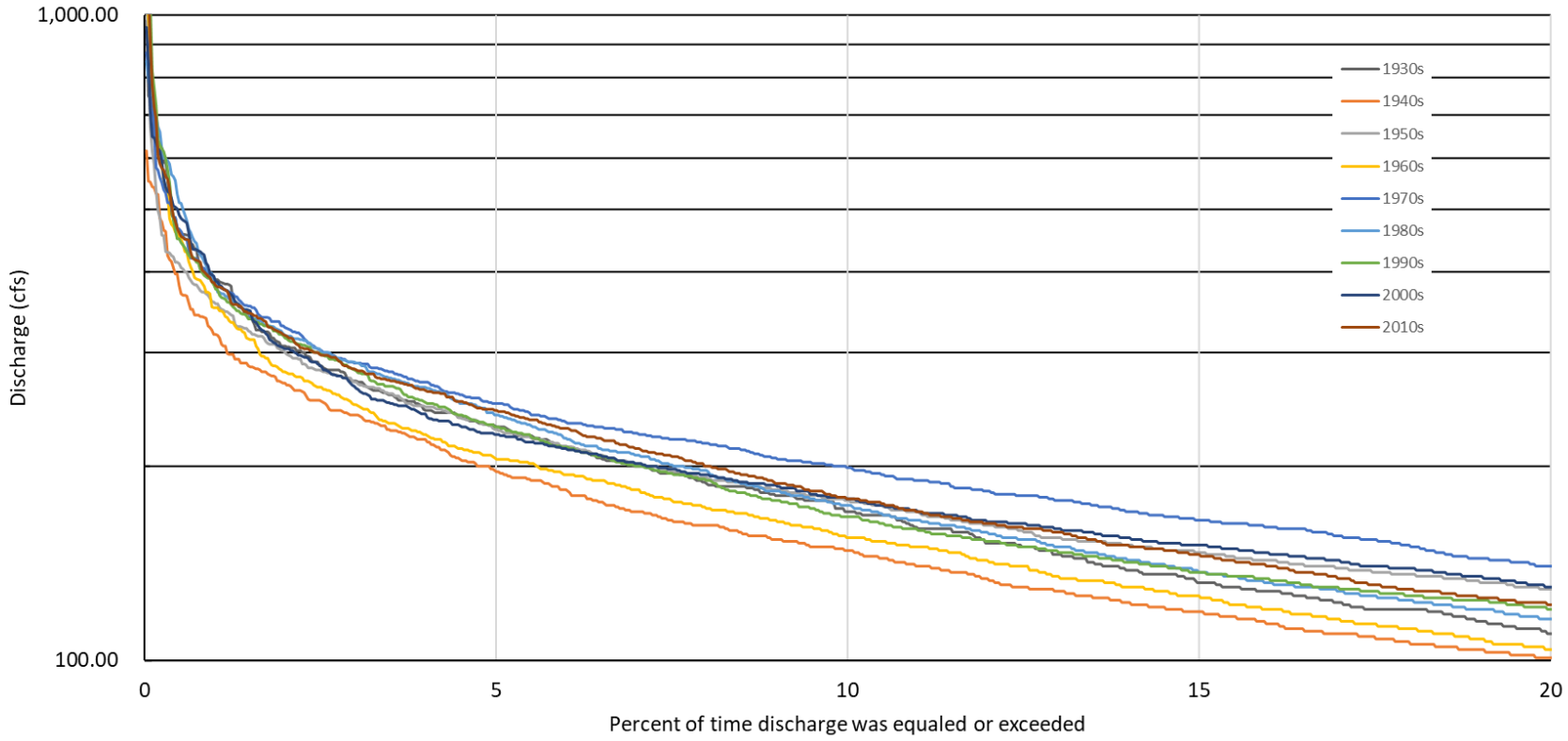

Figure 17. Enlarged section of Figure 15 showing the high flow portion of flow duration curves by decade. Wading River.

Table 9. IHA parameter grouping (Reichold et al., 2010)

Group	IHA parameter	Figure	Examples of Ecosystem Impact
Group 1 Magnitude and timing (12 parameters)	Average monthly flow (1 value for each of the 12 months)	Figure 18	Increased flow variations may lead to wash out or stranding of sensitive species
Group 2 Magnitude and duration (12 parameters)	Average annual 1-day minimum flow	Figure 19	Prolonged low flows, prolonged base flow spikes, and altered inundation period may lead to a change in the concentration of aquatic organisms, reduction or elimination of plant cover, diminished plant species diversity, and loss of floating eggs
	Average annual 3-day minimum flow	Figure 20	
	Average annual 7-day minimum flow	Figure 21	
	Average annual 30-day minimum flow	Figure 22	
	Average annual 90-day minimum flow	Figure 23	
	Average annual 1-day maximum flow	Figure 19	
	Average annual 3-day maximum flow	Figure 20	
	Average annual 7-day maximum flow	Figure 21	
	Average annual 30-day maximum flow	Figure 22	
	Average annual 90-day maximum flow	Figure 23	
	Number of days per year with zero flow	N/A	
	7-day minimum flow divided by mean flow in each year	Figure 24	
Group 3 Timing (2 parameters)	Julian date of the minimum flow	Figure 25	Loss of seasonal flow peaks may disrupt cues for spawning, egg hatching, and migration and lead to loss of fish access to Julian date of the maximum flow wetlands or backwaters
	Julian date of the maximum flow	Figure 25	
Group 4 Frequency and duration (4 parameters)	Number of low pulses	Figure 26	Flow stabilization may lead to invasion of exotic species and reduced water and nutrients to floodplain plant species
	Average duration of low pulse	Figure 27	
	Number of high pulses	Figure 26	
	Average duration of high pulses	Figure 27	
Group 5 Rate of change and frequency (3 parameters)	Rise rate (mean of all positive differences)	Figure 28	Rapid changes in river stage and accelerated flood recession may cause wash out and stranding of aquatic species, failure of seedling establishment
	Fall rate (mean of all negative differences)	Figure 28	
	Number of flow reversals	Figure 29	

Table 10. Potential metrics for evaluating impacts and benefits from changes in land cover

Evaluation Metric	Description	Source	Figure	Unit
Trend Slope	Quantile-Kendall plot	EGRET	Figure 31 & Figure 32	% per year
Variability	Discharge variability over time	EGRET	Figure 30	Unitless
Annual Nutrient (P&N) load export (excluding channel processes)	Pollutant load Export rates	TSC	N/A – will be presented with modeling results in Task 6	lbs/acres/year
Annual surface runoff volume	Runoff yields	TSC	Figure 34	inches/year
Annual Groundwater recharge	Infiltration	TSC	N/A – will be presented with modeling results in Task 6	inches/year
Ecodeficit/Ecosurplus	Flow Duration Curve	TSC	Figure 36	Dimensionless
Composite IHA	Flow Duration Curve		N/A – will be presented with modeling results in Task 6	Dimensionless
$Q_{Bankfull}$	Flooding	TSC	Figure 35	cfs
Richard-Baker Flashiness index	Quicker routing of storm flows to streams and rivers relative to natural conditions	TSC	Figure 33	Dimensionless
Critical Shear Stress (mobilization of particles)	Streambed Mobility/Stability	TSC	N/A – will be presented with modeling results in Task 6	lb-force/ft^2
Evapotranspiration rate	Ecohydrology	TSC	N/A – will be presented with modeling results in Task 6	mm day^{-1}
Latent heat flux	Ecohydrology	TSC	N/A – will be presented with modeling results in Task 6	MJ m^2 day^1

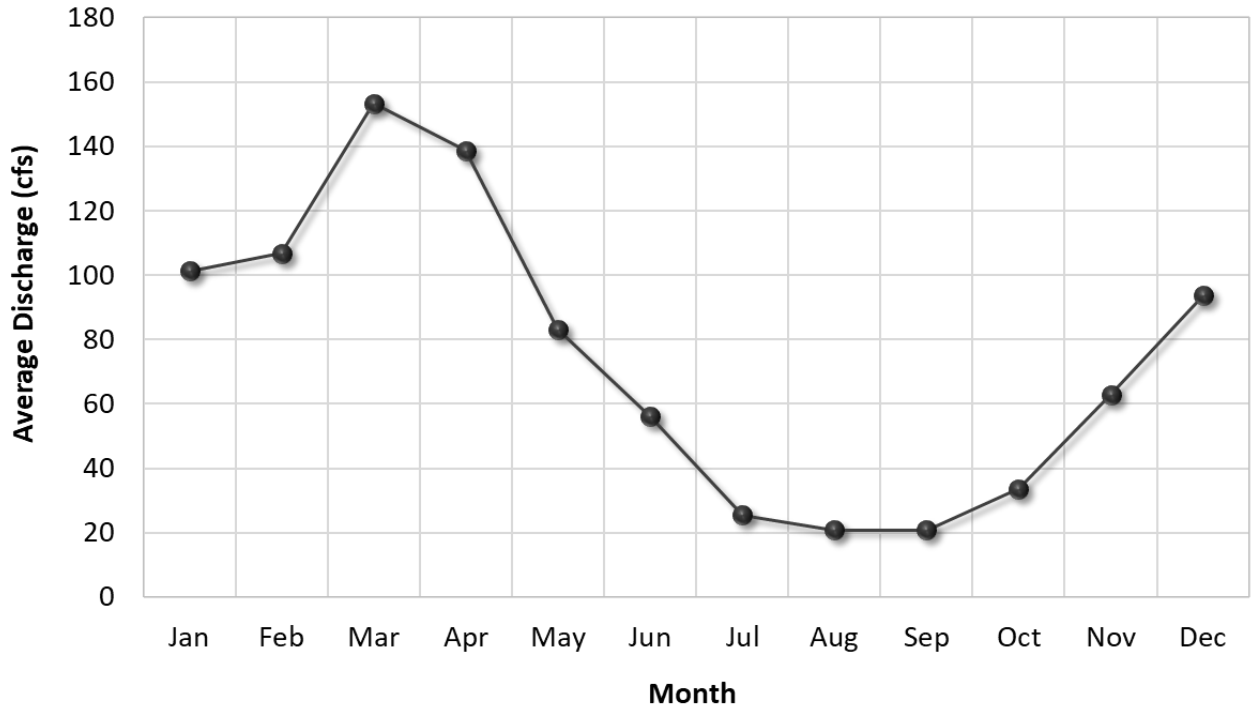

Figure 18. Average monthly flow 1925-2020. Wading River (01109000).

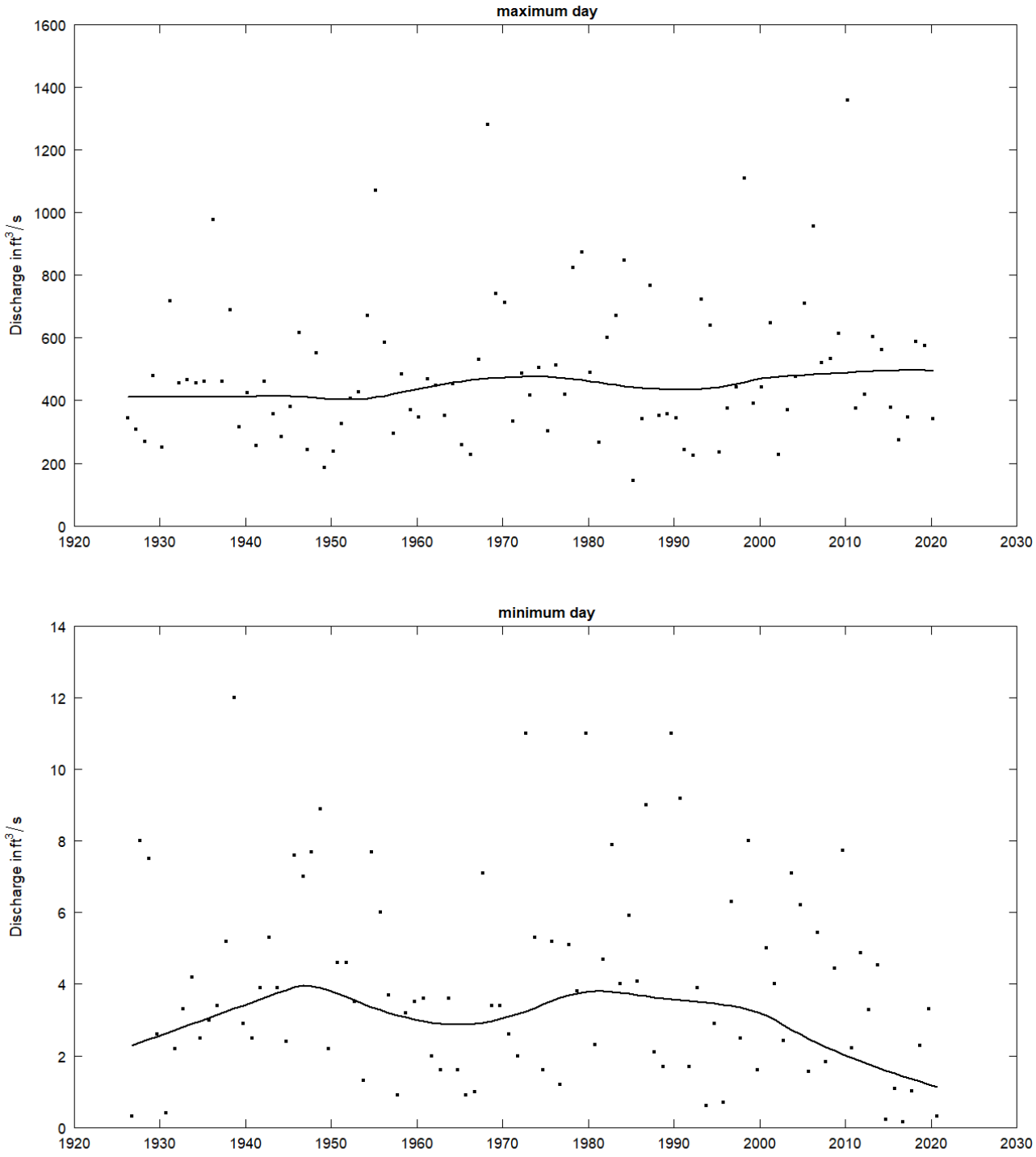

Figure 19. Maximum (top) and minimum (bottom) 1-day mean of daily mean discharges.

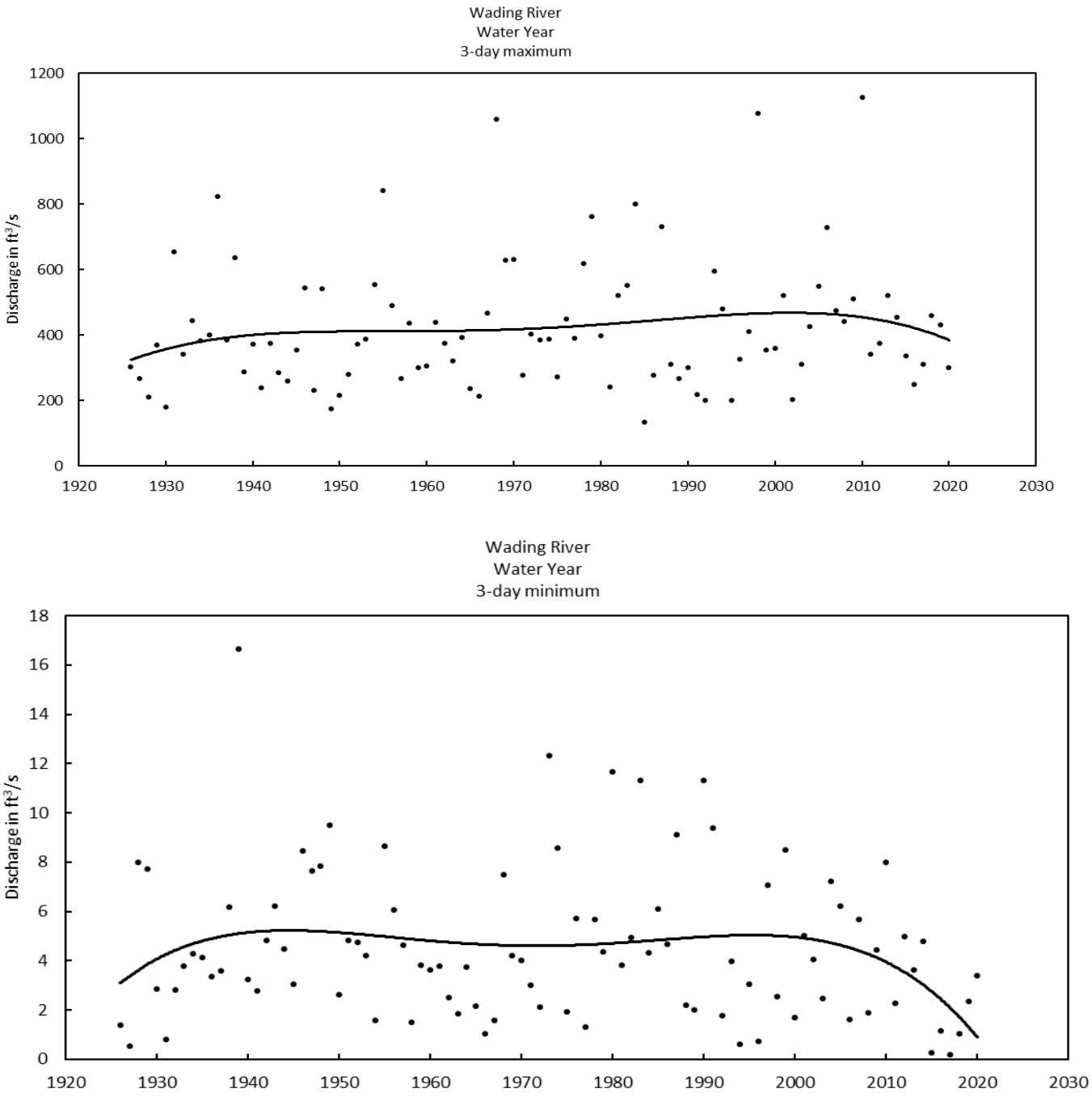

Figure 20. Maximum (top) and minimum (bottom) 3-day mean of daily mean discharges.

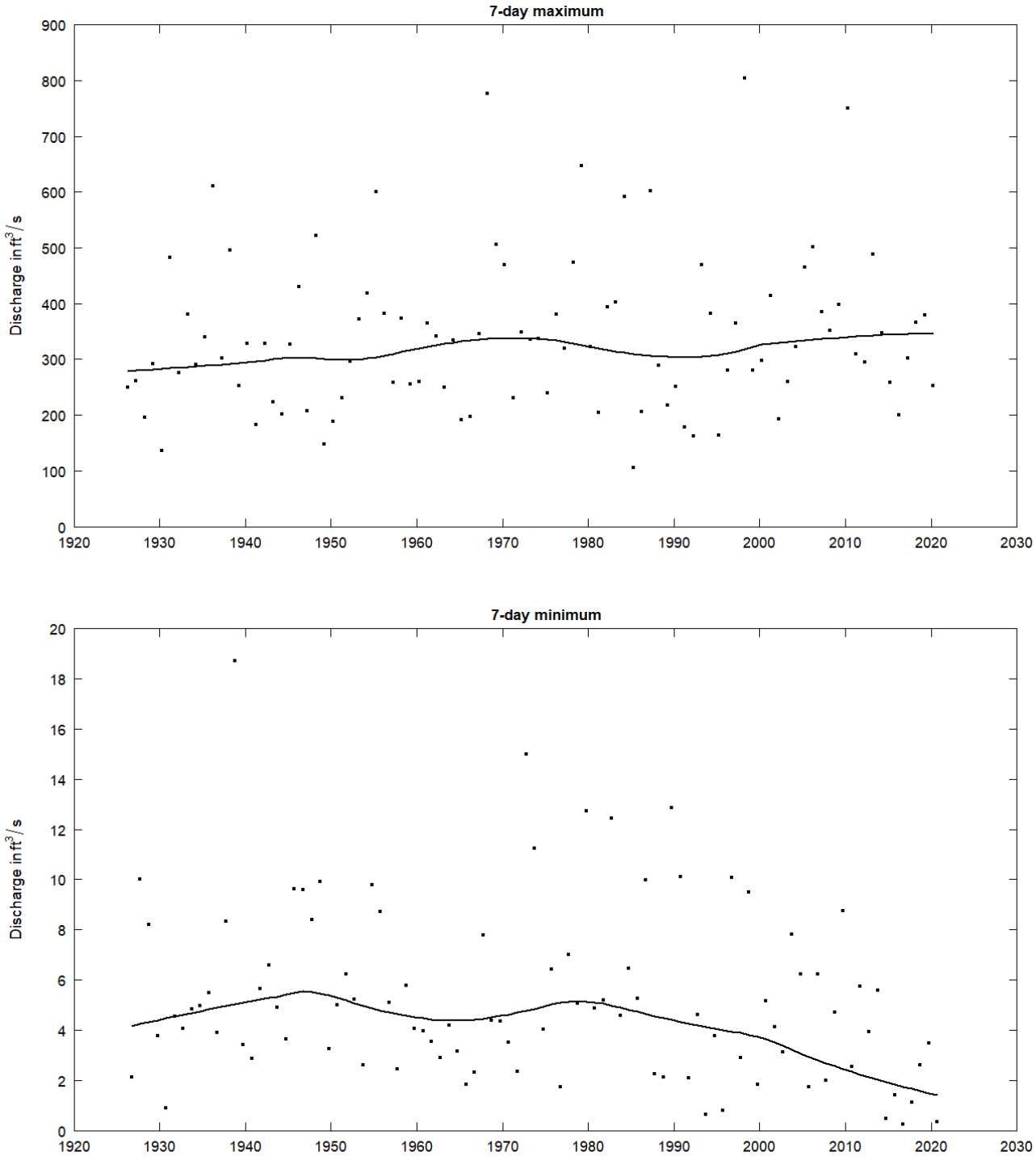

Figure 21. Maximum (top) and minimum (bottom) 7-day mean of daily mean discharges.

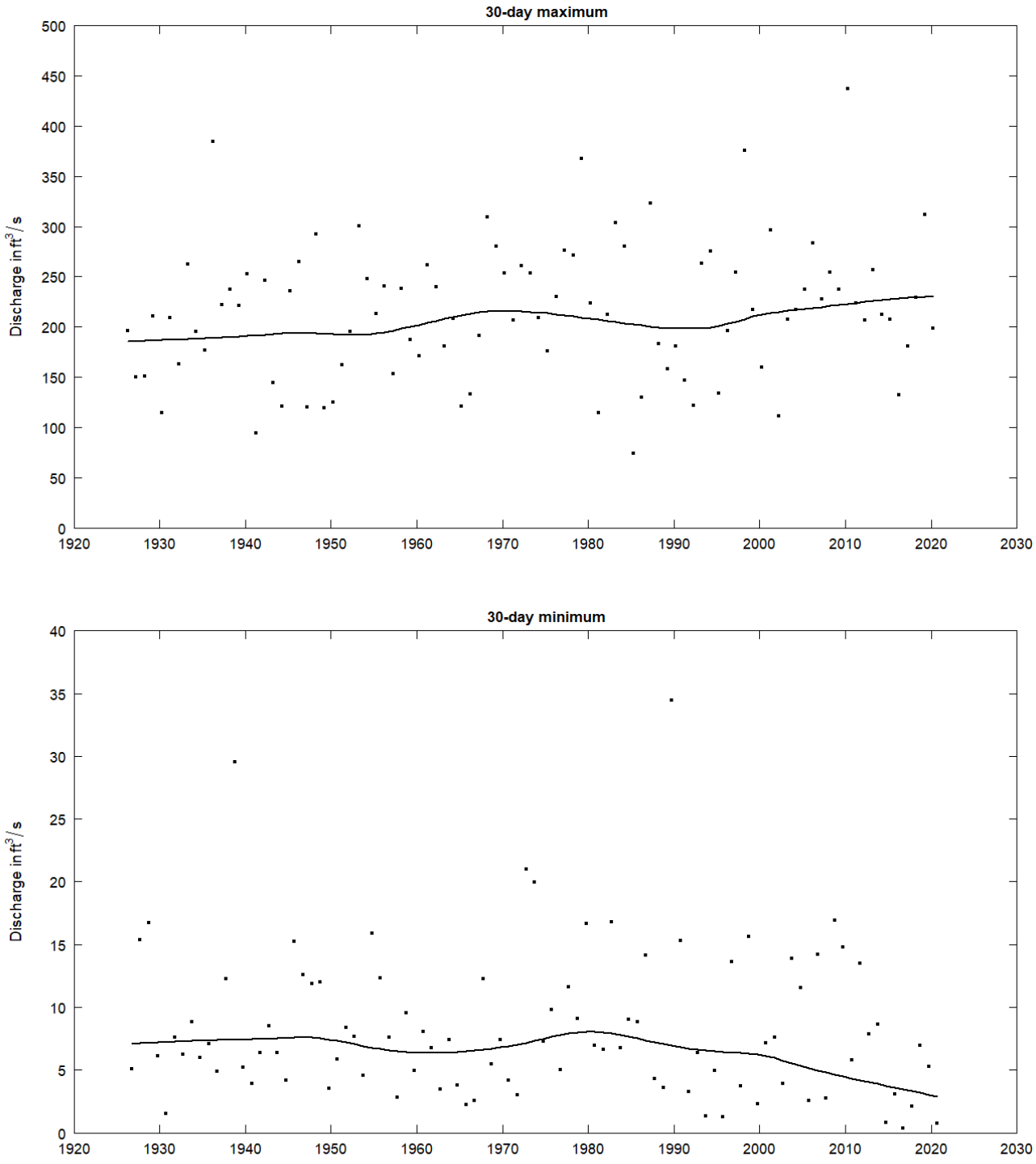

Figure 22. Maximum (top) and minimum (bottom) 30-day mean of daily mean discharges.

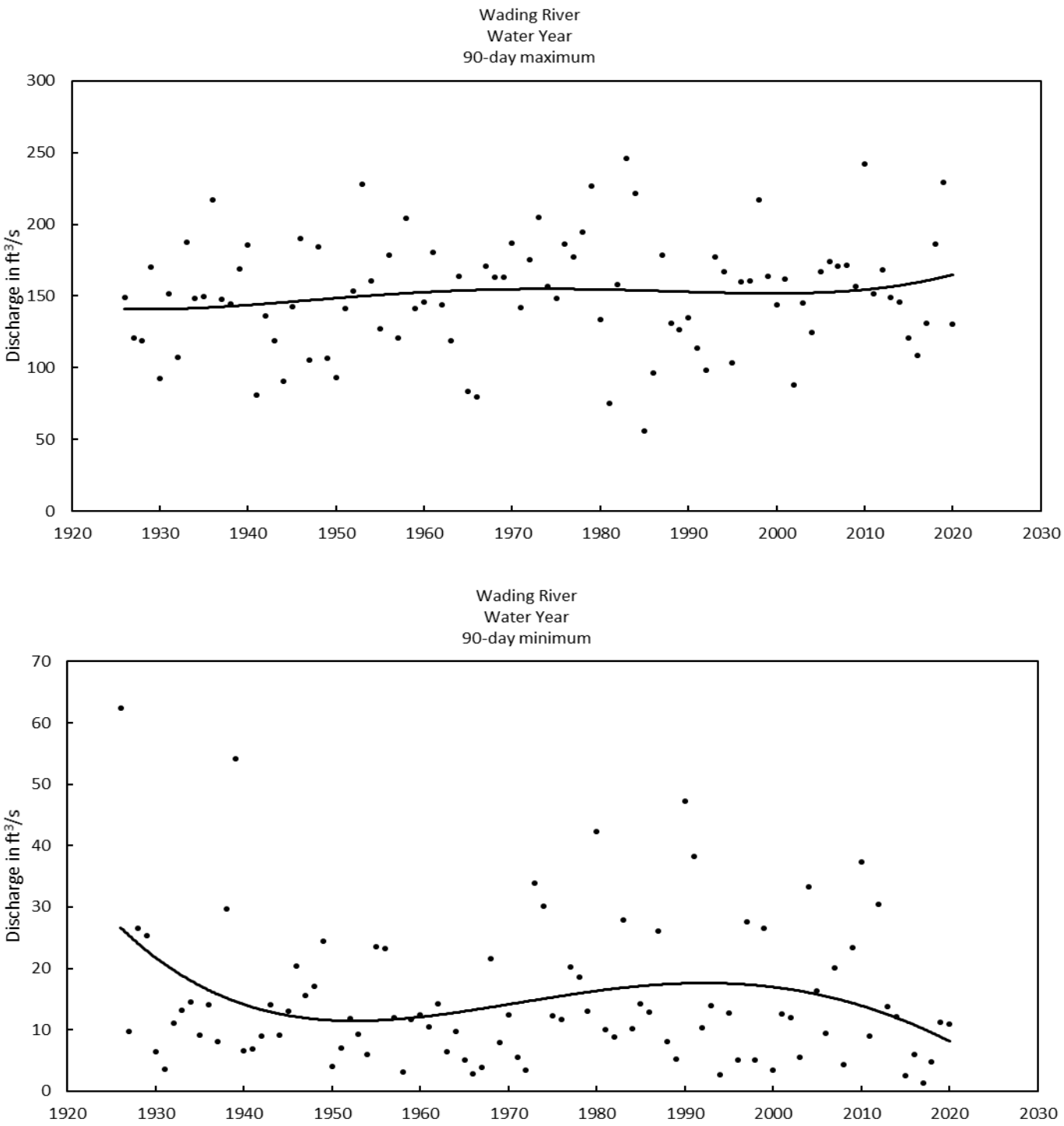

Figure 23. Maximum (top) and minimum (bottom) 90-day mean of daily mean discharges.

Figure 24 presents the minimum 7-day discharge divided by the mean discharge for the respective year. This is a dimensionless baseflow index used to quantify the portion of baseflow to total flows. Figure 24 suggests baseflows are becoming lower in the Wading River. Figure 25 presents Group 3 IHA parameters on the timing of flows. By plotting the Julian day of each year in which the minimum and maximum flows occur, trends may be identified. There does not appear to be any strong trends associated with the dates at which minimum and maximum flows are occurring, suggesting the Wading River is relatively stable with regards to low and high flows shifting their occurrence to earlier or later times in the year. Figure 26 and Figure 27 present the group 4 IHA parameters assessing the frequency and duration of flows. Figure 26 presents the number of high and low pulses for each water year or climate year, respectively. High and low pulses are identified as flows falling into high and low percentiles of the entire record. To help identify whether the choice of percentile impacted the outcome, high and low flows were calculated using the 90^{th} and 10^{th} percentile as well as the 75^{th} and 25^{th} percentile. Overall, there appears to be a considerable amount of variation in the data with no clear trend that low or high flows are occurring more often or for longer periods. However, in Section 5, two distinct periods are compared, resulting in substantial differences in metrics between the two periods.

Figure 28 and Figure 29 present the Group 5 IHA parameters that assess the rate of change and frequency in flows. Figure 28 presents the rise and fall rates over time. These metrics are the mean of all positive and negative differences in daily stream flow, respectively. The metric can assess the flashiness of a system. If a stream or river was becoming flashier over time, it could be expected to see a trend upward and/or downward in the rise and fall rates as differences in daily flow values became greater. Assessment of the changes in rates and frequencies of flows is also facilitated by calculating the number of flow reversals (Figure 29). Flow reversals are counted by summarizing the number of times daily flows change from increasing to decreasing and vice versa.

Additional metrics were included based on feedback from the TSC and the functionality of the EGRET package (Hirsch and De Cicco, 2015). Climate change and increasing imperviousness are often associated with increased variability in hydrologic systems (Jennings and Jarnagin, 2002). Increased flow variability in the Wading River is supported by Figure 30, which presents the standard deviation of the log discharge. Interestingly, there appear to be some systematic oscillations in flow variability throughout the record for the Wading River, and an increasing amount of variability within the last decade.

Figure 31 presents a quantile-Kendall plot. For every year of data, the EGRET package ranks daily discharge values from 1 (the lowest) to 365 (the highest). Each point in the graph represents the estimated trend slope, expressed in percent change per year, for discharge values of the given rank. The x-axis presents daily non-exceedance probability with low flow and their trends on the far left of the graph and high flow and their trends are on the far right. The black and red points indicate that the trend is statistically significant at the given p-value. Figure 31 suggests that many of the lowest flows in the Wading River are becoming significantly ($p < 0.05$-1, $p<0.05$) lower, reducing by between 0.4% to 0.6% a year. Trends were further assessed by season (Figure 32). The trend in lower low flows appears to be a summer phenomenon, which perhaps is unsurprising given it is the period when the lowest flows of the year naturally occur in the region. Additionally, there is a trend during winter flows where high flows are becoming higher. The lowest low flow in winter also appears to be trending higher, although, given the lack of significant trends in other low flows, there is not much to suggest a more general trend.

Figure 33 shows the Richard-Baker Flashiness index (Baker et al., 2004) by water year for the entire period of record and the period 1958-2020. The Wading River appears to have undergone a sustained period whereby the system became less flashy over time and then stabilized. The trend may be a signature of Lake Mirimichi dam's moderating effect on flows. Whereby increased storage in the system resulted in reduced flashiness. It is also possible that the trend is a result of decades of the business-as-usual approach to stormwater management which typically involved the construction of stormwater detention devices whose release of water mitigates peak flows but also results in elevated sustained flows.

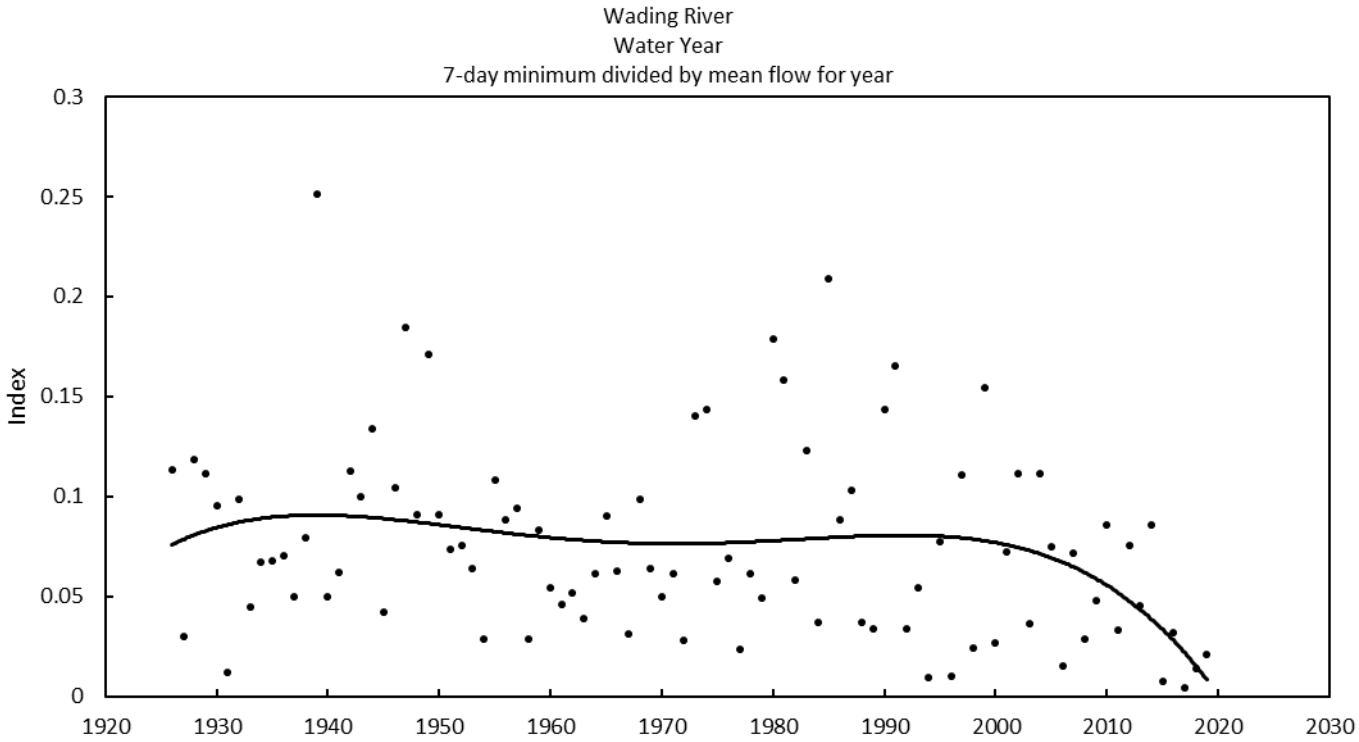

Figure 24. The minimum 7-day mean of daily mean discharges divided by the mean of mean daily discharges for the year.

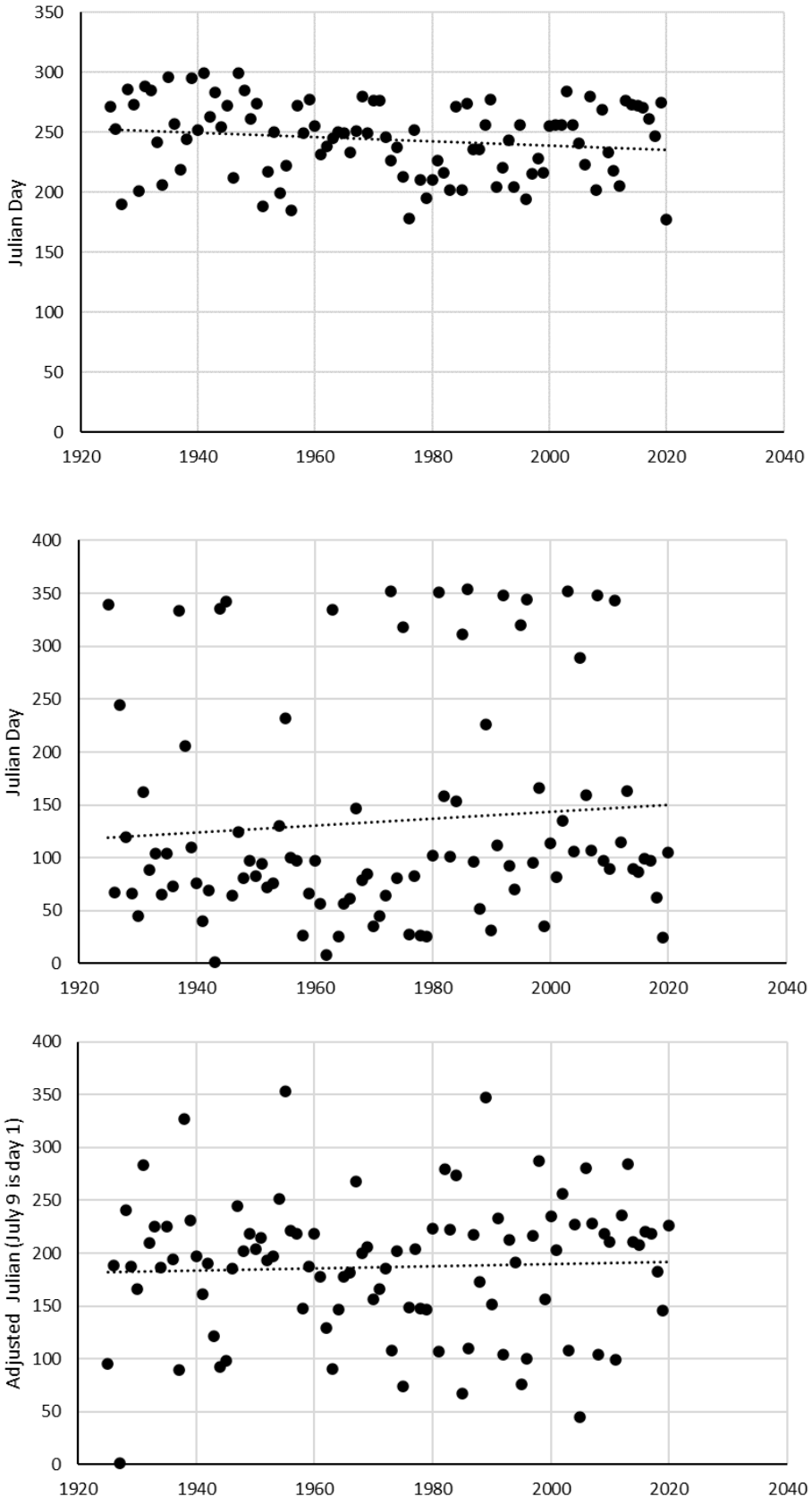

Figure 25. Julian day of minimum (top) and maximum (middle) flows. Maximum flows with an adjusted Julian start date are presented on the bottom graph.

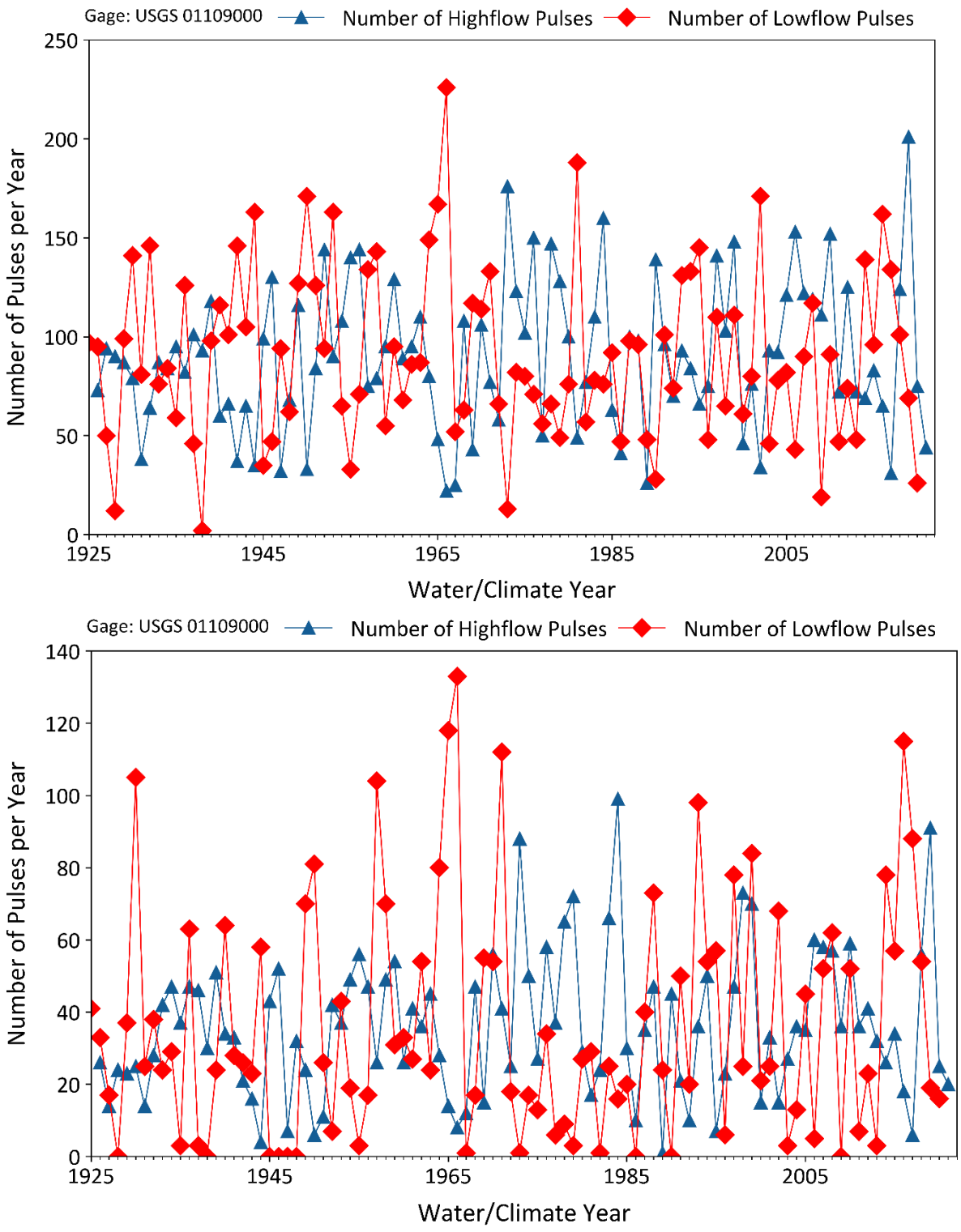

Figure 26. Number of high and low pules. Top graph: 75% (high), 25% (low). Bottom graph: 90% (high), 10% (low).

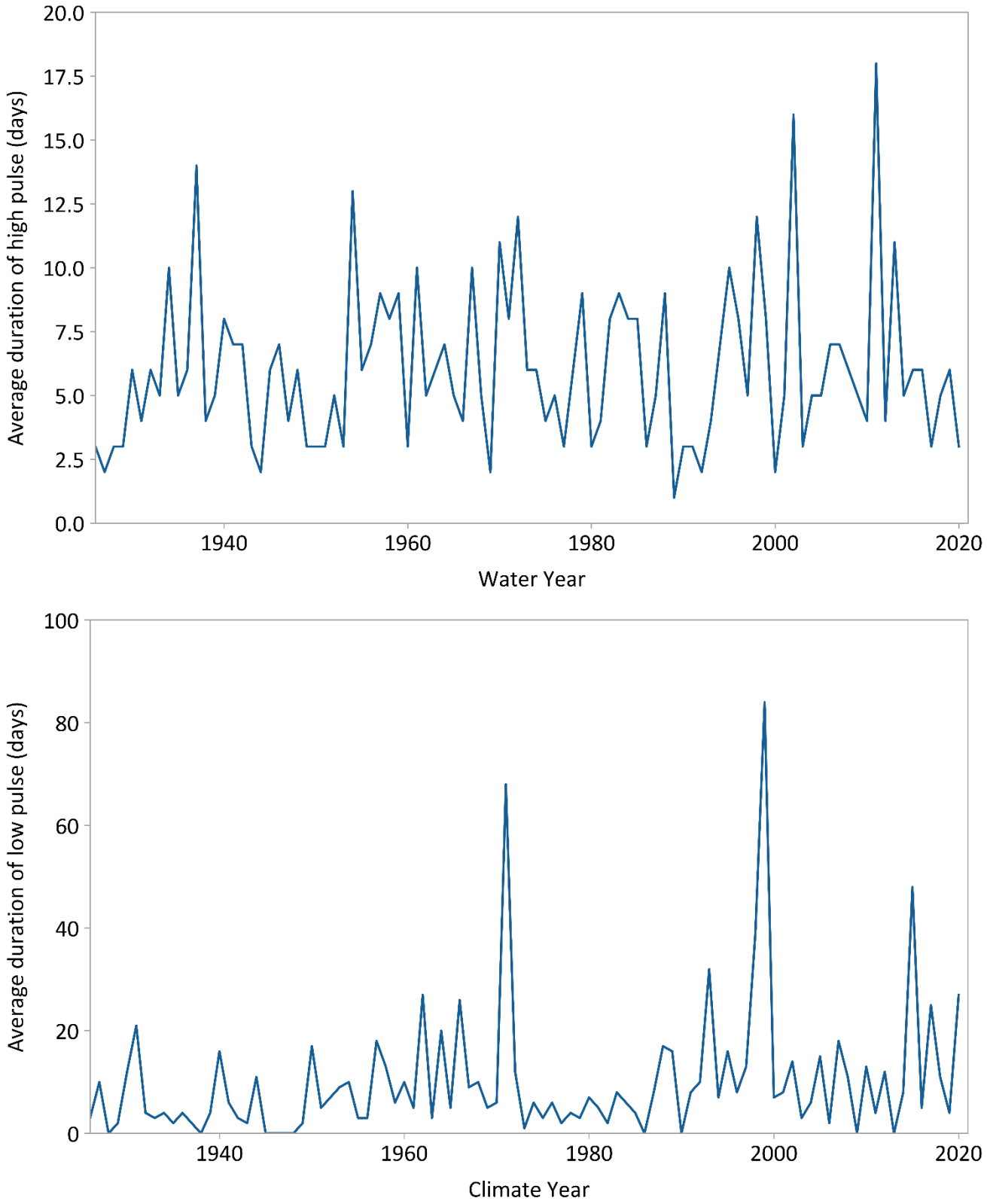

Figure 27. The average duration of high (top) and low (bottom) pulses (90th and 10th percentiles).

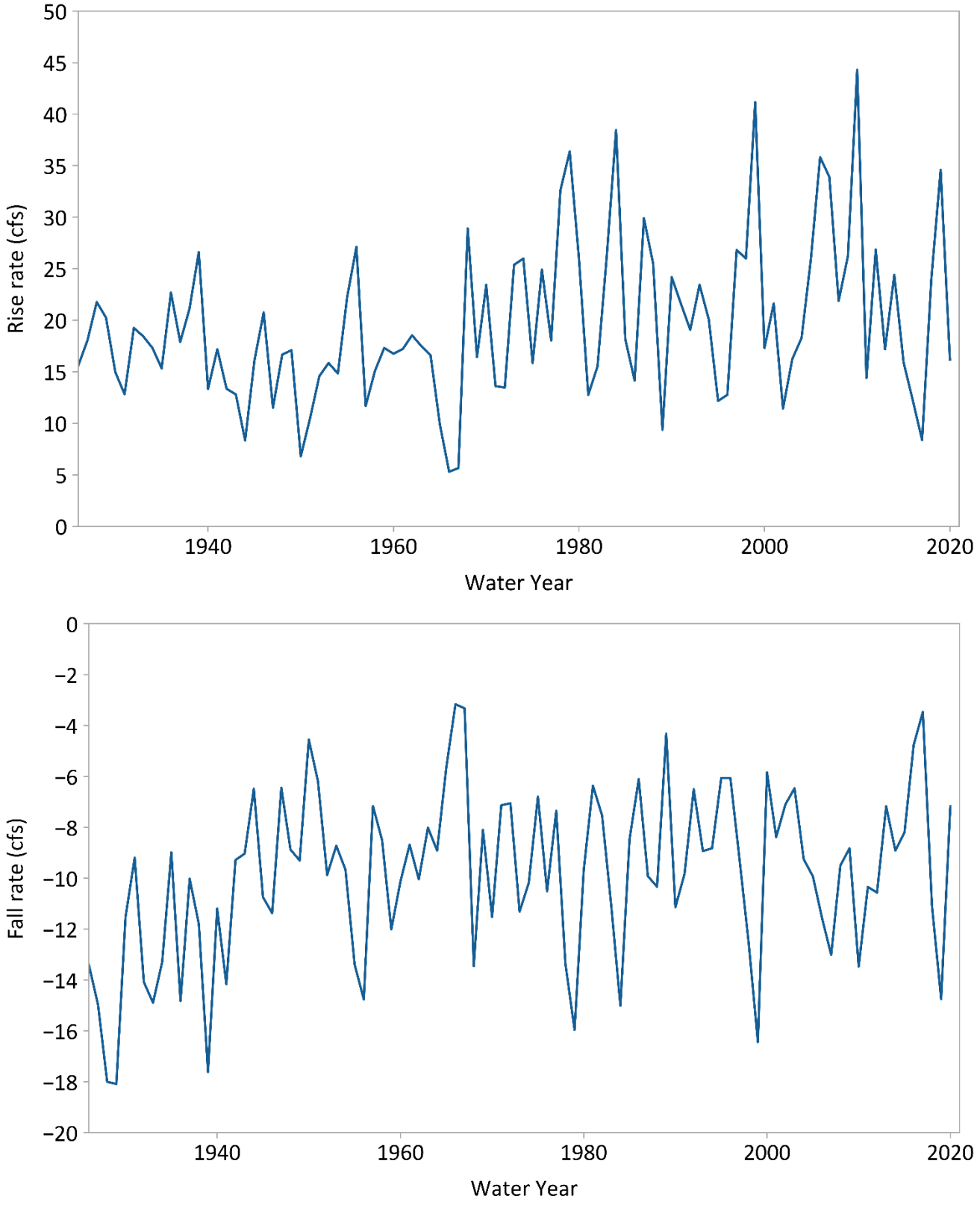

Figure 28. Rise rate (top) and fall rate (bottom).

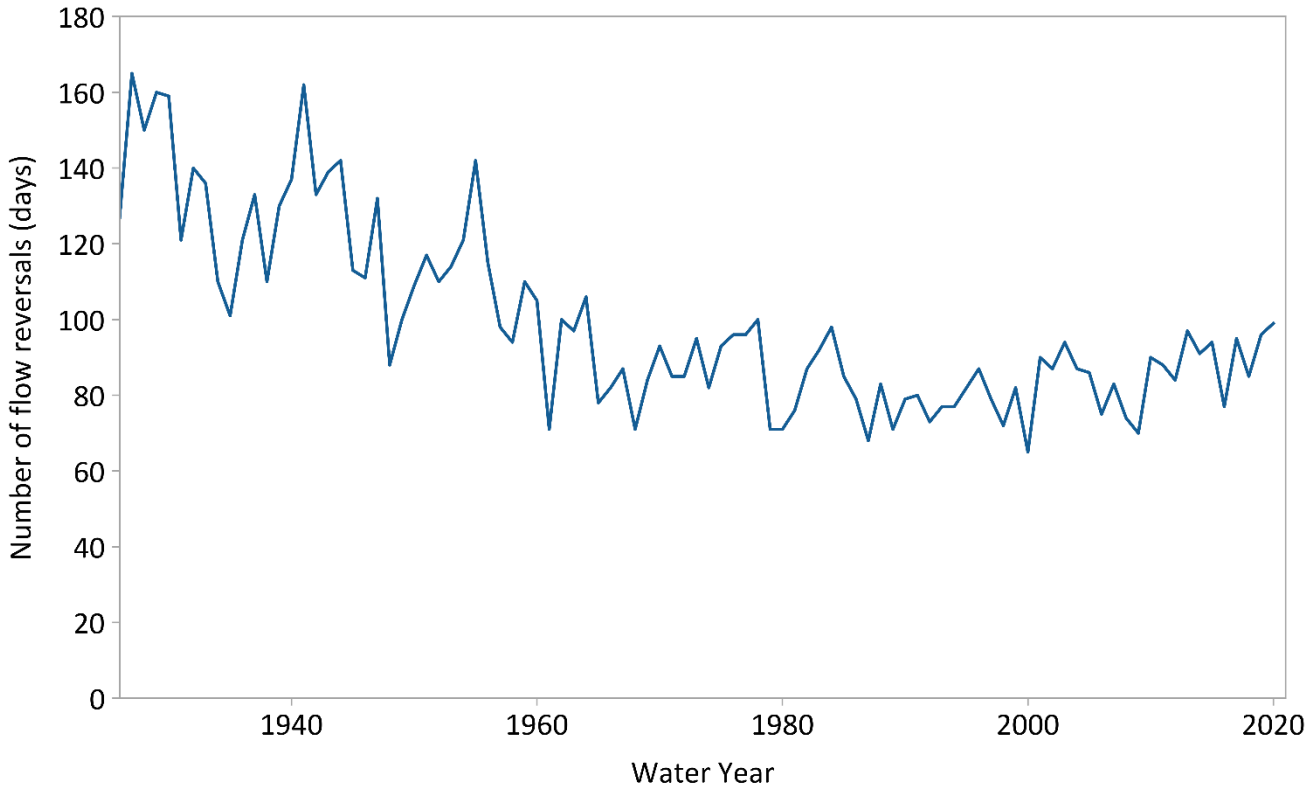

Figure 29. The number of flow reversals.

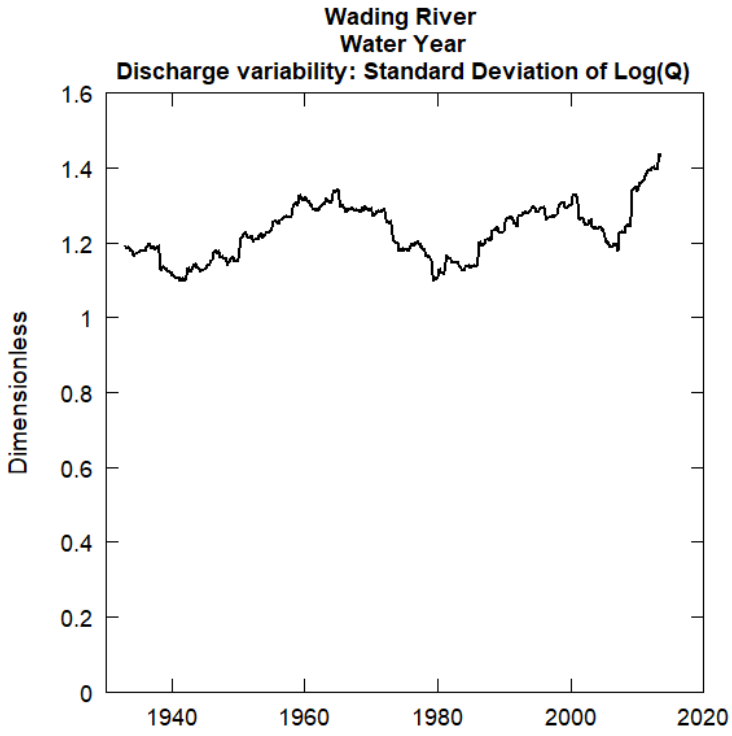

Figure 30. Discharge variability in the Wading River over time.

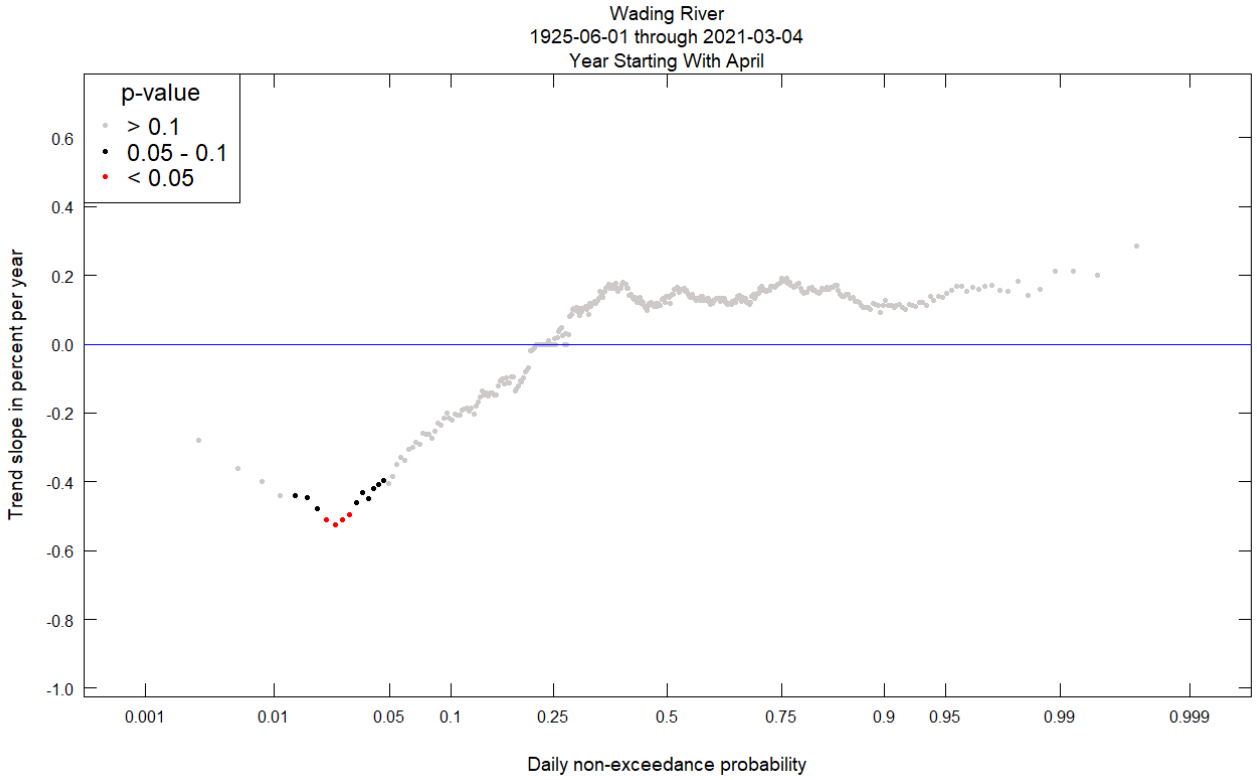

Figure 31. Quantile-Kendall plot 1925-2020.

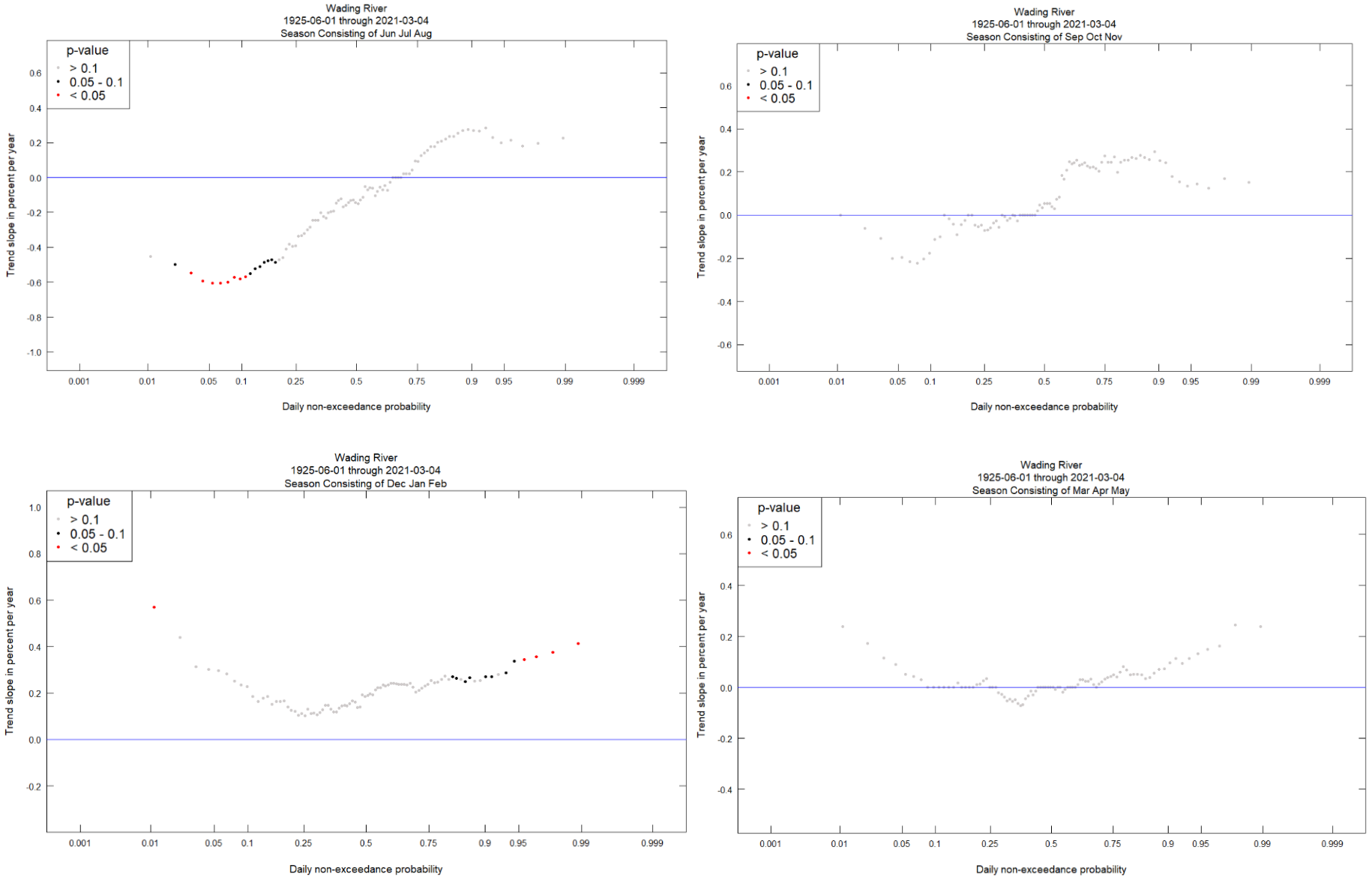

Figure 32. Quantile-Kendall plots 1925-2020 by season. Summer (top left), Fall (top right), Winter (bottom left), Spring (bottom right).

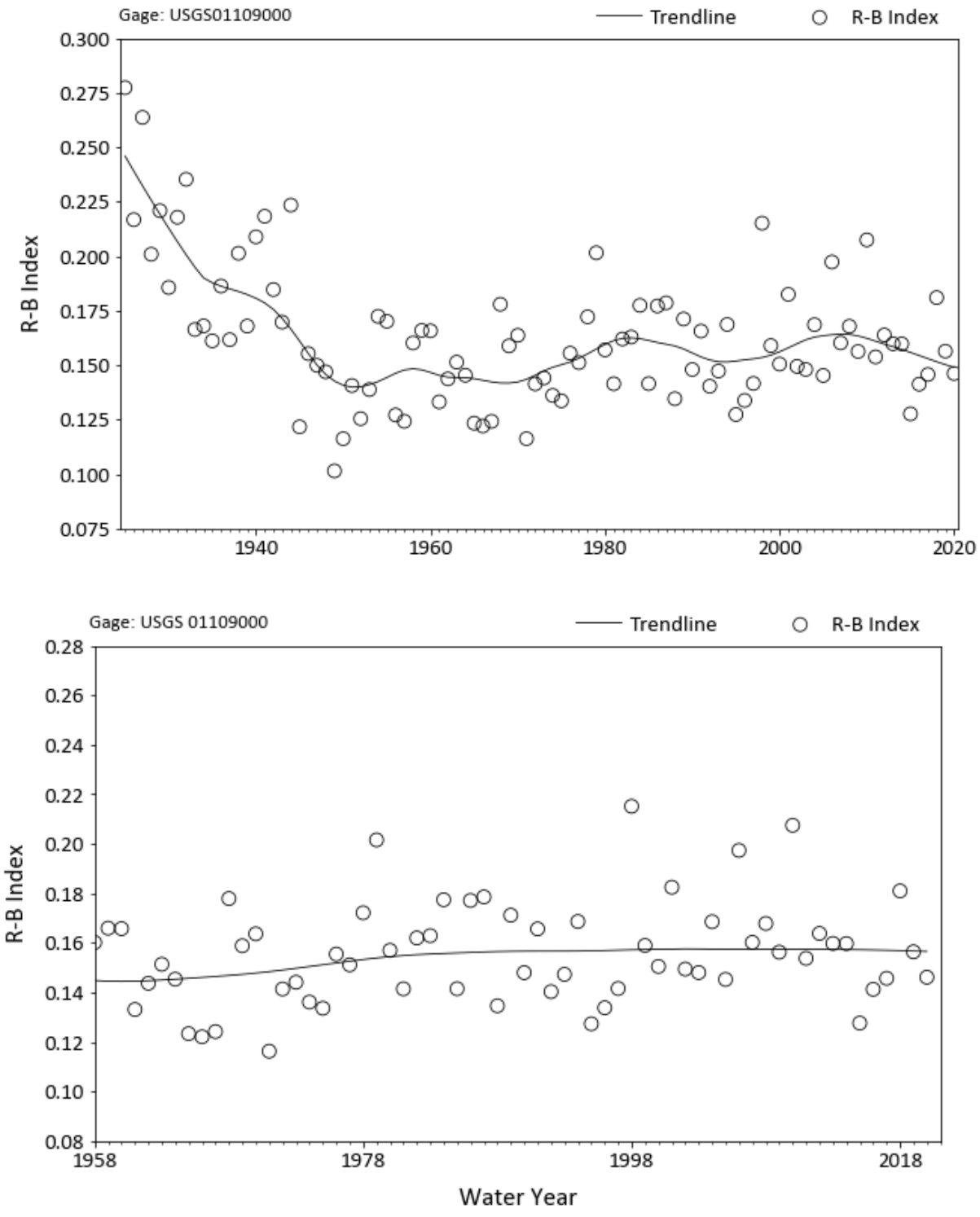

Figure 33. Richard-Baker Flashiness Index (R-B Index) for the Wading River (01109000) by water year based on daily mean discharge for the full period of record (top) and post-1958 (bottom). Trendlines created using the LOWESS function.

Figure 34 presents a time series of runoff coefficients approximated by dividing the total precipitation depth by the total discharge depth ($\frac{discharge\ (ft^3)}{drainage\ area\ (ft^2)}$). The higher the coefficient, the more rainfall was converted to runoff. Overall, there does not appear to be a strong trend in runoff coefficients. Figure 35 presents bankfull frequency in the number of days and number of occurrences. If a bankfull flow was measured for two days in a row, it was counted as two days but only as a single occurrence. It appears that the number of bankfull days has increased in the last few decades. However, bankfull flows can be a problematic metric to assess. Stream channels are dynamic and evolving, especially those changing due to anthropomorphic disturbances such as increased flows from impervious surfaces. A stream may become incised due to an imbalance between stream power and sediment load. Bankfull and larger flows that once accessed the floodplain, may become contained within a stream that is becoming increasingly incised. No robust assessment of Wading River fluvial geomorphology was available to further investigate channel changes over time. Figure 36 presents an assessment of ecosurplus and ecodeficit. Ecosurpluses and ecodeficits are calculated from flow duration curves, providing a simplified assessment of hydrological impacts compared to IHA parameters. An ecosurplus and an ecodeficit represent the overall gain or loss, respectively, in stream flow of the period of analysis (Vogel et al., 2007). Figure 36 compares FDCs for the 2001-2019 period against the long-term historical average period (1925-2019). Figure 36, like the previous figures in this section, uses only observed data to provide an example of the graphical representation that may be used to compare model scenarios in upcoming project tasks and how this information may be conveyed to stakeholders.

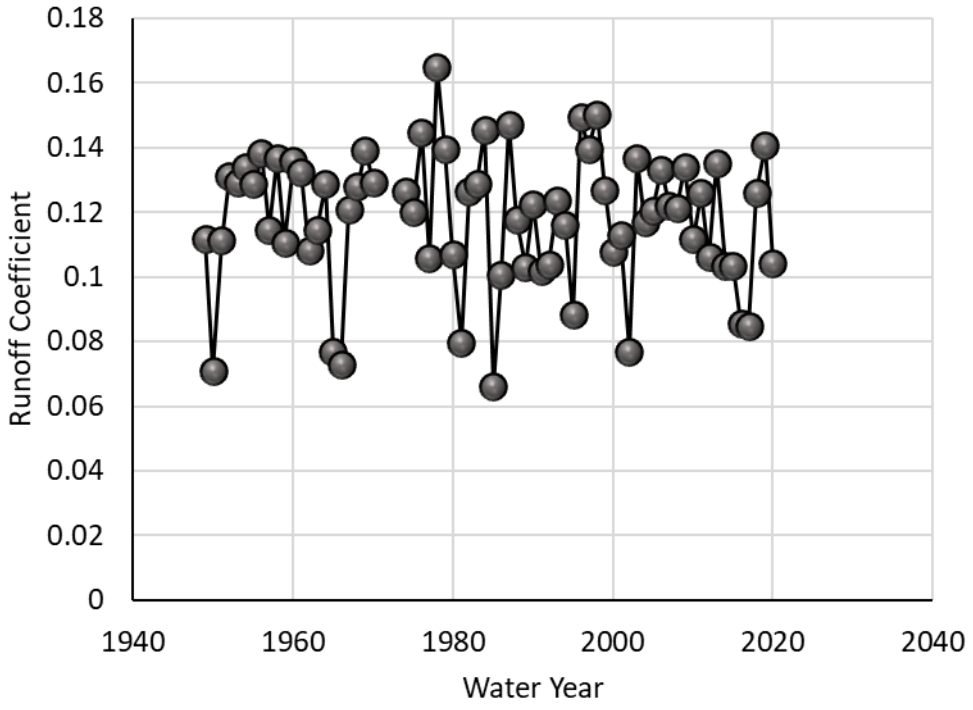

Figure 34. Runoff coefficient by water-year.

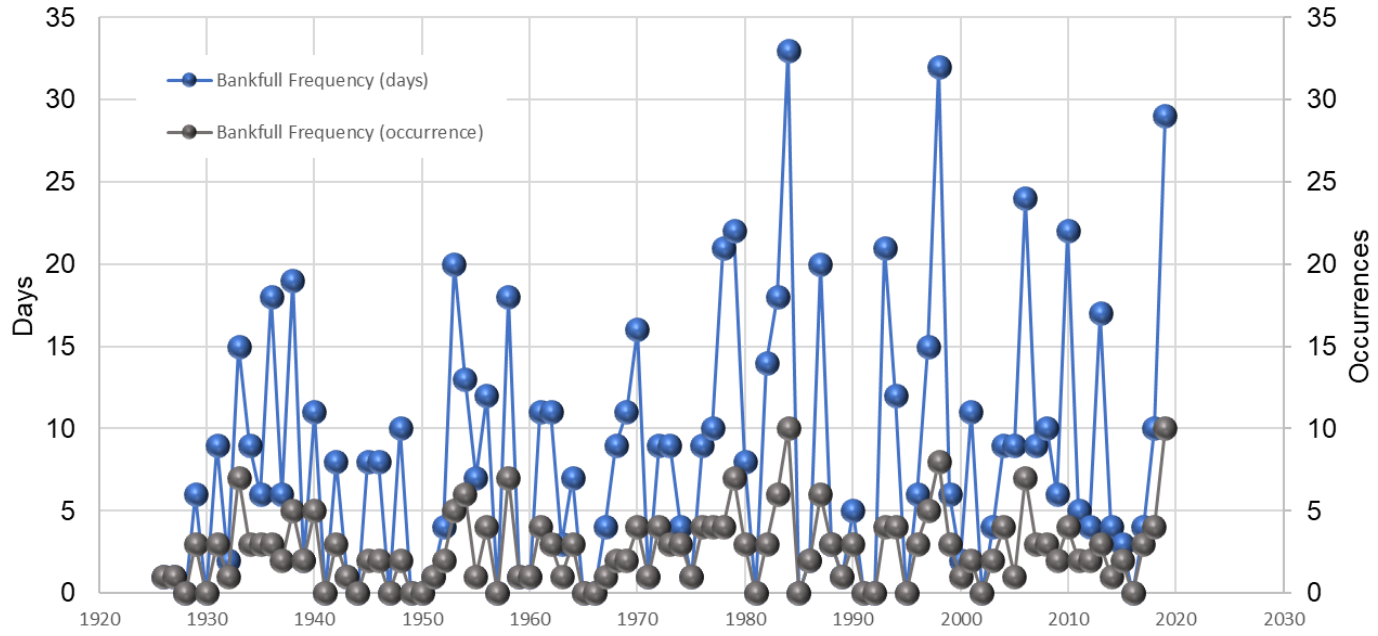

Figure 35. Bankfull frequency by occurrence and total days >= bankfull. Based on a bankfull flow of 295 ft³/s (Bent and Waite, 2013).

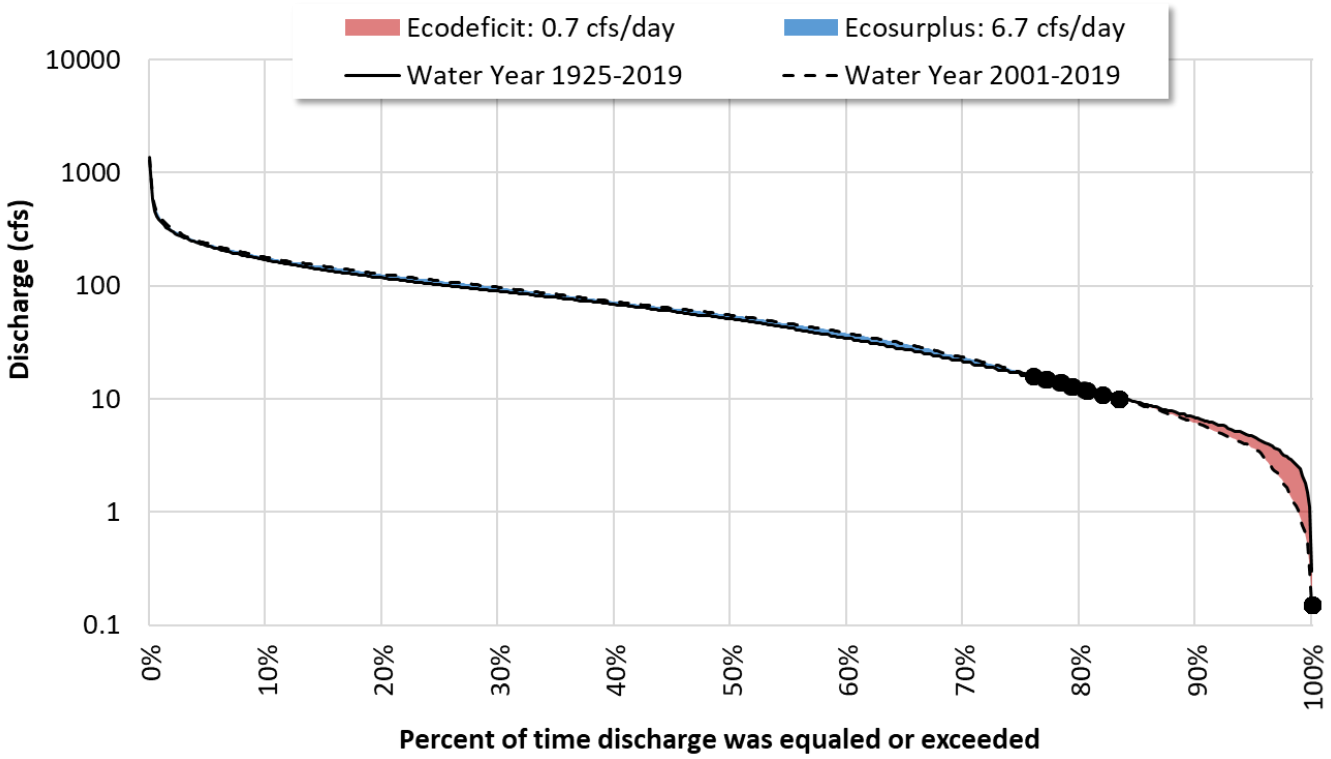

Figure 36. Ecosurplus and ecodeficit for the Wading River for 2001-2019 vs. long-term historical average. Black dots represent inflection points where the two curves change between surplus and a deficit.

2.2 Literature Review and Additional Resources

2.2.1 *HSPF and HEC-RAS Models*

The FDC 1 Project builds upon previous modeling work performed in the Taunton basin (Barbaro and Sorenson, 2013). The previously developed HSPF model subbasins for the Wading River are presented in Figure 37. Additional details for these areas are presented in Table 11. The existing HSPF model accounted for surface and groundwater withdrawals as well as, wastewater return flows, however, these were calculated only for select sub-watersheds and did not include the Wading River. The model accounted for streamflow depletion by groundwater withdrawals using the STRMDEPL program (Barlow, 2000). The program produces a daily time series of total streamflow depletion based on the reported withdrawal record. For wells near a stream and under long-term, steady-state conditions, the total volume of streamflow depletion is very close to the total volume pumped from the well. Withdrawals were taken directly from the stream reaches in the HSPF model and daily values were disaggregated to hourly to match the simulation timestep.

A HEC-RAS model was also developed for the Wading River watershed (Figure 39). Figure 40 presents a cross-section view near the Wading River USGS gage. As of the time of this writing, HEC-RAS models for tributaries to the Wading River, including Hodges Brook, appear to have been developed but are not publicly available. Hodges Brook has been identified as a location for three pilot sub-watersheds (Section 2.3). HEC-RAS models can help facilitate analysis of changes to flooding, stream power, and sheer stress that may result from changes to impervious and next-generation stormwater approaches.

2.2.2 *Evapotranspiration and Carbon Sequestration*

Changes to land use and land cover can affect energy portioning between latent and sensible heat flux. Latent heat is exchanged due to phase changes of water but does not result in a temperature change. Evaporation or condensation are examples of latent heat exchange. Sensible heat is exchanged due to conduction and convection and directly affects the temperature of the atmosphere, such as a warm parking lot radiating heat into a cool night. The ET rate (mm day^{-1}) can be converted to latent heat flux (MJ m^{-2} day^{-1}) using a conversion factor of 2.45 and an assumed temperature of 20°C. Actual ET has been found to have a strong relationship with primary productivity, and therefore carbon sequestration (Lieth and Box, 1972), although the relationship can be impacted by several factors, including water availability, vegetation type, and soil C:N ratio.

Marasco et al (2014) quantified the ET associated with green roofs in urban climates. Evapotranspiration plays an important role in stormwater runoff attenuation and mitigating the urban heat island effect and understanding the benefits and limitations of different prediction methods can help facilitate management strategies. The authors suggest that green roof ET may be better estimated by Penman-based evapotranspiration equations than energy balance methods. However, given large uncertainty in terrestrial ET, modeling approaches are generally limited in their capabilities to investigate how changes in precipitation and land cover may affect ET (Wang and Dickinson, 2012).

Brill et al. (2021) present several approaches for estimating the carbon-related benefits of nature-based solutions. The Nature Capital Project Integrated Valuation of Ecosystem Service and Tradeoffs (InVest) use a relatively simple biomass and soil carbon model to calculated net annual carbon balance following a change in land use/land cover type. The approach uses global datasets for LULC, soil carbon, and other parameters. For each land use – land cover (LULC) type, the model has four fundamental pools of carbon: Above ground biomass, below-ground biomass, soil organic matter, and dead organic matter. The model requires an estimate of the amount of carbon for at least one of these pools. The model then simply calculates the differences between two LULC raster layers, such as a current condition and a future growth map. Table 12 presents an example dataset of carbon pools for various land uses.

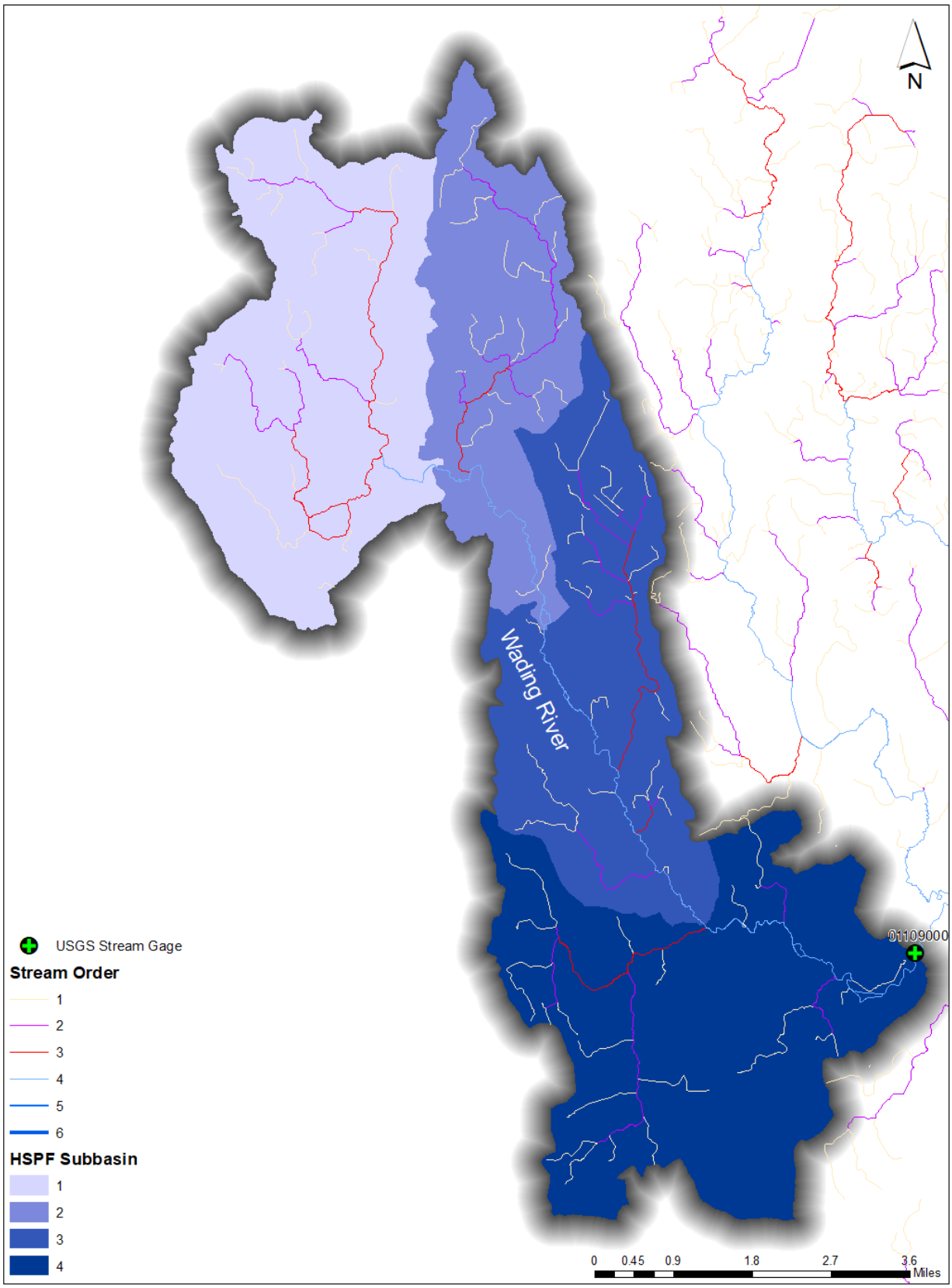

Figure 37. HSPF subbasins for the Wading River.

Table 11. Subbasin and reach representation in HSPF for the Wading River watershed (Barbaro and Sorenson, 2013)

Subbasin/ Reach Number	HSPF subbasin description	Description of reach	Direct drainage area (acres)	Total drainage area (acres)	Upstream reach numbers	Method used to develop FTABLE	Wetlands simulated as virtual reach
1	Wading River headwaters above Lake Mirimichi outlet	Wading River headwaters above Lake Mirimichi outlet	7,732	7,732	--	S	no
2	Wading River above stream gage at West Mansfield (01108500)	Wading River above stream gage at West Mansfield (01108500)	4,727	12,459	1	S	no
3	Wading River above stream gage at Charley (01108700)	Wading River above stream gage at Chartley (01108700)	6,257	18,716	2	S	no
4	Wading River above stream gage near Norton (01109000)	Wading River above stream gage near Norton (01109000)	8,883	27,598	3	S	yes

S: reach was simulated as a stream and an open-channel flow equation was used to compute flow from the reach. No reaches in the Wading River watershed were simulated as reservoirs.

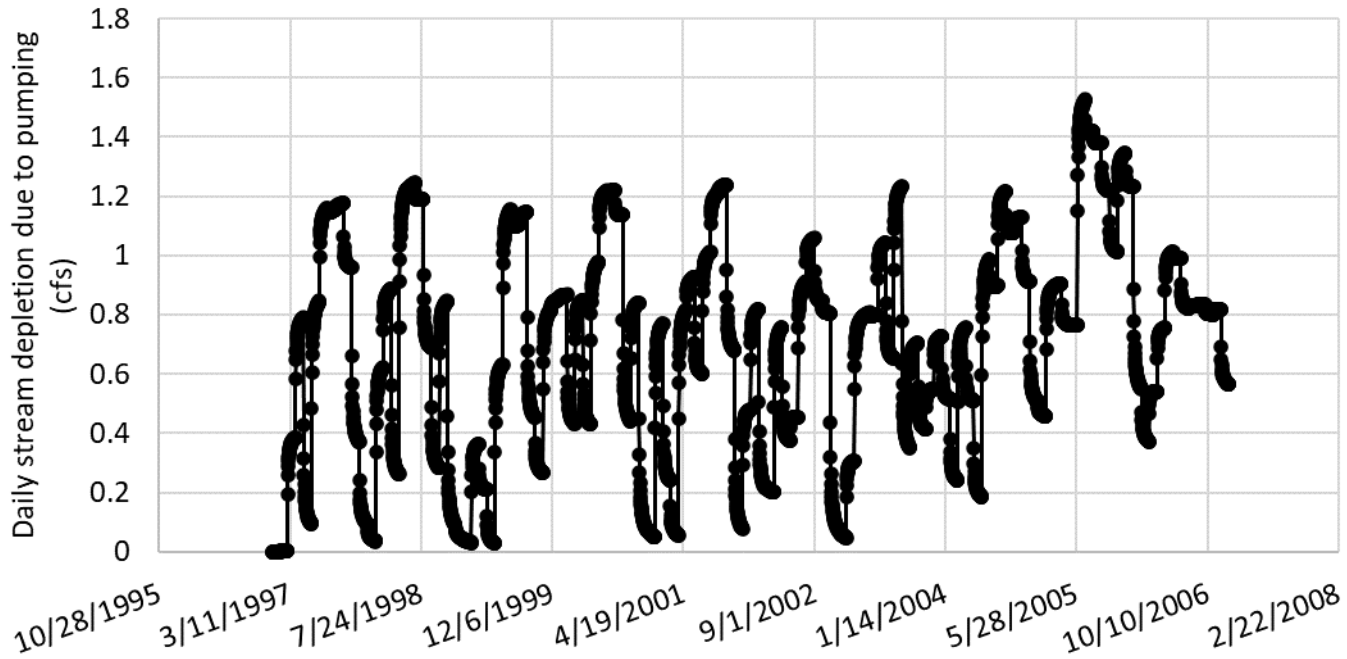

Figure 38. Example STRMDPL time series from the Taunton HSPF model (Barbaro and Sorenson, 2013) for stream depletion due to groundwater pumping.

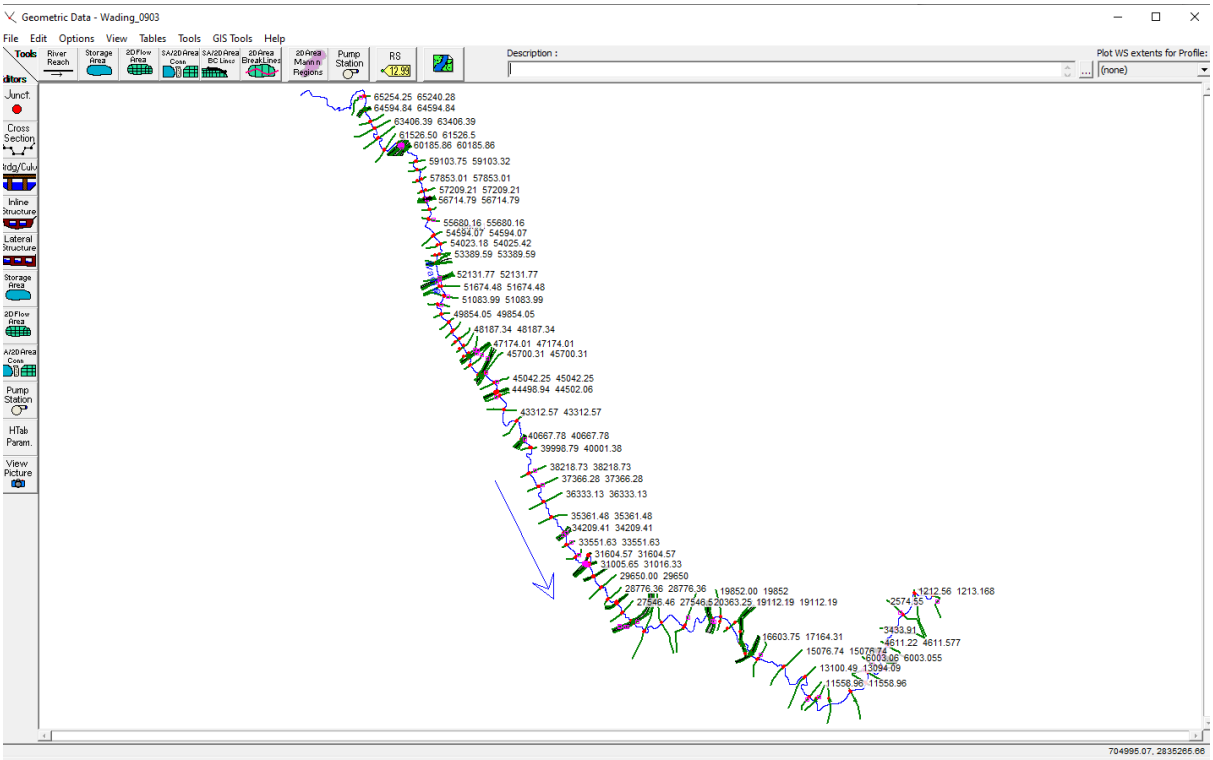

Figure 39. HEC-RAS stream and cross-sections for the Wading River.

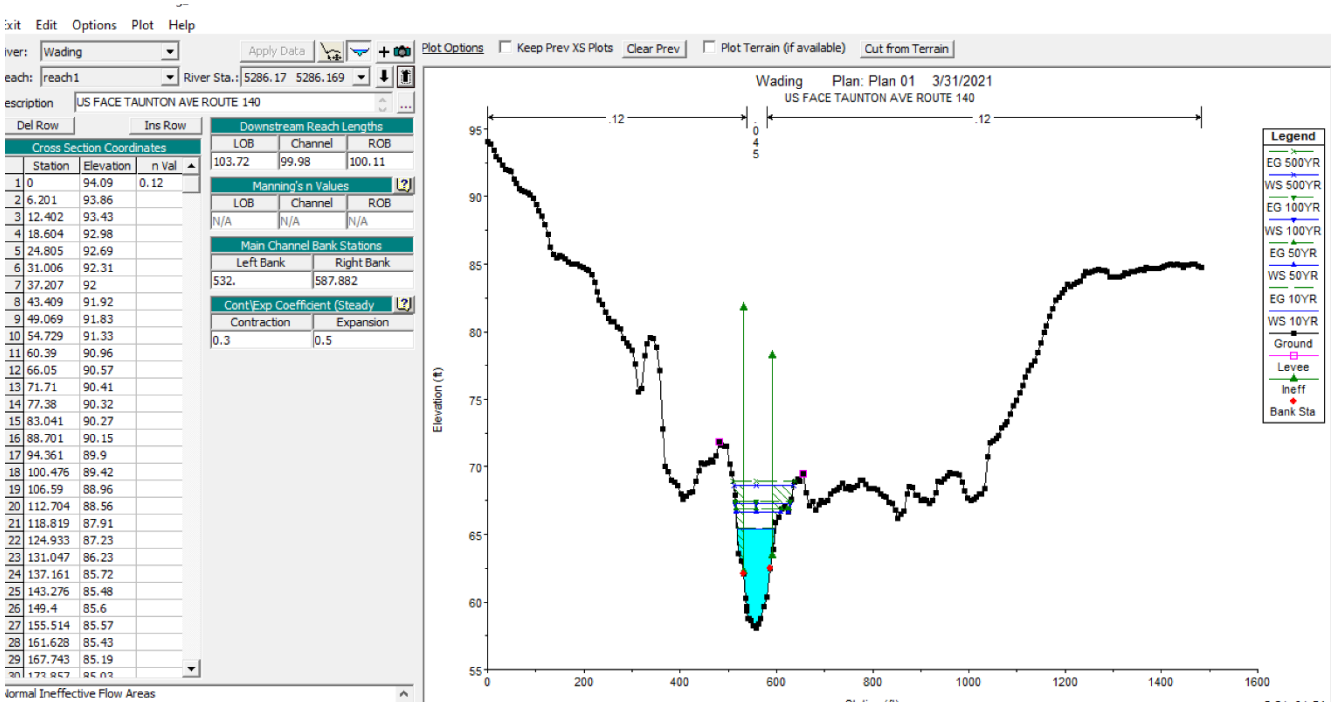

Figure 40. HEC-RAS cross-section view of the Wading River near USGS gage 01109000.

Table 12. Example dataset for calculating carbon balances based on changes in land use/land cover (Source: Natural Capital Project, 2021)

	Carbon (megagrams/ha)			
LULC_Name	above ground	Below ground	Soil organic matter	dead organic matter
Residential 0-4 units/acre	15	10	60	1
Residential 4-9 units/acre	5	3	20	0
Residential 9-16 units/acre	2	1	5	0
Residential >16 units/acre	0	0	0	0
Vacant	10	20	10	5
Commercial	0	0	0	0
Commercial/Industrial	0	0	0	0
Industrial	0	0	0	0
Industrial & Commercial	0	0	0	0
Residential & Commercial	0	0	0	0
Upland Forest open	75	45	85	20

Generally, the lifecycle of most green stormwater infrastructure may result in more carbon emissions than that which is sequestered by the devices (Kavehei et al., 2018; Moore and Hunt, 2013). Kavehei (2018) conducted a systematic literature review and found that rain gardens provide the highest carbon sequestration potential for offsetting their carbon footprint. Carbon sequestration of bioretention basins, green roofs, vegetated swales, and stormwater ponds can mitigate approximately 70%, 68%, 45%, and 8% of their carbon footprint respectively. Alternatively, Moore and Hunt (2013) reviewed the carbon footprint of several stormwater control measures (SCMs) including green roofs, permeable pavement, sand filters, bioretention cells, constructed stormwater wetlands, level spreader-grassed filter strips, grassed swales wet ponds, and rainwater harvesting. The authors found that even after accounting for sequestration by vegetation in these systems, only stormwater wetlands and grassed swales were predicted to store more carbon that was released through their construction and maintenance.

2.2.3 *The Massachusetts Sustainable-Yield Estimator*

The Massachusetts Sustainable-Yield Estimator (MA SYE) is a statewide, interactive decision-support tool to help resource managers better understand and quantify the potential, unregulated flows in a stream and the flows that result from competing for water resource demands (Archfield et al., 2009). Figure 41 presents a comparison of flow duration curves derived from observed flows and Wading River and MA SYE estimates of unaltered conditions. The Wading River gage (01109000) was used as a reference gage for the MA SYE for which estimates at other, ungage streams are based on. Importantly, the estimated unaltered flows from MA SYE do not account for the effects of climate change, septic-system discharge, impervious area, non-public water supply withdrawals less than 100,000 gallons per day, and impounded surface-water bodies.

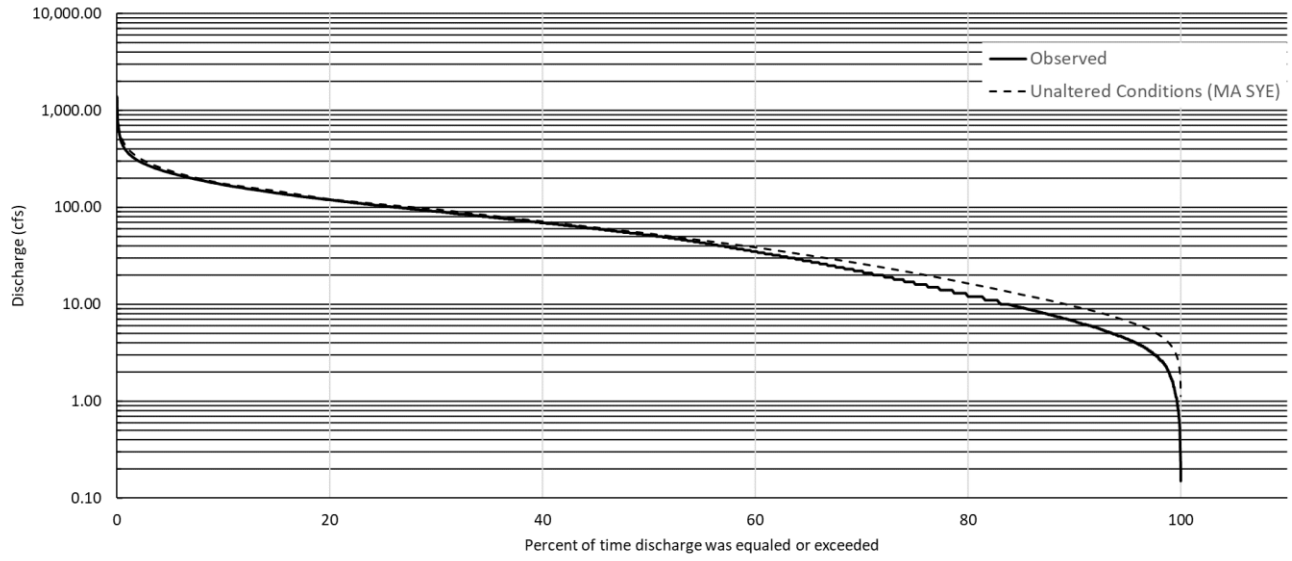

Figure 41. Observed flow duration curve for Wading River for the period of record and the estimated unaltered condition flow duration curve generated from the Massachusetts Sustainable-Yield Estimator.

2.2.4 *The Watershed Management Optimization Support Tool (WMOST)*

The EPA's Watershed Management Optimization Support Tool (WMOST) is a spreadsheet-based decision support tool that facilitates integrated water management at the local or small watershed scale. WMOST estimates a potential reduction in runoff and pollutant loads from best management practices and uses the Network-Enabled Optimization System (NEOS) online service to perform optimization. WMOST has been applied to the Wading-Three Mile River Watershed to assess future growth and climate scenarios (Detenbeck and Weaver, 2018). The authors used four combinations of changes in temperature and precipitation to roughly bound the extremes of temperature and precipitation changes reflected in the collection of general circulation models (GCMs). Hourly temperature and precipitation time series representing future climate scenarios were generated by uniformly adjusting historical (observed/baseline) temperature and precipitation time series by the corresponding changes from the scenarios. Temperatures were adjusted based on absolute value and precipitation was adjusted based on percentage. Therefore, if the overall temperature was predicted to increase 2 degrees and precipitation was expected to increase 10%, every hourly record of temperature and precipitation was adjusted by those values, respectively.

2.3 Candidate Sub-watersheds Identification and Prioritization

Wading River watershed (HUC12-010900040302) is 43.3 mi^2, contains 1st through 4th order streams, and is in the Taunton basin. The Wading River is 13.9 miles long and is a tributary to the Three Mile River. The watershed includes Chartley Brook, Meadow Brook, Henkes Brook, Hodges Brook, Cocasset River, Mirimichi Lake, and Turnpike Lake. The outlet of the watershed has long-term, continuous monitoring data from USGS gage 01109000. The Wading River watershed was selected to configure and calibrate the LSPC model because of long-term flow data available at the mouth of the river.

Three sub-watersheds were selected from the Wading River watershed for which future modeling tasks, including baseline and management scenario simulations, will be performed (Figure 42). The three sub-watersheds, Pilot Tributary, Lower Hodges Brook, and Upper Hodges Brook have second and third-order streams at their outlets. Pilot Tributary does not represent an actual stream name, it is an unnamed brook. Pilot Tributary, Lower Hodges Brook, and Upper Hodges Brook have impervious surface areas comprising 4%, 20%, and 32% of the total sub-watershed area, respectively (Figure 42). Note that Upper Hodges Brook is nested within Lower Hodges Brook. These three sub-watersheds were selected based on their drainage to low-order stream reaches (i.e., 2nd and 3rd) within the Wading River watershed and varying levels of development ranging from very rural to more highly developed with distinctly different amounts of impervious cover (IC) (e.g., very rural (less than10% IC); rural/suburban (15%-25% IC); and suburban to urban (greater than 30%)), suitable for further assessment and modeling analysis.

Table 13 and Figure 43 present 2016 land use/land cover area distribution for the Wading River watershed and selected sub-watersheds. The forest land cover is dominated (31%) followed by wetlands (22%) and developed open space (11%) in the Wading River watershed. The total impervious cover is 10% in the Wading River watershed. The forest is also the dominant land cover in all three selected sub-watersheds. The Upper Hodges sub-watershed is more urban with 17% industrial impervious cover and 20% developed open space as compared to more rural pilot tributary sub-watershed with only 4% total impervious cover.

Table 14, Figure 44, Table 15, and Figure 45 present available SSURGO and STATSGO2 soil data, respectively. While SSURGO has a higher resolution dataset, STATSGO2 is more complete, therefore STATSGO2 was used to fill in data gaps present in SSURGO. One-third of the Wading River watershed has high infiltration soil type A. The selected sub-watersheds have similar proportions of soil types A, C, and D, roughly 20% each. Elevation and slope data are presented in Table 16, Table 17, and Figure 46, respectively.

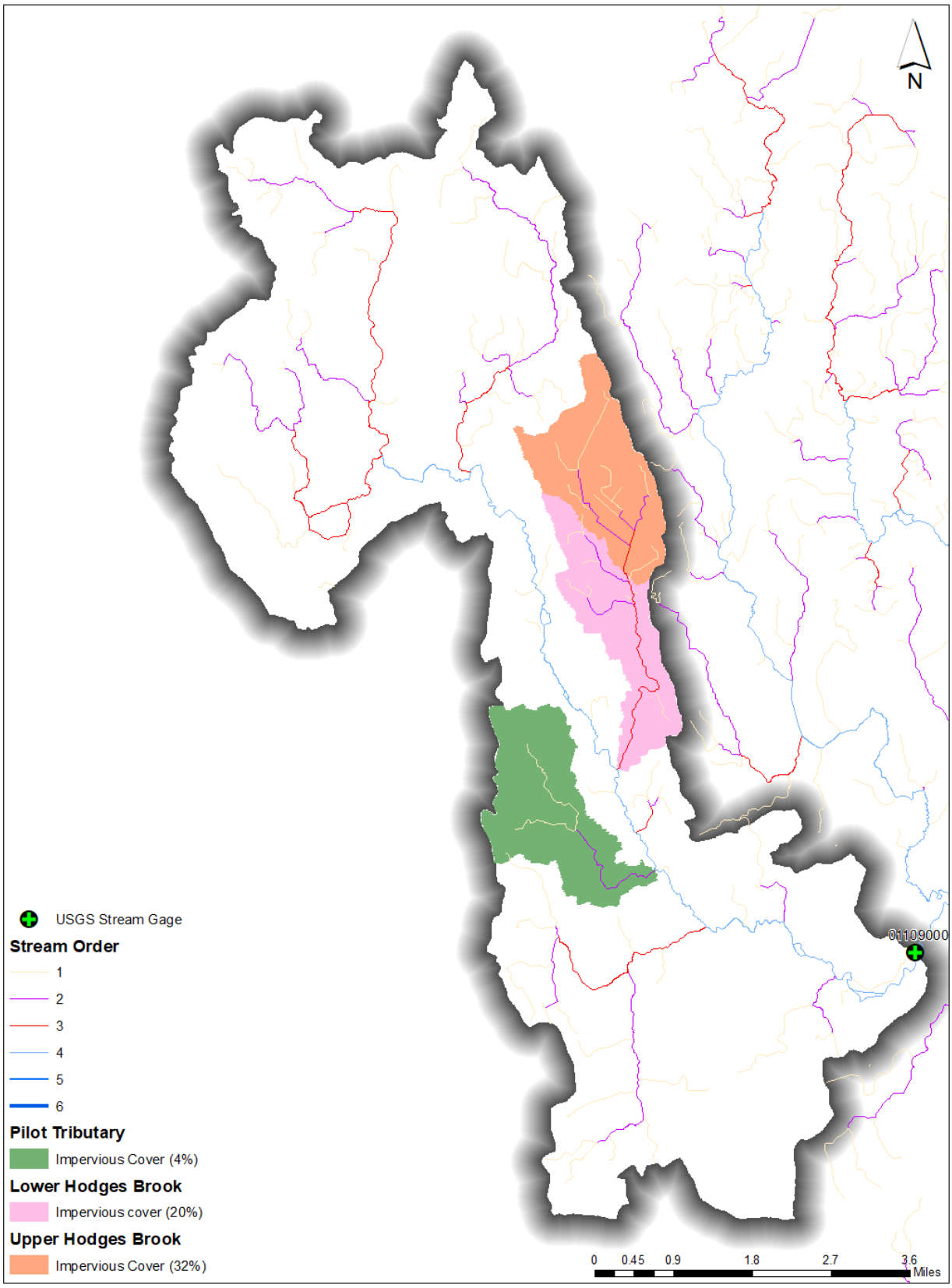

Figure 42. Selected sub-watersheds in the Wading River watershed.

Table 13. Land use – Land cover area distribution in Wading River watershed and pilot sub-watersheds

Land Use - Land Cover	Wading River	Pilot Tributary	Lower Hodges	Upper Hodges
	Acres	Acres	Acres	Acres
Residential - single family	778.30	26.29	61.91	17.70
Residential - multi-family	147.79	4.85	9.65	8.26
Residential - other	7.13	0.47	2.86	1.89
Commercial	375.75	0.64	49.24	45.60
Industrial	366.21	0.24	223.28	223.30
Mixed use, primarily residential	13.39	0.00	0.00	0.00
Mixed use, primarily commercial	0.02	0.00	0.00	0.00
Mixed use, other	0.23	0.00	0.00	0.00
Other Impervious	249.04	1.17	10.90	10.04
Right-of-way	956.59	23.51	152.87	116.92
Cultivated	62.25	1.52	1.91	0.00
Pasture/Hay	234.92	0.63	12.02	2.23
Developed Open Space	3,151.86	84.71	396.18	265.12
Deciduous Forest	8,591.74	579.07	605.94	286.39
Evergreen Forest	4,944.03	213.60	456.90	174.70
Grassland	631.52	30.35	16.35	3.58
Scrub/Shrub	233.92	42.02	16.15	11.95
Bare Land	203.16	14.76	16.23	8.32
Forested Wetland	5,281.34	355.10	448.53	147.59
Non-forested Wetland	719.87	77.14	19.98	8.49
Saltwater Wetland	0.48	0.00	0.00	0.00
Water	440.44	0.75	1.81	1.66
Unconsolidated Shore	0.00	0.00	0.00	0.00
Aquatic Bed	208.64	0.09	2.46	2.46
Total	**27,598.62**	**1,456.95**	**2,505.17**	**1,336.21**

Table 14. SSURGO Hydrologic Soil Group area distribution in Wading River watershed and pilot sub-watersheds

Hydrologic Soil Group	Wading River	Pilot Tributary	Lower Hodges	Upper Hodges
	Acres	Acres	Acres	Acres
NoData	2,610.7	0.9	239.2	239.2
A	9,174.3	309.6	670.8	263.8
A/D	1,592.4	71.3	103.5	26.3
B	2,633.7	78.0	170.8	65.3
B/D	3,589.9	170.2	271.8	66.4
C	3,081.1	322.5	335.7	194.7
C/D	1,828.2	171.8	294.2	211.1
D	3,090.9	332.6	419.1	269.3
Total	**27,601.2**	**1,456.9**	**2,505.2**	**1,336.2**

Table 15. STATSGO2 Hydrologic Soil Group area distribution in Wading River watershed and pilot sub-watersheds

Hydrologic Soil Group	Wading River	Pilot Tributary	Lower Hodges	Upper Hodges
	Acres	Acres	Acres	Acres
NoData	0.0	0.0	0.0	0.0
A	12,136.0	264.1	575.9	14.2
A/D	0.0	0.0	0.0	0.0
B	2,950.0	0.0	0.0	0.0
B/D	0.0	0.0	0.0	0.0
C	11,557.4	1,192.9	1,929.3	1,322.0
C/D	0.0	0.0	0.0	0.0
D	957.9	0.0	0.0	0.0
Total	**27,601.2**	**1,456.9**	**2,505.2**	**1,336.2**

Table 16. Elevation range in Wading River watershed and pilot sub-watersheds

Range	Elevation (m)			
	Wading River	Pilot Tributary	Lower Hodges	Upper Hodges
Minimum	18.3	30.1	31.9	42.4
Mean	55.0	40.3	53.1	60.3
Max	134.8	52.2	92.8	92.8

Table 17. Slope category area distribution in Wading River watershed and pilot sub-watersheds

Slope Category	Wading River	Pilot Tributary	Lower Hodges	Upper Hodges
	Acres	Acres	Acres	Acres
Low	20,686.8	1,407.2	2,343.4	1,235.6
Med	5,321.9	48.9	150.9	92.3
High	1,591.5	1.8	12.6	9.5
Total	**27,600.2**	**1,457.9**	**2,506.9**	**1,337.3**

The elevation ranges from 18m to 135m in the Wading River watershed. Overall, the Wading River watershed has a low slope (75% of the area) with only 6% of the high slope areas. More than 92% of the areas have a low slope and less than 1% of the areas have a high slope in the selected sub-watersheds.

Table 18 and Figure 47 show the impervious area comparison from NLCD and MassGIS data sources for different periods (the year 2001, 2005, 2006, 2011, and 2016) in the Wading River watershed and selected three sub-watersheds.

Figure 48 shows the 2016 land use/land cover distribution and Figure 49 shows water use locations in the Wading River watershed and the selected sub-watersheds. Figure 50 presents aquifer locations and Figure 51 presents the locations of FEMA Special Flood Hazard Areas (FHAs). During SCM optimization in future tasks, the FHA layer will be used as one of the screening categories in which SCM placement will be avoided. Figure 52 and Figure 53 present available SSURGO and STATSGO2 soil maps, respectively. Elevation and slope maps are presented in Figure 54 and Figure 55, respectively.

Table 18. Total Impervious Cover comparison by a data source in Wading River watershed and pilot sub-watersheds

Data Source	Wading River	Pilot Tributary	Lower Hodges	Upper Hodges
	Acres	Acres	Acres	Acres
NLCD 2001	2,658.3	43.4	523.6	433.3
NLCD 2006	2,849.6	49.2	556.7	464.1
NLCD 2011	3,066.8	52.5	578.3	483.1
NLCD 2016	3,113.7	52.6	580.6	485.1
Mass-Imp 2005	3,192.6	72.5	506.0	413.0
Mass-LULC 2016	2,894.2	57.2	511.1	424.1

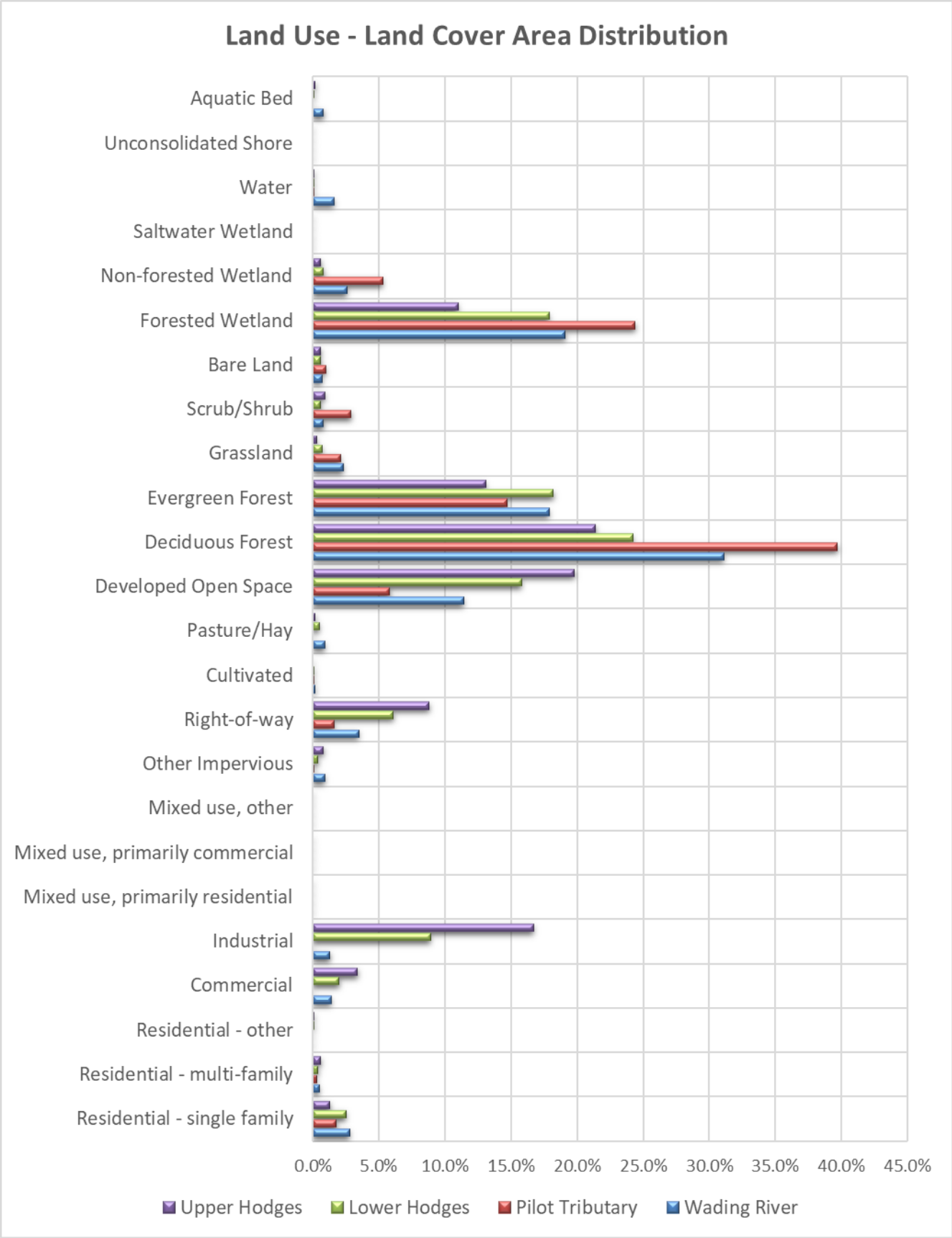

Figure 43. Land use – Land cover area distribution in Wading River watershed and pilot sub-watersheds.

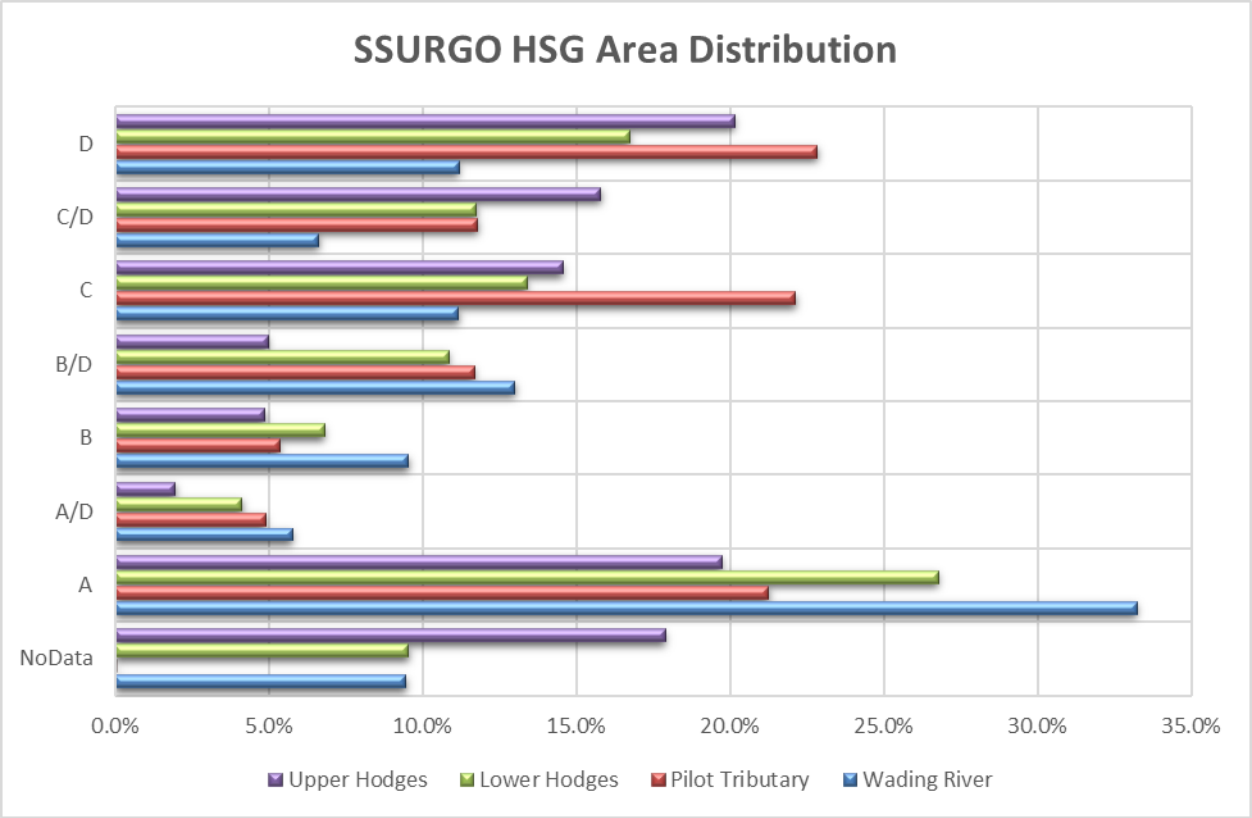

Figure 44. SSURGO Hydrologic Soil Group area distribution in Wading River watershed and pilot sub-watersheds.

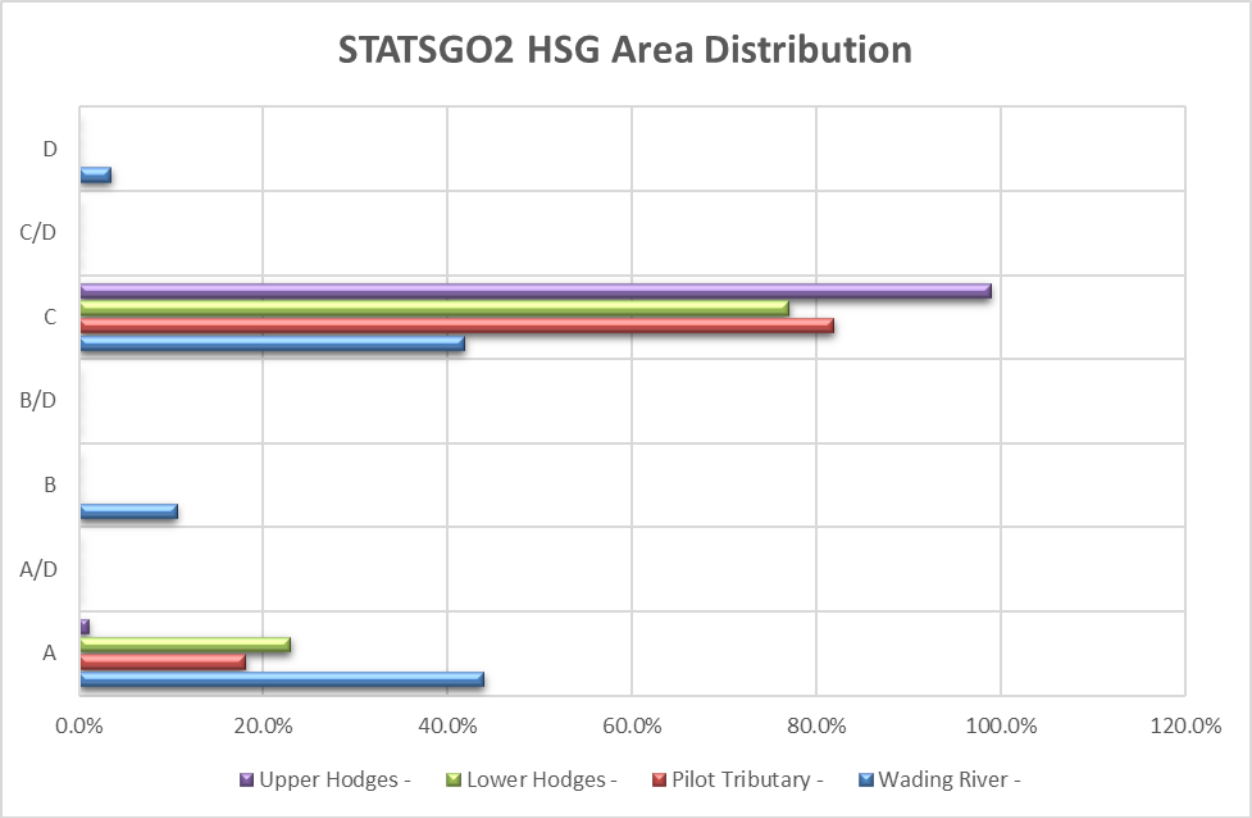

Figure 45. STATSGO2 Hydrologic Soil Group area distribution in Wading River watershed and pilot sub-watersheds.

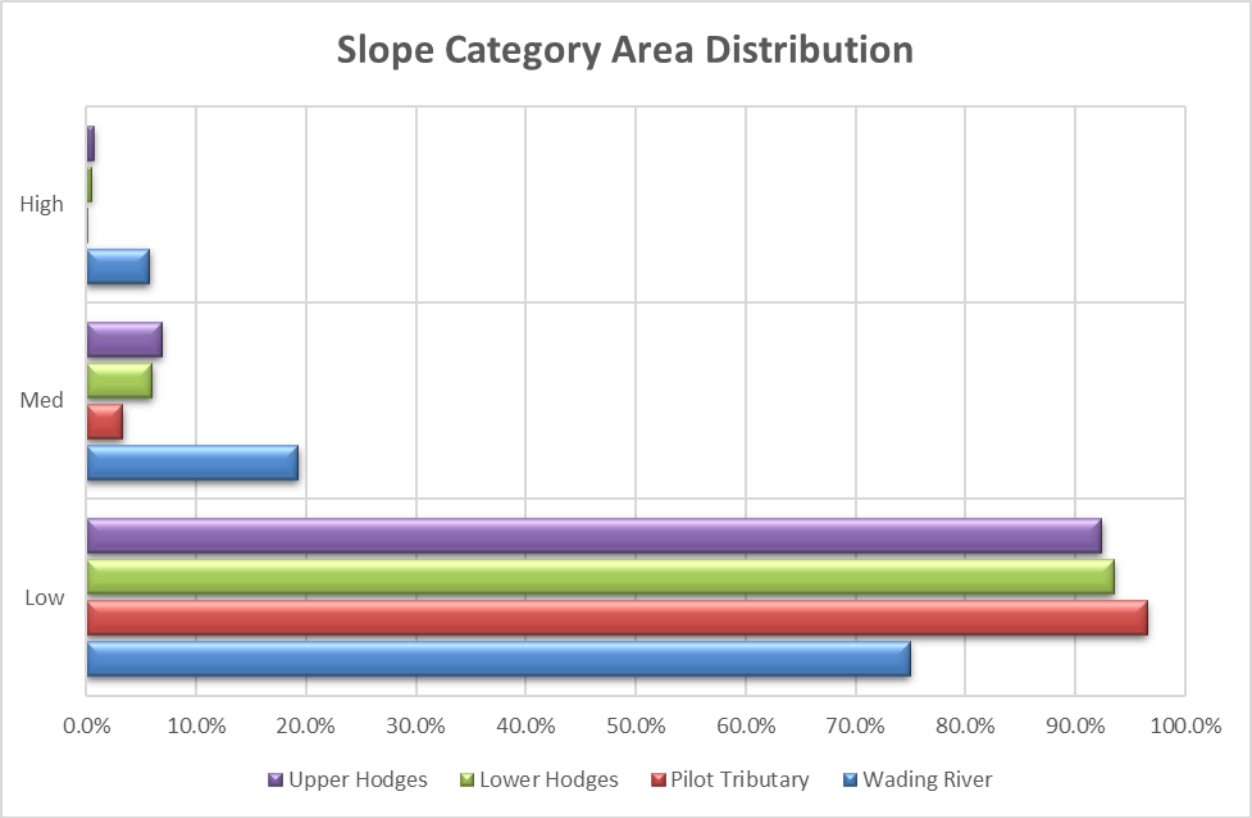

Figure 46. Slope Group area distribution in Wading River watershed and pilot sub-watersheds.

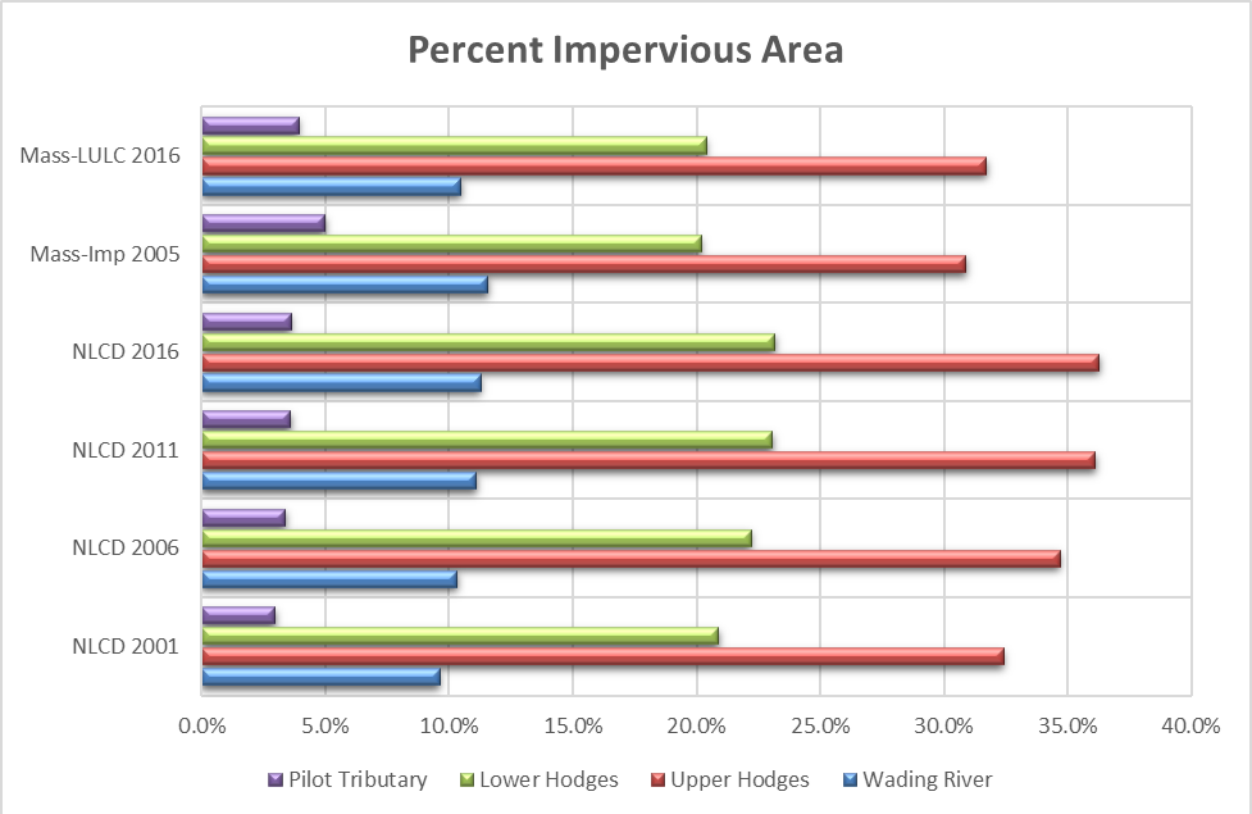

Figure 47. Total Impervious Cover comparison by a data source in Wading River watershed and pilot sub-watersheds.

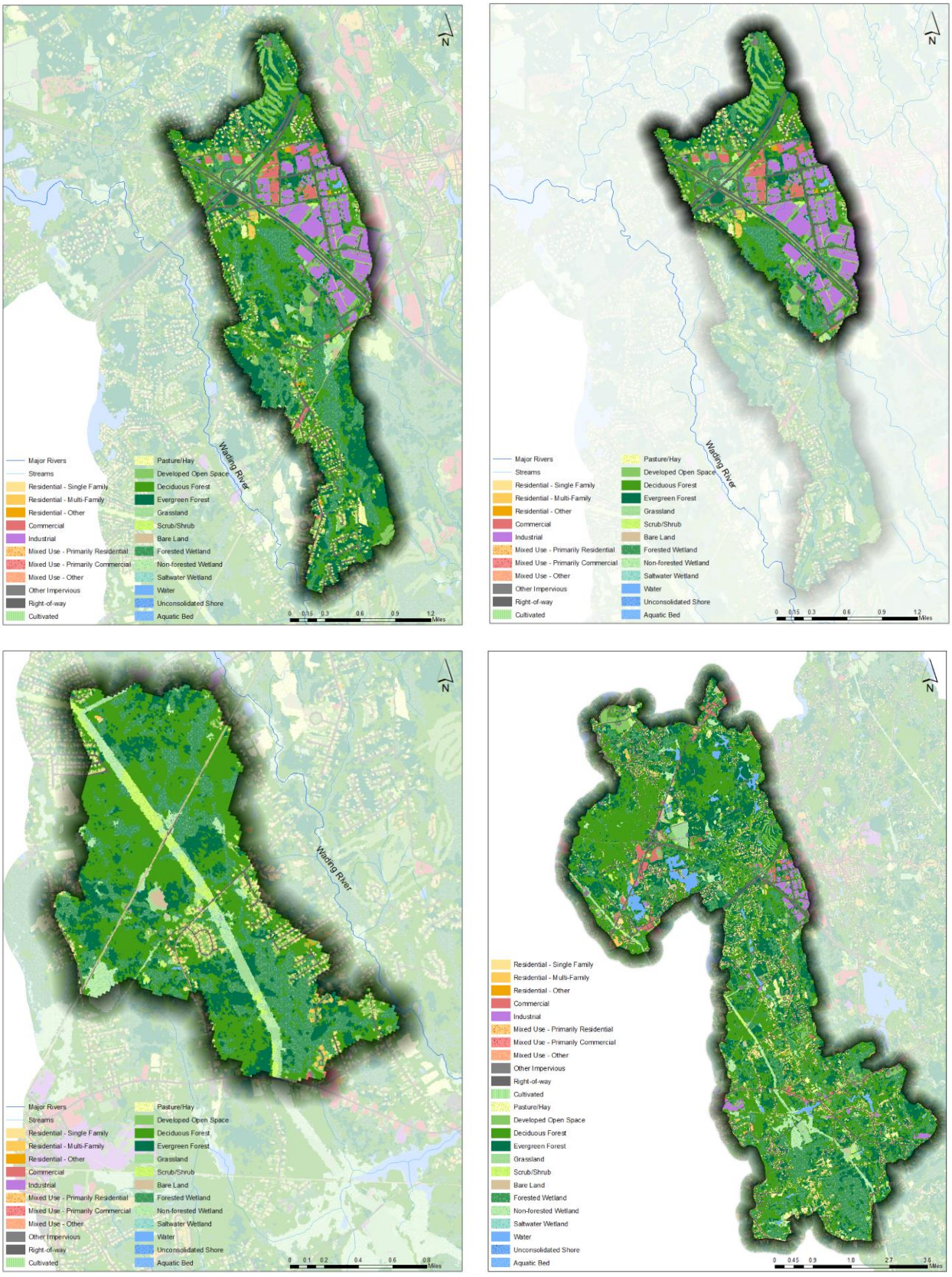

Figure 48. 2016 Land use – Land cover for Lower Hodges Brook (top left), Upper Hodges Brook (top right), Pilot Tributary (bottom left), and Wading River (bottom right).

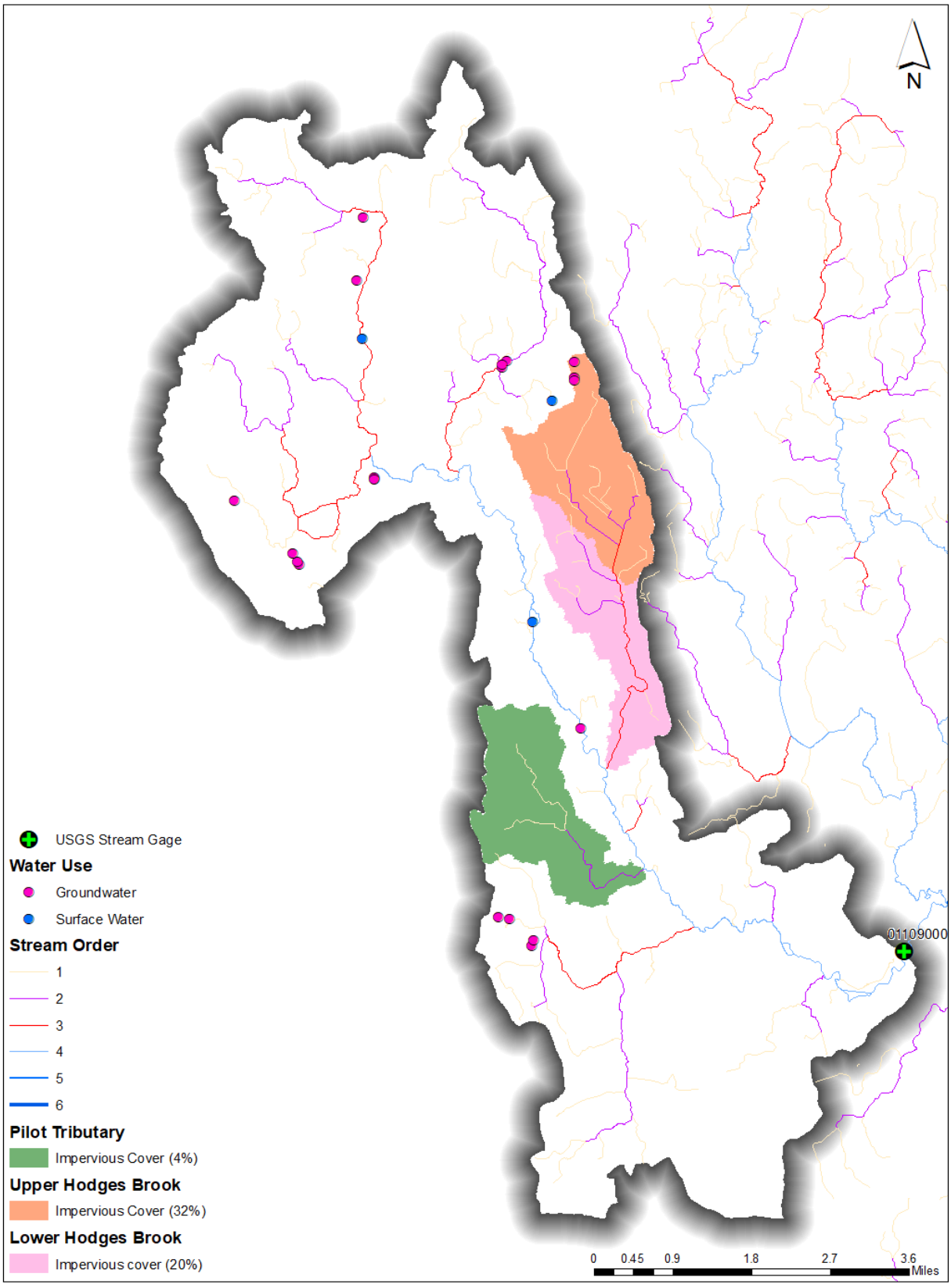

Figure 49. Water use locations and selected sub-watersheds in the Wading River watershed.

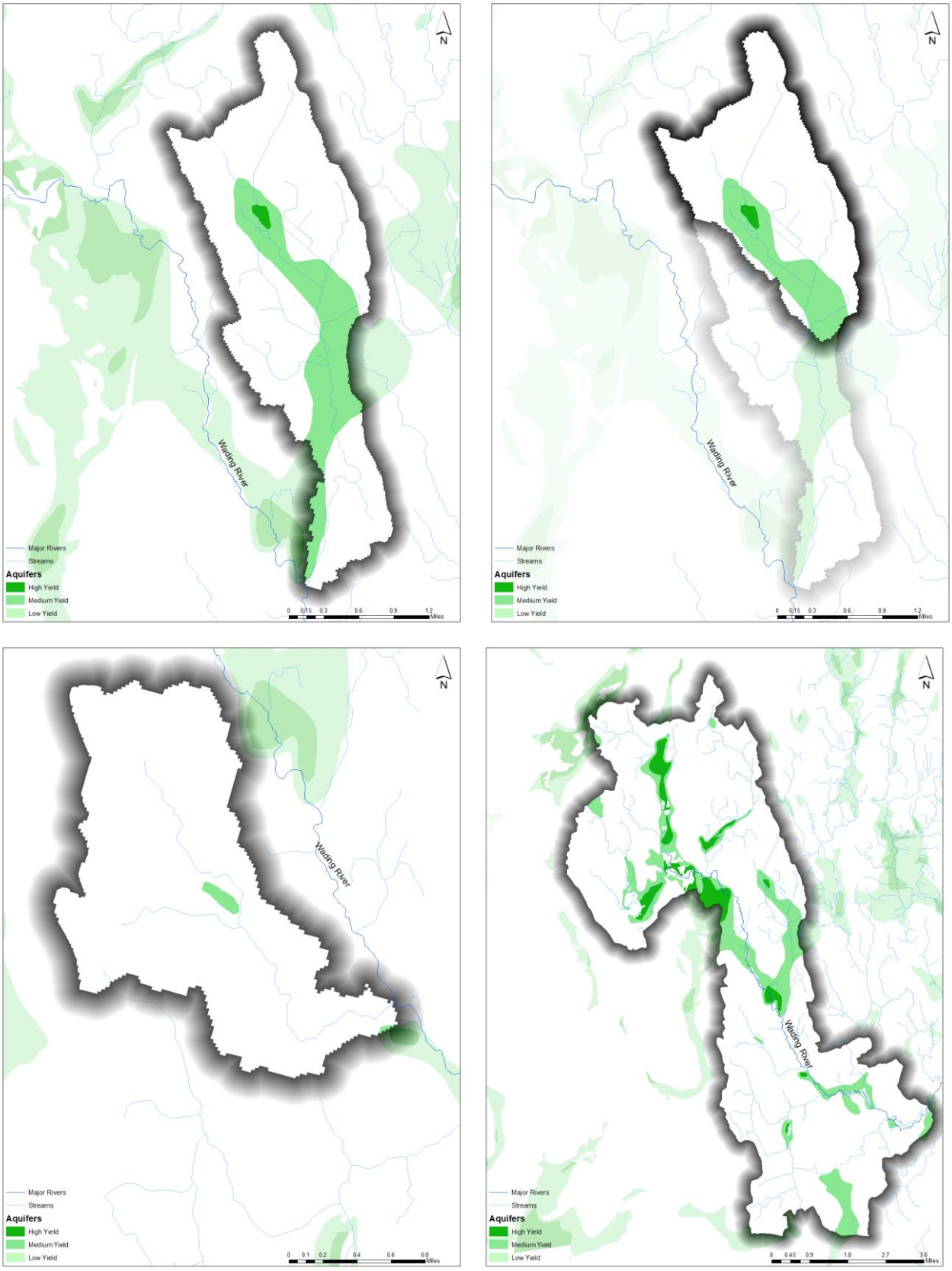

Figure 50. Aquifer locations in Lower Hodges Brook (top left), Upper Hodges Brook (top right), Pilot Tributary (bottom left), and Wading River (bottom right).

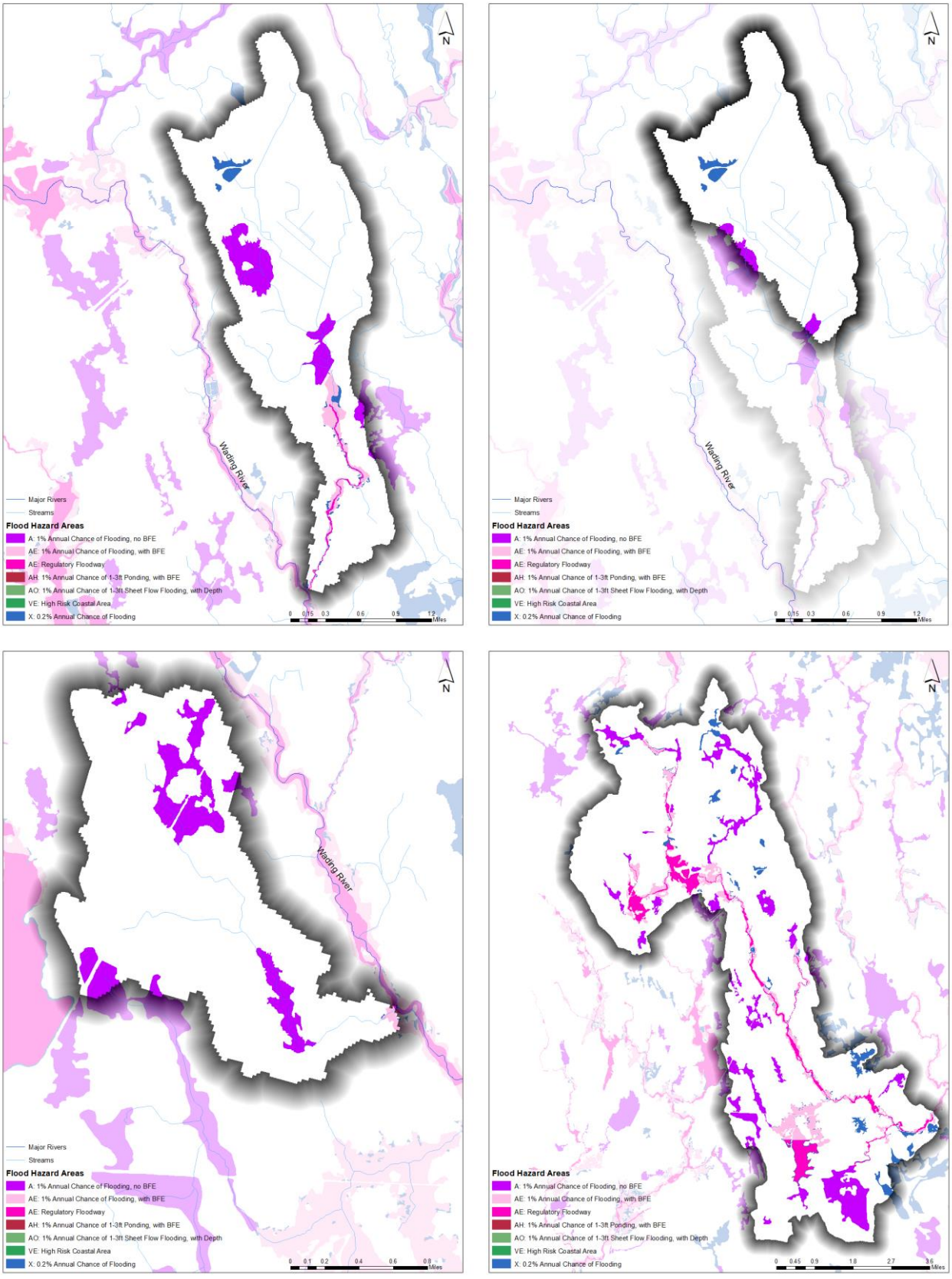

Figure 51. FEMA Special Flood Hazard Areas locations in Lower Hodges Brook (top left), Upper Hodges Brook (top right), Pilot Tributary (bottom left), and Wading River (bottom right).

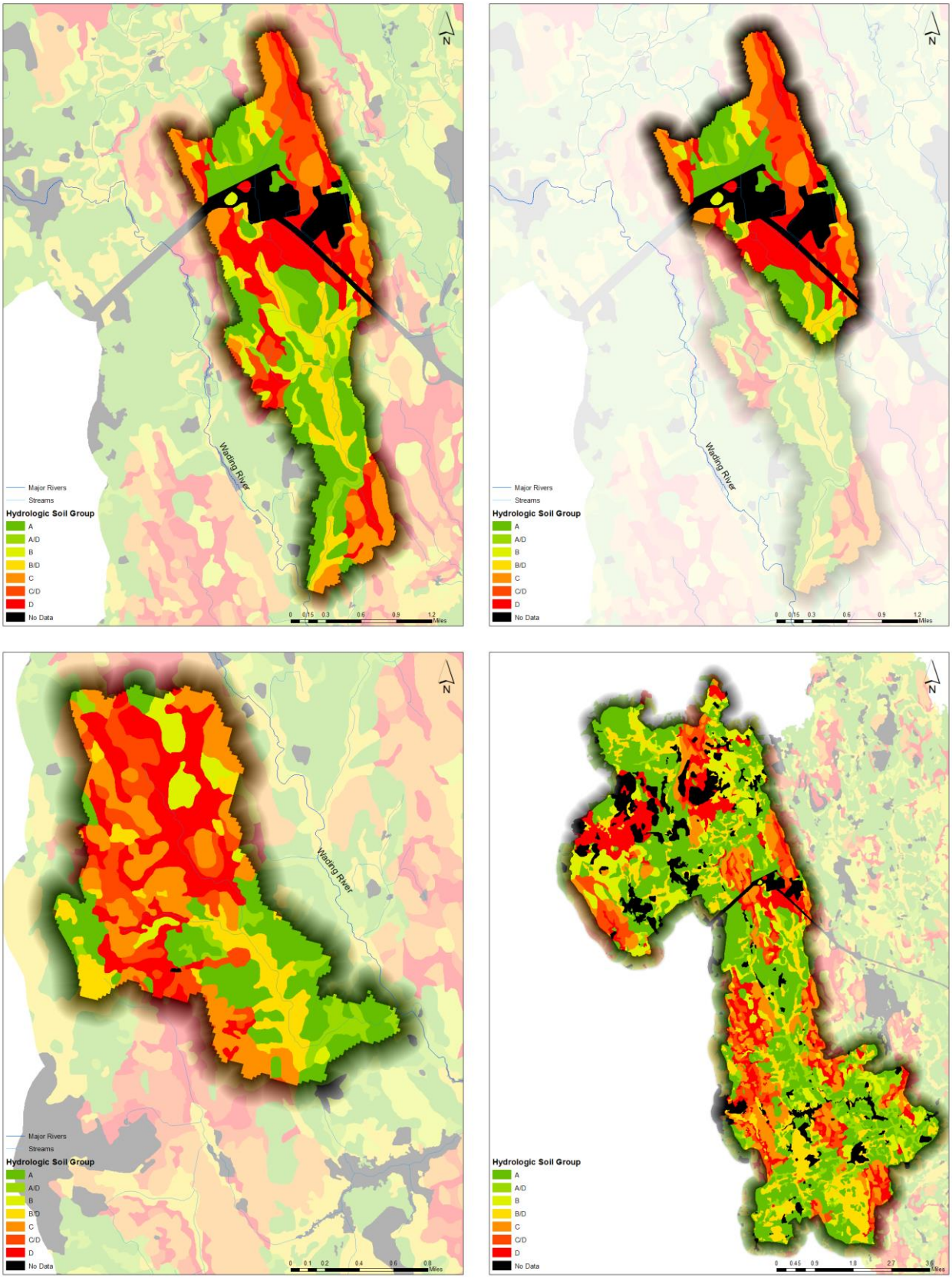

Figure 52. SSURGO information for Lower Hodges Brook (top left), Upper Hodges Brook (top right), Pilot Tributary (bottom left), and Wading River (bottom right).

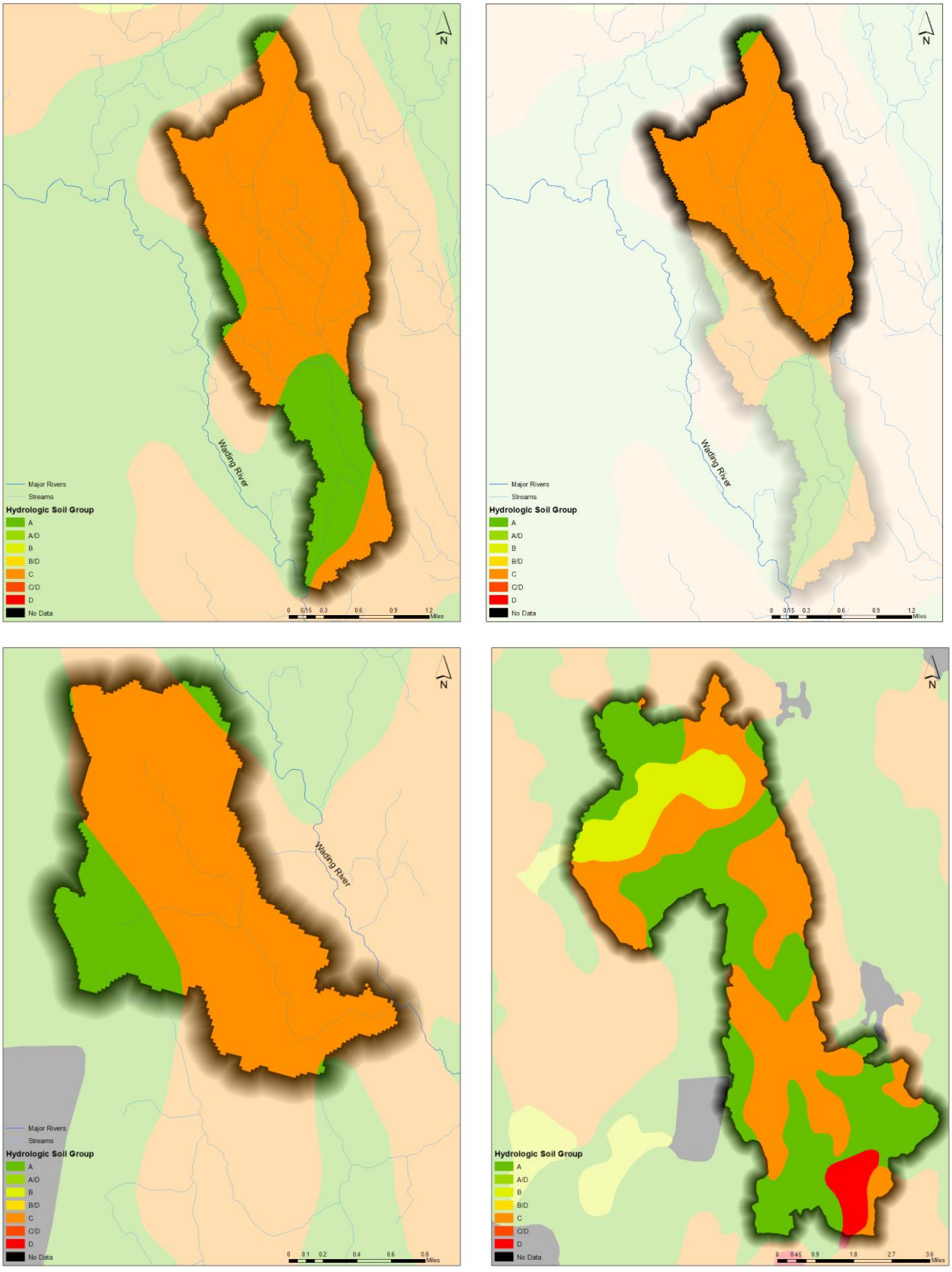

Figure 53. STATSGO2 information for Lower Hodges Brook (top left), Upper Hodges Brook (top right), Pilot Tributary (bottom left), and Wading River (bottom right).

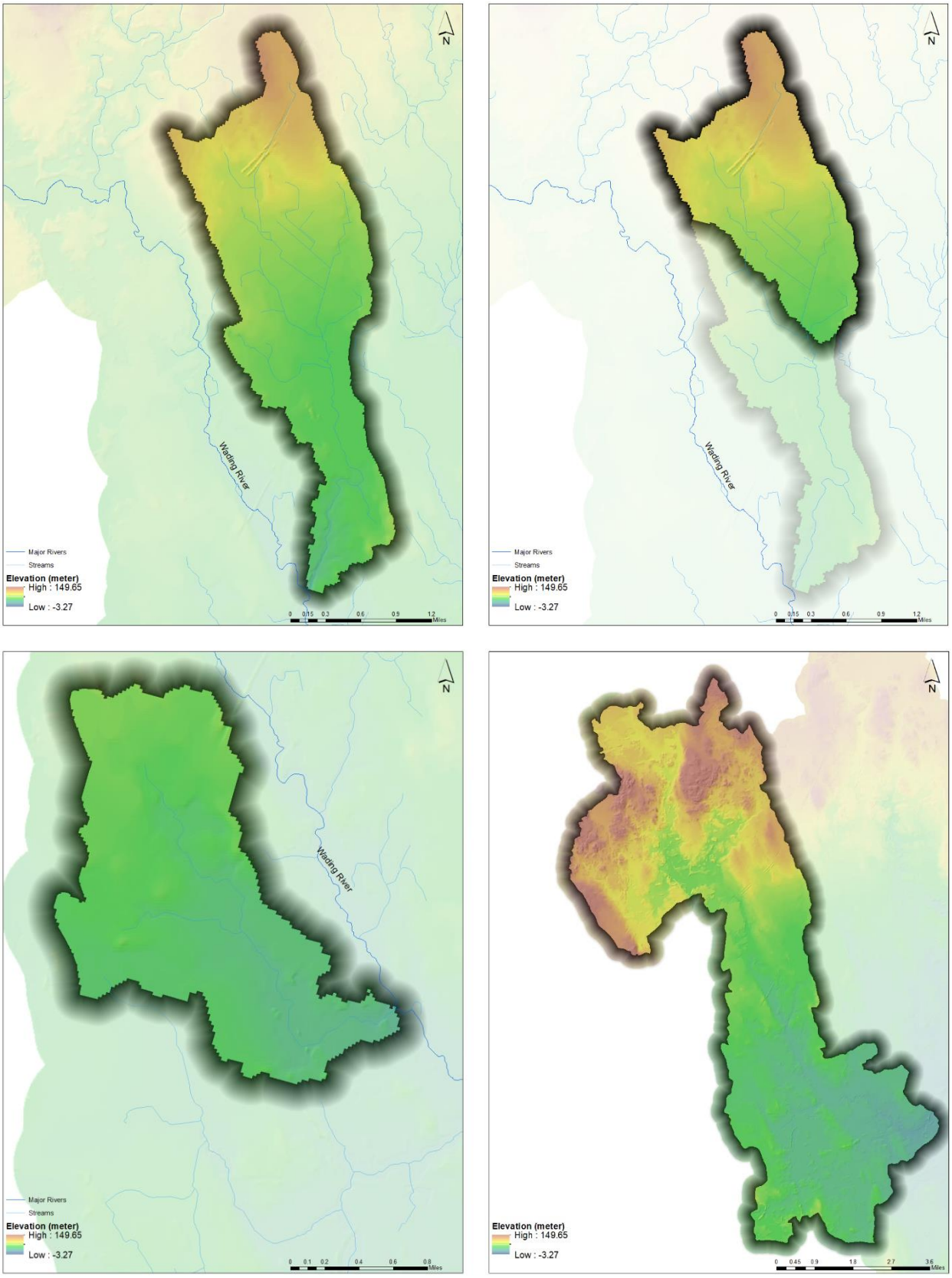

Figure 54. Elevation information for Lower Hodges Brook (top left), Upper Hodges Brook (top right), Pilot Tributary (bottom left), and Wading River (bottom right).

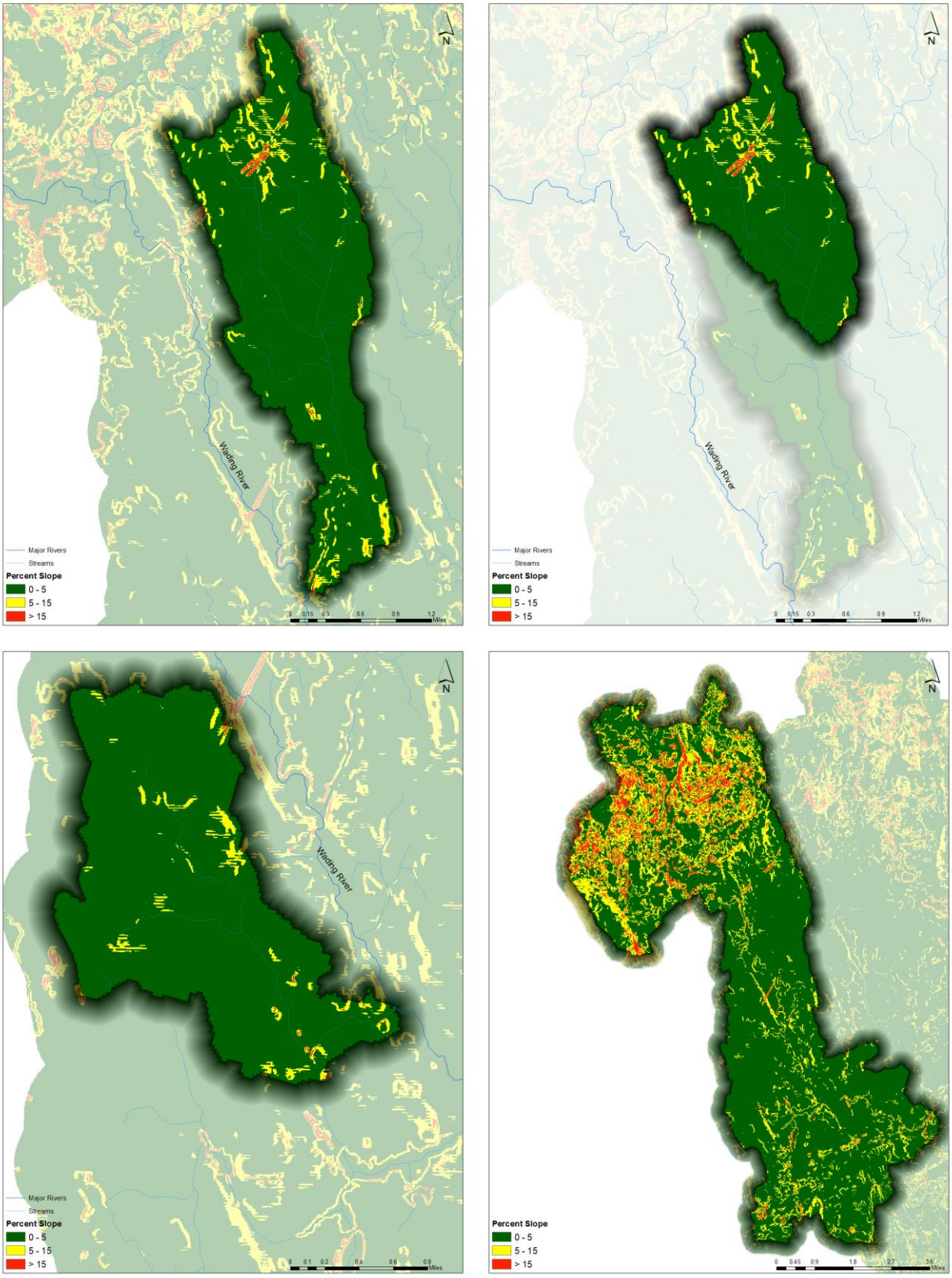

Figure 55. Slope information for Lower Hodges Brook (top left), Upper Hodges Brook (top right), Pilot Tributary (bottom left), and Wading River (bottom right).

3 TASK 5B. PAST, CURRENT AND FUTURE CLIMATE DATA ANALYSIS

The climate of Massachusetts is changing; the state has warmed by more than two degrees Fahrenheit in the last century and experiences heavier, more frequent rainstorms (EPA, 2016). Within the Taunton basin, both maximum and minimum temperatures are expected to continue to increase through the end of the century. Winters are expected to have more precipitation while summers may see an increase or decrease in precipitation (Northeast Climate Adaptation Science Center, 2018). In response, the state has produced Climate Resilience Design Standards and Guidelines (Resilient Massachusetts Action Team, 2020) to incorporate climate resilience into the State's capital planning process. The design standards are intended to inform the climate resilience design of assets and include design criteria for extreme precipitation. Best practice guidance from the Climate Resilience Design Standards includes embedding future capacity into projects and designing for uncertainty. The approach encourages that assets (such as stormwater SCMs) be implemented in locations that (1) reduce exposure to climate hazards, (2) mitigate adverse climate impacts and provide benefits and (3) protect, conserve, and restore critical natural resources on-site and off-site.

Climate variability and changes to land use/land cover are two interwoven factors that impact hydrologic systems and improving the understanding of these two factors is the subject of research programs around the globe and an important part of sustainable water resource management.

3.1 Historic Trends

Figure 56 presents monthly rainfall for the period of record for T.F. Green Airport. Precipitation data is also presented in Figure 57 as annual averages, average depth for the period of record, and rolling 10 and 30-year averages. Overall, there does not appear to be a strong increasing trend in terms of annual precipitation depths. Additionally, the historic precipitation data was analyzed to produce 24-hour rainfall depths for the 1, 2, 5, 10, 25, 50, 100, and 500-year storms. These storms relate to approximately 100%, 50%, 20%, 10%, 4%, 2%, 1%, and 0.2% that these depths will fall within a 24-hour period in any given year. Figure 58 presents daily minimum and maximum temperatures. There appears to be a strong trend of increasing temperatures based on visual inspection of annual averages, the average temperature for the period of record, and tolling 10 and 30-year averages (Figure 59).

3.2 Current Conditions

Streamflow data in the Wading River over the last over the 95 years of record between 1925 and 2020 contain signatures of natural climate variability mixed with hydrological impacts caused by anthropogenic development activity. The period between 2001 and 2019 was identified as being representative of present-day development impacts based on available land use data. Analysis of historical precipitation data was conducted to identify a past 19-year period having the closest average precipitation, storm-size distribution, and average monthly/temporal pattern of rainfall as the 2001-2019 period. The data summary previously shown in Table 5 was resampled using a rolling 19-year period to calculate the following sets of statistics for evaluation:

1. Average rainfall for each rolling 19-year period,
2. Average number of days per year for four bins of storms (≥0.1-, ≥0.5-, ≥1.0-, and ≥1.5-inches),
3. Average monthly volume and number of wet days for each rolling 19-year period.

Figure 60 shows average monthly rainfall and number of wet days for the long-term average (1949-2019), historical (1972-1990), and most recent (2001-2019) periods. Figure 61 presents annual precipitation totals and rainfall distribution differences throughout record precipitation at T.F. Green Airport. The 19-year historical period between 1972 and 1990 had the closest average rainfall and storm distribution as the 2001-2019 period.

Table 19. Data source and methodologies for extreme precipitation design criteria (Source: Resilient Massachusetts Action Team, 2020)

Design Criteria	Data Sources & Methodologies		
	Tier 3 - High Level of Effort	Tier 2 - Average Level of Effort	Tier 1 - Low Level of Effort
Total Precipitation Depth for 24-hour Design Storms	Downscaled GCMs (from ResilientMA.org or LOCA dataset) and extreme value distribution analysis	NCA4 CSSR values and increase the NOAA Atlas 14 values by the change percentage as indicate	Atlas-14 90% of the upper 90% C.I (DEP proposed approach)
Peak intensity for 24-hour design storms[1]	Type III distribution to future design storms estimated from downscaled GCMs and extreme value distribution analysis	Type III distribution to future design storms estimated using NCA4 CSSR method	Type III distribution to future design storms estimated using Atlas-14 90% of the upper 90% C.I
Riverine peak discharge[1]	Hydrologic/hydraulic modeling at watershed/sub-watershed scale using future design storms		StreamStats using Zariello's Equation
Riverine peak flood elevation[1]	Hydrologic/hydraulic modeling at watershed/sub-watershed scale using future design storms		Use Stage Discharge Curve from corresponding gage location used in StreamStats
Duration of flooding for design storm	Hydrologic/hydraulic modeling at watershed/subwatershed scale using future design storms	Not needed.	
Flood Pathways[1]		Not needed.	

1. These criteria are calculated based on precipitation depths affected by climate change. The methods to calculate these criteria are consistent with existing industry practices, but they should use the future precipitation depths.

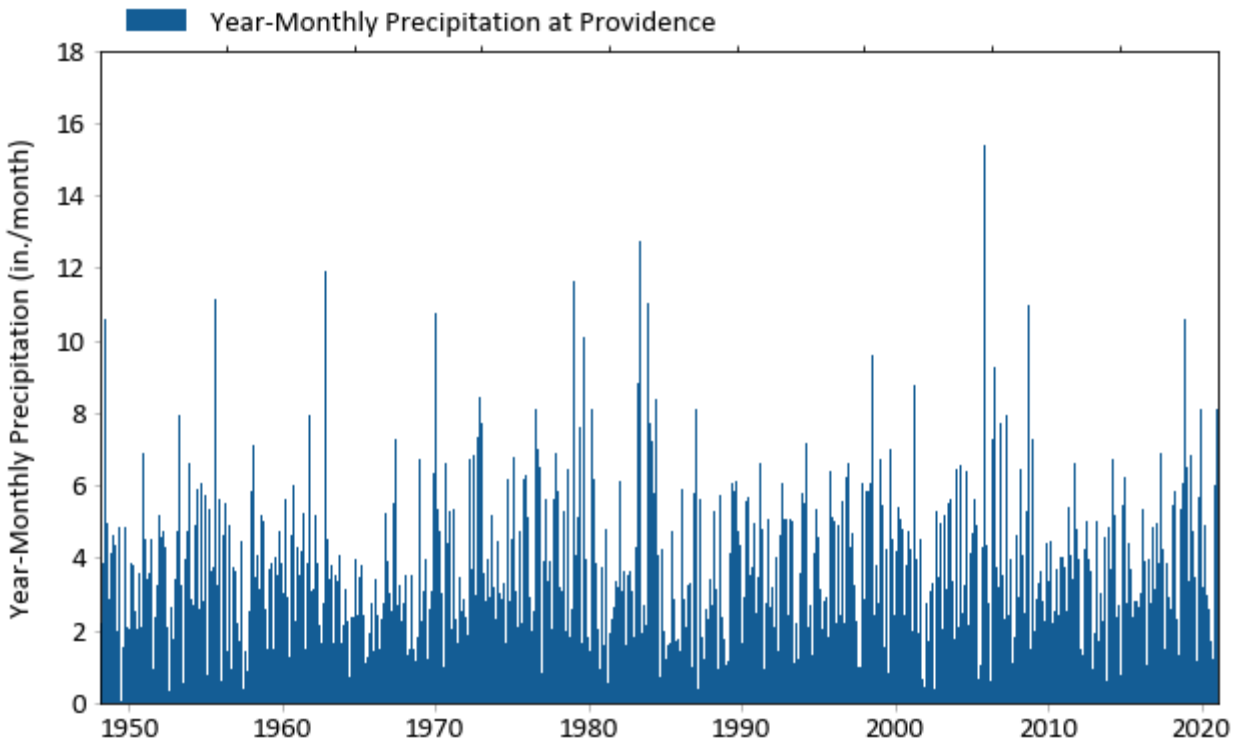

Figure 56. Monthly rainfall.

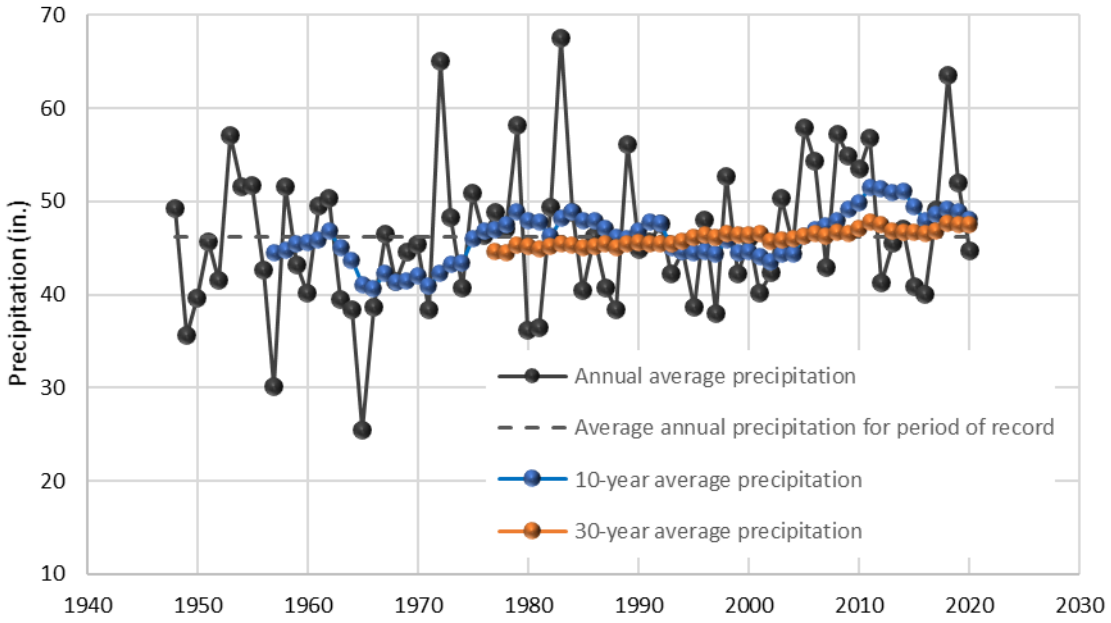

Figure 57. Precipitation trends (T.F. Green Airport).

Table 20. Precipitation depths for 24-hour events based on analysis of historical data

Description		Return Period	24-hour Rainfall Depth (in)
1	Small	1-yr	2.1
2		2-yr	2.8
3	Medium	5-yr	3.3
4		10-yr	3.9
5	Large	25-yr	5.1
6		50-yr	6.5
7	Extreme	100-yr	8.4
8		500-yr	16.63

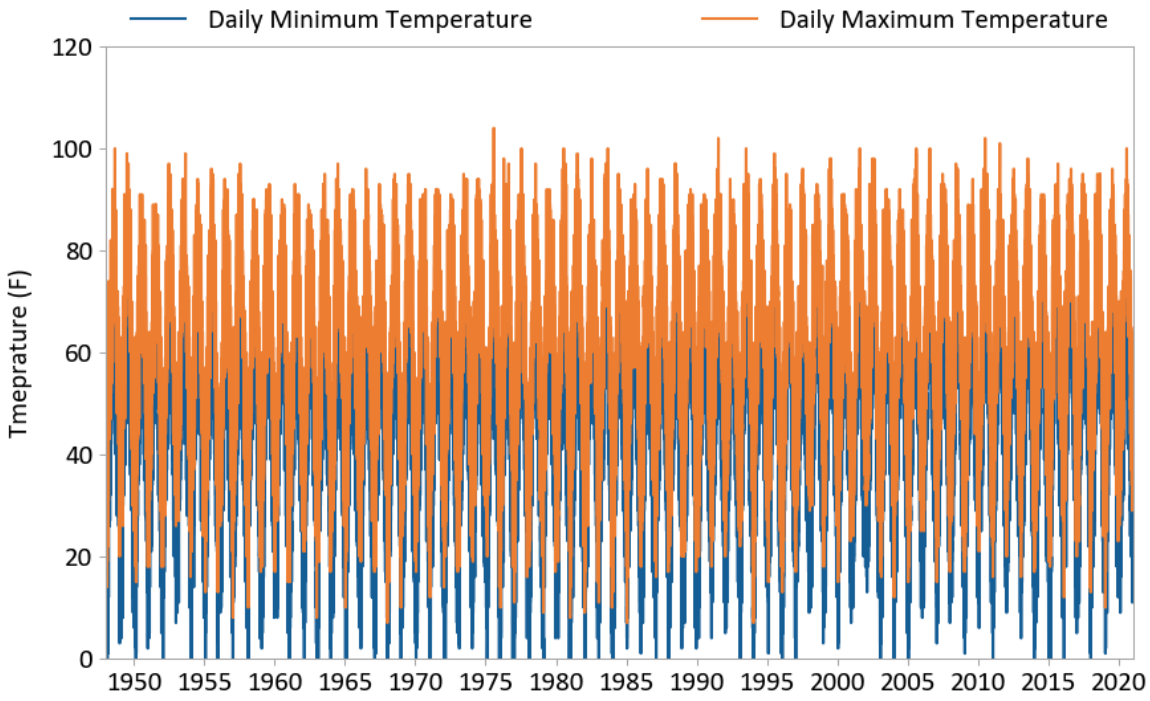

Figure 58. Daily minimum and maximum temperatures (T.F. Green Airport).

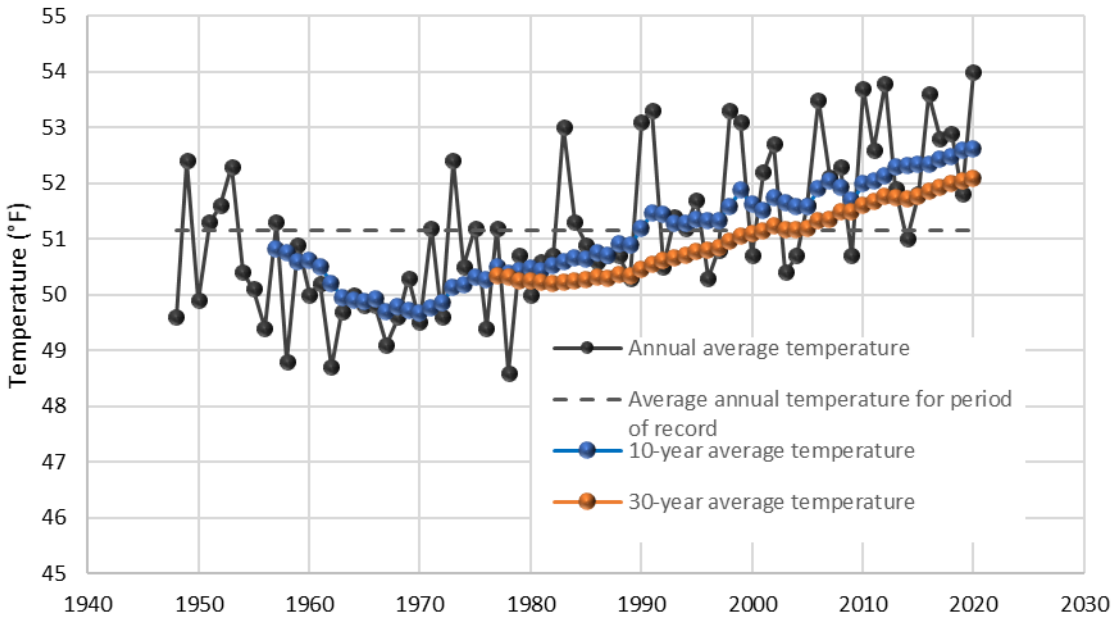

Figure 59. Annual average temperature trends (T.F. Green Airport).

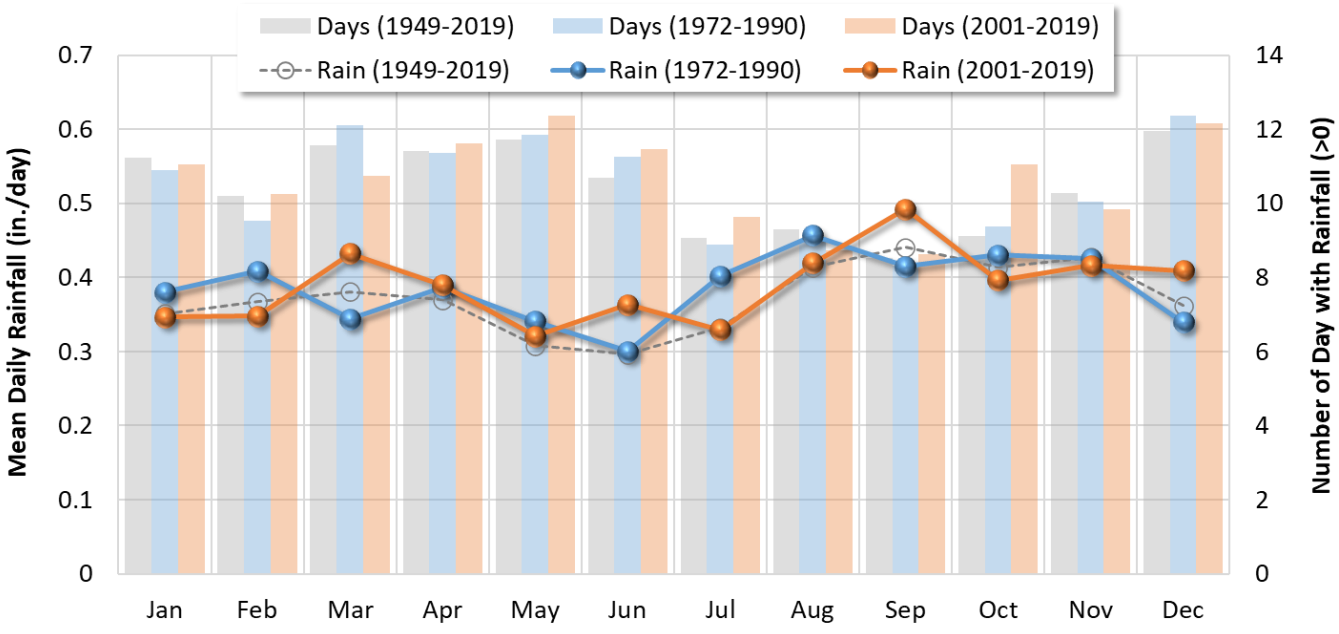

Figure 60. Average monthly rainfall and number of wet days for the long-term average (1949-2019), historical (1972-1990), and most recent (2001-2019) periods.

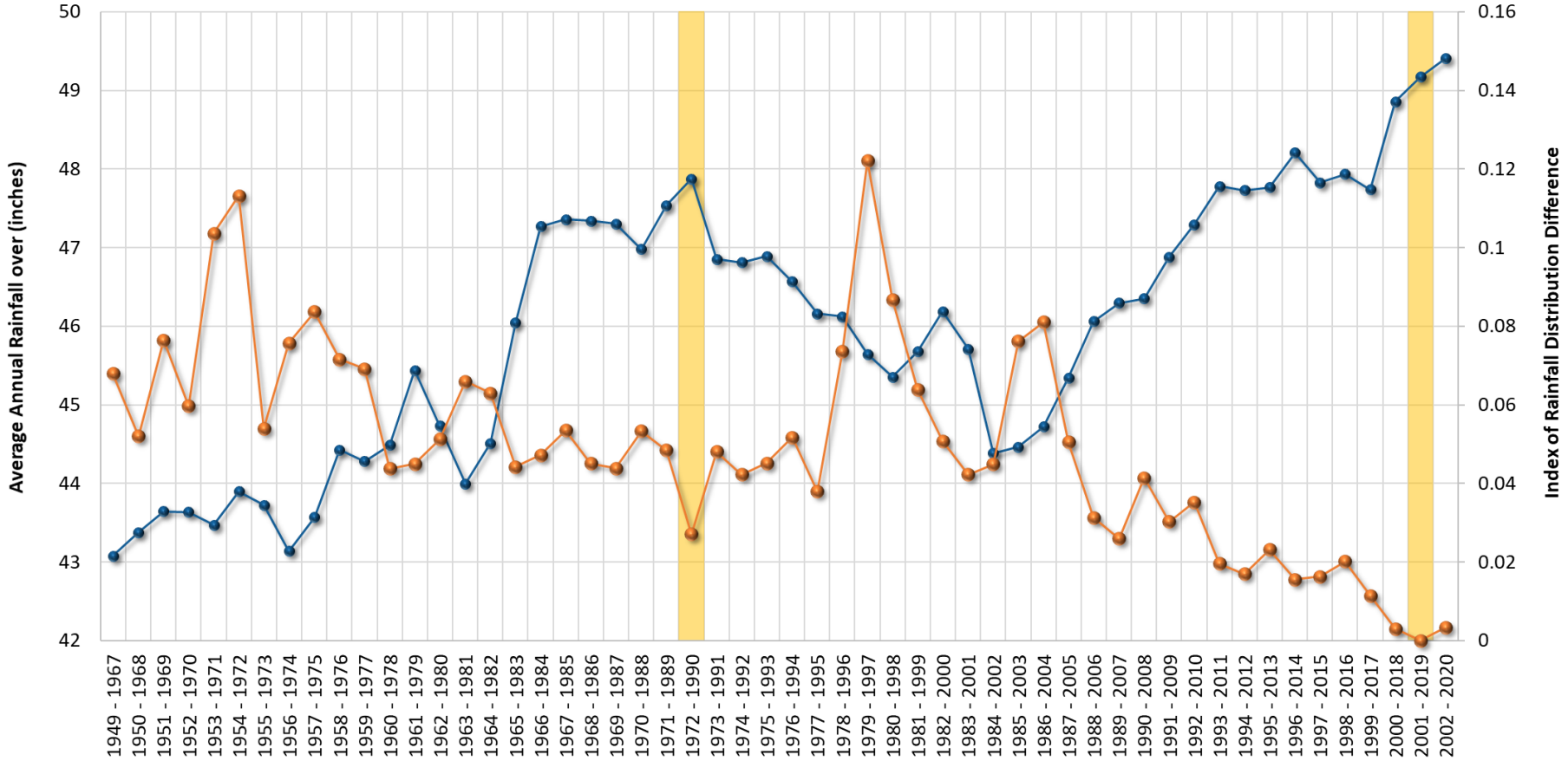

Figure 61. Average annual rainfall depth and distribution (T.F. Green Airport).

Average temporal variability represented as average monthly rainfall depth and the number of wet days, was also evaluated for the historical and the 2001-2019 period. The Student's t-test was used to assess how different the seasonal variability of 2001-2019 was from other 19-year periods in the historical record. Those results are summarized in Table 21. The p-values are presented on a gradient scale between 0% and 100%, where months with p-values <5% are flagged as significantly different from corresponding months in the 19 years between 2001 and 2019. To account for both storm depth and number of wet days, the statistic used for this test was average inches per wet day. The results suggest that between 1949 and 1989, the month of October had significantly different rainfall patterns than 2001-2019. Furthermore, between 1973 and 1999, the month of March had significantly different rainfall patterns than 2001-2019. Periods between 1982 and 2019 showed less significant difference mainly because of overlapping years in the rolling 19-year window. Of the 53 rolling 19-year windows evaluated, three periods, 1972-1990, 1980-1998, and 1982-2000 showed no significant difference in monthly rainfall distribution relative to 2001-2019; however, 1972-1990 was selected as a representative historical period because:

1. It was the farthest removed from development signatures associated with the 2001-2019 period,
2. It had the most similar average rainfall, average storm distribution, and average temporal distribution as the 2001-2019 period,
3. It had no overlapping years with the 2001-2019 period.

3.3 Future Conditions

The Massachusetts Climate Change Report (MA EOEE, 2011) presents estimates that annual precipitation will increase 5-8% in 2035-2064 and 7-14% in the period 2070-2099, with increased precipitation rates especially occurring during winter months (Hayhoe et al., 2006). These estimates are based on general circulation models (GCMs), which typically produce output at relatively coarse temporal and spatial resolutions. Temporal resolutions are often monthly timesteps and spatial resolutions are often grid cells of 1 or more degrees (~60-200 miles). However, most hydrological and water quality models require data at hourly timesteps or finer, and higher spatial resolutions depending on watershed size. Statistical downscaling allows modelers to create fine resolution climate time series using coarse resolution datasets by identifying statistical relationships between the coarse and fine resolution data. Raw climate model data has been downscaled from monthly resolution to daily resolution by a consortium of researchers (Northeast Climate Adaptation Science Center, 2018) and is publicly available (www.resilientma.org). However, further downscaling was necessary to generate the required hourly data.

The specific downscaling techniques used depend on the variable being downscaled. Precipitation data presents challenges in downscaling due to its high spatial and temporal variability. Fortunately, there are existing techniques developed to overcome these challenges. Local Constructed Analogs (LOCA) has been shown to successfully downscale similarly variable climate data and was selected to downscale precipitation for the Taunton basin. While estimates of future precipitation are available at a daily timestep, the LSPC/Opti-Tool modeling requires hourly data. The LOCA approach examines historical hourly data to identify "analog days" that can be used to disaggregate represent the future daily precipitation. The process iterates over each day in the modeled future precipitation. For each day of data, the process also extracts rainfall estimates for the preceding and following days to create a three-day time series of daily rainfall. Then, the LOCA approach searches through historical hourly rainfall data to find three-day periods with similar rainfall. It compares the hourly rainfall against the modeled daily rainfall and the historical three-day period with the most similar rainfall becomes the analog day.

LOCA has also been used to generate hourly downscaled wind data. However, it is not expected that hourly wind data is needed for this study. Model results are unlikely to be sensitive to hourly wind speed, and daily averages are expected to be adequate. The remaining variables typically exhibit predictable diurnal cycles making the use of sophisticated algorithms like LOCA unnecessary. To downscale evapotranspiration, penman-monteith will be used to calculate daily evapotranspiration using the daily resolution climate data. Then, an hourly diurnal evapotranspiration cycle will be derived for each season using observed data. This cycle will be scaled to the daily evapotranspiration values, to generate hourly evapotranspiration.

Table 21. P-values of Student's t-test results of monthly rainfall variability of 2001-2019 vs. 53 19-year periods between 1949 and 2019

Start	End	Jan	Feb	Mar	Apr	May	Jun	Jul	Aug	Sep	Oct	Nov	Dec
1949	1967	33.2%	61.3%	51.3%	63.3%	50.0%	6.7%	86.8%	25.3%	65.1%	**1.1%**	73.5%	18.2%
1950	1968	22.9%	71.3%	64.9%	60.8%	50.5%	7.1%	84.3%	17.8%	92.0%	**1.0%**	70.7%	31.7%
1951	1969	26.9%	82.7%	71.4%	74.5%	54.1%	6.6%	63.8%	11.8%	99.6%	**1.6%**	86.4%	38.7%
1952	1970	17.4%	95.7%	63.1%	76.0%	55.2%	6.5%	49.5%	14.8%	92.7%	**0.8%**	96.8%	35.1%
1953	1971	16.6%	76.1%	78.2%	94.1%	49.6%	81.9%	35.2%	14.2%	85.5%	**0.6%**	96.7%	20.2%
1954	1972	12.5%	98.5%	89.9%	87.4%	57.0%	83.7%	26.7%	12.1%	69.3%	**0.7%**	27.3%	15.7%
1955	1973	23.1%	88.8%	74.8%	81.4%	51.5%	96.9%	16.8%	49.7%	69.8%	**0.8%**	27.0%	12.0%
1956	1974	20.4%	86.8%	82.2%	84.4%	46.5%	93.6%	30.8%	32.3%	68.1%	**0.5%**	20.8%	13.4%
1957	1975	27.2%	91.5%	75.5%	72.0%	53.5%	86.5%	20.2%	32.9%	72.7%	**1.3%**	40.0%	15.6%
1958	1976	27.8%	97.5%	62.6%	57.5%	58.5%	92.0%	10.1%	32.9%	73.2%	**1.4%**	47.1%	11.3%
1959	1977	42.3%	90.7%	59.8%	62.4%	82.5%	91.5%	5.9%	32.0%	78.1%	**1.6%**	45.2%	16.5%
1960	1978	56.2%	34.3%	64.7%	58.8%	94.7%	93.5%	6.8%	33.7%	90.1%	**1.0%**	46.5%	23.4%
1961	1979	73.0%	35.6%	65.2%	51.6%	97.3%	85.6%	13.2%	43.4%	86.4%	**0.9%**	18.7%	20.9%
1962	1980	62.4%	33.9%	71.0%	65.1%	95.5%	80.7%	13.7%	37.5%	45.3%	**0.3%**	13.4%	14.4%
1963	1981	42.0%	33.8%	15.5%	73.9%	99.6%	84.6%	12.8%	55.7%	44.0%	**0.6%**	8.5%	16.0%
1964	1982	63.6%	33.9%	12.2%	66.9%	87.8%	78.9%	10.3%	58.5%	75.0%	**1.2%**	10.1%	12.8%
1965	1983	66.1%	30.8%	14.8%	55.2%	79.3%	86.1%	7.7%	61.2%	79.1%	**1.2%**	14.2%	22.4%
1966	1984	57.9%	30.5%	19.7%	42.4%	81.5%	81.6%	**5.0%**	65.1%	79.8%	**0.7%**	20.0%	25.3%
1967	1985	48.9%	31.7%	20.1%	41.4%	86.9%	84.8%	7.2%	98.3%	62.7%	**1.6%**	18.8%	16.9%
1968	1986	82.0%	31.0%	12.1%	64.0%	84.5%	91.8%	**4.9%**	95.9%	48.2%	**2.1%**	22.8%	18.4%
1969	1987	91.0%	30.5%	9.6%	61.0%	83.5%	88.3%	5.9%	90.7%	28.9%	**1.7%**	27.8%	18.5%
1970	1988	90.6%	29.2%	12.7%	57.6%	80.5%	85.7%	9.1%	71.1%	60.3%	**2.4%**	52.3%	12.8%
1971	1989	92.9%	31.1%	13.3%	85.6%	82.3%	87.8%	8.3%	73.7%	63.6%	**2.4%**	54.7%	11.6%
1972	1990	89.4%	32.6%	5.4%	99.4%	83.1%	22.7%	8.2%	70.7%	58.8%	6.0%	84.4%	14.4%
1973	1991	77.1%	32.9%	**2.3%**	64.0%	75.2%	18.5%	15.2%	63.8%	52.1%	7.2%	86.6%	15.7%
1974	1992	53.1%	35.4%	**2.6%**	92.5%	74.0%	19.4%	23.5%	92.7%	65.5%	12.8%	91.1%	16.0%
1975	1993	57.5%	33.0%	**2.0%**	77.8%	74.2%	18.0%	25.7%	96.3%	54.7%	29.5%	79.6%	24.3%
1976	1994	61.8%	33.4%	**2.5%**	87.0%	68.9%	36.1%	52.7%	96.3%	56.0%	36.5%	87.0%	32.8%

Start	End	Jan	Feb	Mar	Apr	May	Jun	Jul	Aug	Sep	Oct	Nov	Dec
1977	1995	67.0%	32.8%	**2.8%**	83.3%	66.4%	39.6%	76.7%	92.5%	75.4%	22.9%	88.5%	30.4%
1978	1996	83.7%	32.9%	**2.7%**	67.8%	42.4%	35.5%	69.9%	98.1%	64.3%	20.2%	66.4%	25.8%
1979	1997	89.6%	92.5%	**2.1%**	79.5%	27.6%	47.4%	82.8%	94.7%	55.9%	16.0%	55.8%	14.9%
1980	1998	97.1%	97.9%	6.3%	84.5%	29.1%	51.6%	52.1%	87.2%	51.3%	12.4%	34.8%	11.1%
1981	1999	97.6%	79.4%	**4.5%**	74.5%	37.6%	42.7%	59.9%	97.5%	49.2%	20.2%	45.5%	15.4%
1982	2000	70.7%	85.5%	14.9%	64.0%	36.6%	41.4%	63.7%	66.3%	49.1%	22.4%	24.0%	19.2%
1983	2001	88.0%	70.2%	21.7%	60.5%	49.9%	77.2%	89.8%	70.9%	24.7%	35.3%	33.8%	21.3%
1984	2002	97.9%	40.1%	19.7%	22.8%	56.5%	72.1%	99.6%	74.6%	21.7%	30.6%	43.8%	13.2%
1985	2003	99.7%	37.5%	22.9%	15.5%	52.2%	70.8%	88.2%	69.6%	26.0%	52.6%	59.3%	27.9%
1986	2004	95.0%	74.6%	22.6%	34.1%	45.4%	67.7%	89.9%	26.9%	42.2%	49.1%	52.7%	33.6%
1987	2005	73.7%	75.0%	35.1%	59.2%	40.5%	68.2%	70.7%	46.8%	75.1%	28.2%	50.4%	46.1%
1988	2006	69.8%	83.3%	20.7%	52.4%	48.3%	71.8%	73.8%	43.3%	65.4%	29.5%	45.5%	36.8%
1989	2007	66.4%	64.6%	18.5%	66.5%	47.2%	78.6%	79.7%	21.4%	69.5%	30.7%	67.2%	30.9%
1990	2008	68.5%	72.9%	30.1%	86.1%	42.1%	78.8%	85.4%	20.1%	93.5%	49.6%	62.9%	33.2%
1991	2009	82.1%	70.0%	31.4%	99.6%	38.8%	78.1%	95.8%	17.5%	97.2%	43.3%	85.2%	42.9%
1992	2010	93.2%	99.6%	67.5%	61.4%	38.4%	83.1%	98.0%	16.3%	97.6%	43.9%	77.3%	82.2%
1993	2011	57.9%	64.9%	72.2%	77.0%	39.6%	67.9%	83.8%	22.3%	82.3%	35.2%	49.1%	85.2%
1994	2012	61.2%	84.0%	68.0%	77.2%	45.5%	69.7%	88.1%	25.0%	92.6%	40.4%	53.7%	68.8%
1995	2013	45.6%	75.4%	77.0%	72.8%	44.7%	56.7%	87.2%	25.8%	96.6%	44.9%	57.5%	65.1%
1996	2014	47.1%	75.3%	80.9%	95.0%	44.4%	80.9%	76.2%	46.5%	84.7%	73.3%	46.5%	70.8%
1997	2015	44.8%	76.6%	83.9%	86.5%	89.3%	89.8%	99.3%	97.3%	91.0%	77.8%	44.5%	74.2%
1998	2016	79.5%	59.7%	80.0%	79.0%	90.1%	97.0%	89.0%	93.5%	91.4%	98.1%	39.8%	73.5%
1999	2017	69.7%	81.0%	92.9%	98.6%	87.6%	85.7%	85.7%	100.0%	94.5%	92.8%	77.5%	72.3%
2000	2018	99.6%	95.9%	83.5%	95.8%	95.1%	94.9%	85.3%	97.7%	95.3%	98.9%	56.2%	91.6%
2001	2019	100.0%	100.0%	100.0%	100.0%	100.0%	100.0%	100.0%	100.0%	100.0%	100.0%	100.0%	100.0%

	Zero difference				*Somewhat Different*		*Significantly Different*				*Completely Different*	
P-value Gradient:	100.0%	80.0%	60.0%	40.0%	20.0%	10.0%	**5.0%**	**4.0%**	**3.0%**	**2.0%**	**1.0%**	**0.0%**

To downscale air temperature, an hourly diurnal temperature cycled will be derived for each season using observed temperature data. This cycle will be scaled to the daily temperature values to generate hourly air temperature. To downscale solar radiation, an hourly diurnal temperature cycled will be derived for each season using observed radiation data. This cycle will be scaled to the daily solar radiation values to generate hourly solar radiation. Hourly dew point data will be calculated by scaling the hourly downscaled air temperature.

4 TASK 5C. BASELINE UNIT-AREA MODELING ANALYSIS

This section describes the methodology to develop a set of unique hydrologic response units (HRUs) representing the land use, land cover, soil, and slope characteristics in the Taunton basin. Each HRU represents areas of similar physical characteristics attributable to core processes identified through GIS overlays. The HRU layer combines spatial information into a single raster layer with identified 36 unique categories. The unit-area HRU time series for the baseline conditions will be developed using the most recent 20-year period of observed meteorological boundary conditions and calibrating the rainfall-runoff response on each HRU along with reach routing processes in the LSPC model under Task 6. The estimates of the changes in average annual volumes of runoff, recharge, ET, and pollutant load export for each source HRU category will also be performed under Task 6 when the LSPC model is calibrated.

4.1 HRUs Development

Within LSPC, the land is categorized into HRUs, which are the core hydrologic modeling land units in the watershed model. Each HRU represents areas of similar physical characteristics attributable to certain processes. The HRU development process uses these three primary data types that are typically closely associated with hydrology in the watershed.

- **Land Use – Land Cover:** *Land use describes the principal programmatic use and/or vegetation type. The programmatic, or zoning, element of this attribute is critical for water quality simulation. The land cover defines landscape as having either pervious or impervious cover.*
- **Hydrologic Soil Group:** *Represents one of four soil classes (i.e., A, B, C, and D) commonly associated with a spectrum of infiltration rates with HSG-A having the highest and HSG-D having the lowest.*
- **Landscape Slope:** *Represents the overland flow slope derived from a digital elevation model. The percent slope was categorized into three groups: low (<5%), medium (5% - 15%), and high (>15%).*

The HRU-based approach reflects the key physical features that influence runoff and pollutant loadings such as land use, slope, soils, and impervious cover and is based on the best available local datasets characterizing existing conditions for the Taunton basin. The raster combination of these dataset characteristics determined the number of possible HRU categories considered for the model. Ultimately, some consolidation of HRUs was implemented to balance the need for spatial resolution with model simulation efficiency, resulting in a set of meaningful HRUs for model configuration. Figure 62 shows the three spatial layers used to create the mapped HRU raster.

4.1.1 *Land Use – Land Cover Reclassification*

Land use categories indicate activities taking place at the parcel-scale (e.g., industrial use) and are important for characterizing the hydrologic and water quality responses from those areas (Huang et al., 2013; Tong and Chen, 2002; Tunsaker and Levine, 1995). Land cover designations supplement land use categories by providing additional texture to parcel descriptions, enabling their hydrologic and water quality response to be further characterized (Wilson, 2015). MassGIS (Bureau of Geographic Information) 2016 land use – land cover layer contains both land use and land cover information as separate attributes and can be accessed independently or in a useful combination with one another. For example, it is possible to measure the

portions of pervious and impervious surfaces for a commercial parcel. The land cover information in this layer is consistent with Coastal Change Analysis Program(C-CAP)'s high-resolution land cover classification scheme. For more information on the data development process and data accuracy reporting, see the full detailed description (PDF) document. For HRU development, the MassGIS 2016 land use – land cover attributes were reclassified to 15 unique either pervious or impervious land segments as shown in Table 22.

4.1.2 *Hydrologic Soil Group Reclassification*

HSGs characterize the propensity for precipitation to saturate and percolate through the subsurface or contribute to runoff. Soils with similar hydrologic and physical properties (e.g., texture, permeability) are grouped by HSGs (USDA, 2003, Table 23). HSG-A generally has the highest infiltration and lowest runoff potential whereas HSG-D has the lowest infiltration and highest runoff potential. HSG classifications are used within the model as a basis for setting certain hydrologic parameters including infiltration rates.

HSG designations for the Taunton basin were obtained from the Natural Resources Conservation Service (NRCS) Soil Survey Geographic Database (USDA, 2019)s and the State Soil Geographic (STATSGO2) Database. As shown in Table 23, some HSG designations were unspecified in the SSURGO database which were assigned a HSG from the STATSGO2 database or contained dual HSG assignments, therefore a conservative assumption to assign all as HSG-D was applied.

4.1.3 *Slope Group Reclassification*

A DEM is a raster-based dataset describing the elevation of the landscape across a regular grid. DEMs are useful for performing drainage studies in determining flow direction and are used to derive the landscape slope, defined as the change in elevation over a set distance. The slope was calculated from the USGS National Elevation Dataset (NED) product for the contiguous United States and clipped to the Taunton basin (USGS, 2002). Slopes were categorized as low (< 5%), medium (5% - 15%) and high (> 15%) as shown in Table 24.

4.1.4 *Mapped HRU Categories*

Each of the three spatial datasets described above (land use - land cover, HSG, and slope) were spatially joined in GIS to derive a composite raster. The resulting raster and attribute table were reclassified into 36 unique mapped HRUs (Table 25).

The spatial distribution of mapped HRUs for the Taunton basin is shown in Figure 63. The spatial distribution of mapped HRUs for Lower Hodges Brook, Upper Hodges Brook, Pilot Tributary, and Wading River are shown in Figure 64.

Table 22. Land use – Land cover reclassification

Land Cover Code	Land Cover Description	Land Use Code	Land Use Description	Land Use Reclassification	Cover Type
2	Impervious	0	Unknown	Paved Open Land	Impervious
2	Impervious	2	Open land	Paved Open Land	Impervious
2	Impervious	3	Commercial	Paved Commercial	Impervious
2	Impervious	4	Industrial	Paved Industrial	Impervious
2	Impervious	6	Forest	Paved Forest	Impervious
2	Impervious	7	Agriculture	Paved Agriculture	Impervious
2	Impervious	8	Recreation	Paved Open Land	Impervious
2	Impervious	9	Tax exempt	Paved Open Land	Impervious
2	Impervious	10	Mixed use, primarily residential	Paved Medium Density Residential	Impervious
2	Impervious	11	Residential - single family	Paved Low Density Residential	Impervious
2	Impervious	12	Residential - multi-family	Paved High Density Residential	Impervious
2	Impervious	13	Residential - other	Paved Medium Density Residential	Impervious
2	Impervious	20	Mixed use, other	Paved Open Land	Impervious
2	Impervious	30	Mixed use, primarily commercial	Paved Commercial	Impervious
2	Impervious	55	Right-of-way	Paved Transportation	Impervious
2	Impervious	88	Water	Paved Open Land	Impervious
5	Developed Open Space	N/A	N/A	Developed Open Space	Pervious
6	Cultivated	N/A	N/A	Agriculture	Pervious
7	Pasture/Hay	N/A	N/A	Agriculture	Pervious
8	Grassland	N/A	N/A	Agriculture	Pervious
9	Deciduous Forest	N/A	N/A	Forest	Pervious
10	Evergreen Forest	N/A	N/A	Forest	Pervious
12	Scrub/Shrub	N/A	N/A	Agriculture	Pervious
13	Palustrine Forested Wetland	N/A	N/A	Forested Wetland	Pervious
14	Palustrine Scrub/Shrub Wetland	N/A	N/A	Non-Forested Wetland	Pervious
15	Palustrine Emergent Wetland	N/A	N/A	Non-Forested Wetland	Pervious
18	Estuarine Emergent Wetland	N/A	N/A	Water	Pervious
19	Unconsolidated Shore	N/A	N/A	Water	Pervious
20	Bare Land	N/A	N/A	Developed Open Space	Pervious
21	Water	N/A	N/A	Water	Pervious
22	Palustrine Aquatic Bed	N/A	N/A	Water	Pervious

Table 23. Soil – HSG reclassification

HSG - SSURGO	HSG - STATSGO2	HSG Reclassification	Justification
No Data	A	A	When no other information was available, the STATSGO2 data layer was used to fill the gaps. -
No Data	B	B	
No Data	C	C	
No Data	D	D	
A	N/A	A	
A/D	N/A	D	Dual HSGs were represented, and their undrained condition ('D') was selected as a conservative choice.
B	N/A	B	-
B/D	N/A	D	Dual HSGs were represented, and their undrained condition ('D') was selected as a conservative choice.
C	N/A	C	-
C/D	N/A	D	Dual HSGs were represented, and their undrained condition ('D') was selected as a conservative choice.
D	N/A	D	-

Table 24. Percent slope reclassification

Percent Slope	Slope Reclassification
<5%	Low
5% - 15%	Medium
>15%	High

Table 25. Final HRU categories

HRU Code	HRU Description	Land Use	Soil	Slope	Land Cover
1001	Paved Forest	Paved Forest	N/A	N/A	Impervious
2001	Paved Agriculture	Paved Agriculture	N/A	N/A	Impervious
3001	Paved Commercial	Paved Commercial	N/A	N/A	Impervious
4001	Paved Industrial	Paved Industrial	N/A	N/A	Impervious
5001	Paved Low Density Residential	Paved Low Density Residential	N/A	N/A	Impervious
6001	Paved Medium Density Residential	Paved Medium Density Residential	N/A	N/A	Impervious
7001	Paved High Density Residential	Paved High Density Residential	N/A	N/A	Impervious
8001	Paved Transportation	Paved Transportation	N/A	N/A	Impervious
9001	Paved Open Land	Paved Open Land	N/A	N/A	Impervious
10110	Developed OpenSpace-A-Low	Developed OpenSpace	A	Low	Pervious
10120	Developed OpenSpace-A-Med	Developed OpenSpace	A	Med	Pervious
10210	Developed OpenSpace-B-Low	Developed OpenSpace	B	Low	Pervious
10220	Developed OpenSpace-B-Med	Developed OpenSpace	B	Med	Pervious
10310	Developed OpenSpace-C-Low	Developed OpenSpace	C	Low	Pervious
10320	Developed OpenSpace-C-Med	Developed OpenSpace	C	Med	Pervious
10410	Developed OpenSpace-D-Low	Developed OpenSpace	D	Low	Pervious
10420	Developed OpenSpace-D-Med	Developed OpenSpace	D	Med	Pervious
11000	Forested Wetland	Forested Wetland	N/A	N/A	Pervious
12000	Non-Forested Wetland	Non-Forested Wetland	N/A	N/A	Pervious
13110	Forest-A-Low	Forest	A	Low	Pervious
13120	Forest-A-Med	Forest	A	Med	Pervious
13210	Forest-B-Low	Forest	B	Low	Pervious
13220	Forest-B-Med	Forest	B	Med	Pervious
13310	Forest-C-Low	Forest	C	Low	Pervious
13320	Forest-C-Med	Forest	C	Med	Pervious
13410	Forest-D-Low	Forest	D	Low	Pervious
13420	Forest-D-Med	Forest	D	Med	Pervious
14110	Agriculture-A-Low	Agriculture	A	Low	Pervious
14120	Agriculture-A-Med	Agriculture	A	Med	Pervious
14210	Agriculture-B-Low	Agriculture	B	Low	Pervious
14220	Agriculture-B-Med	Agriculture	B	Med	Pervious
14310	Agriculture-C-Low	Agriculture	C	Low	Pervious
14320	Agriculture-C-Med	Agriculture	C	Med	Pervious
14410	Agriculture-D-Low	Agriculture	D	Low	Pervious
14420	Agriculture-D-Med	Agriculture	D	Med	Pervious
15000	Water	Water	N/A	N/A	Pervious

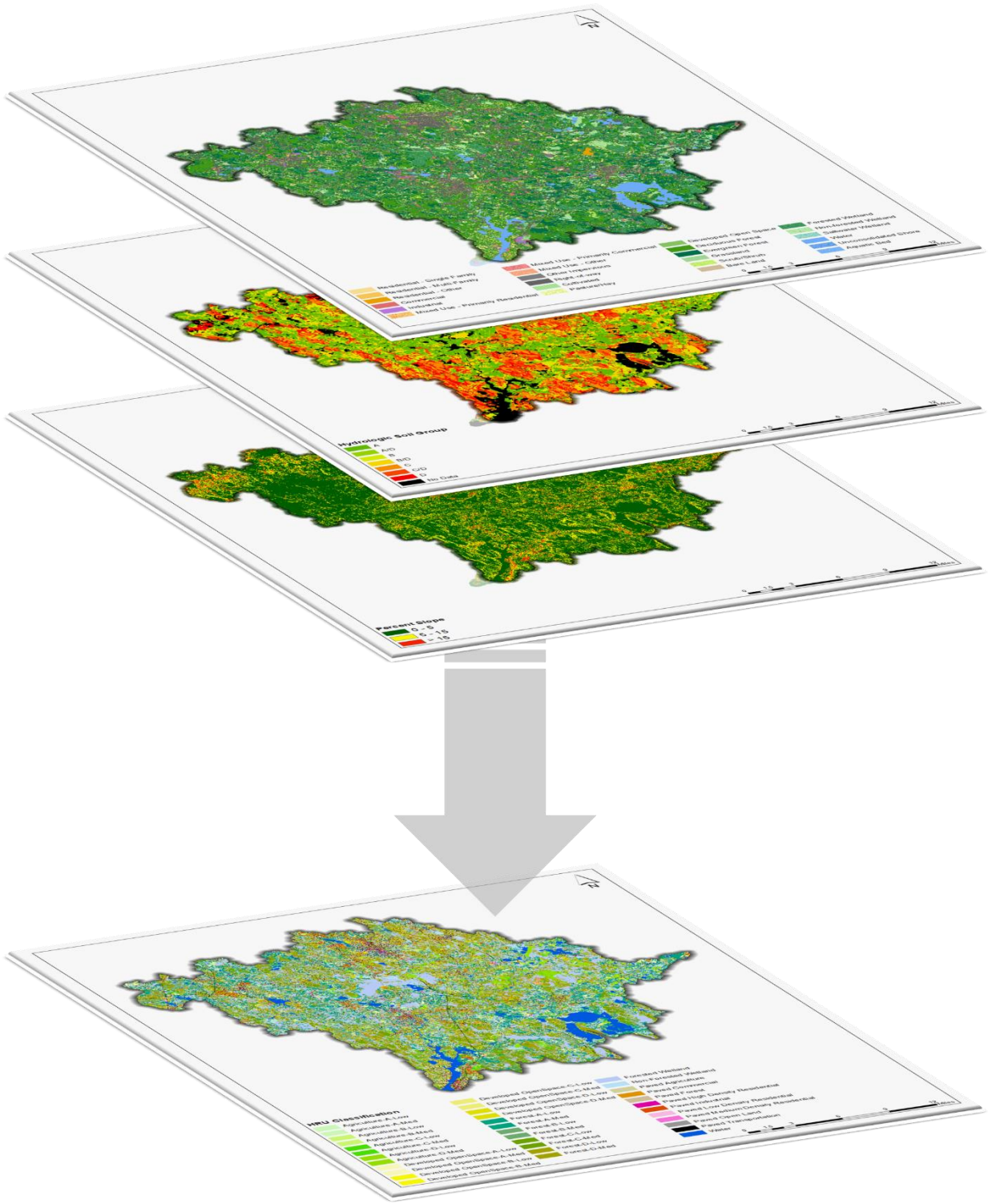

Figure 62. Mapped HRUs process (spatial overlay of land use – land cover, soil, and slope layers).

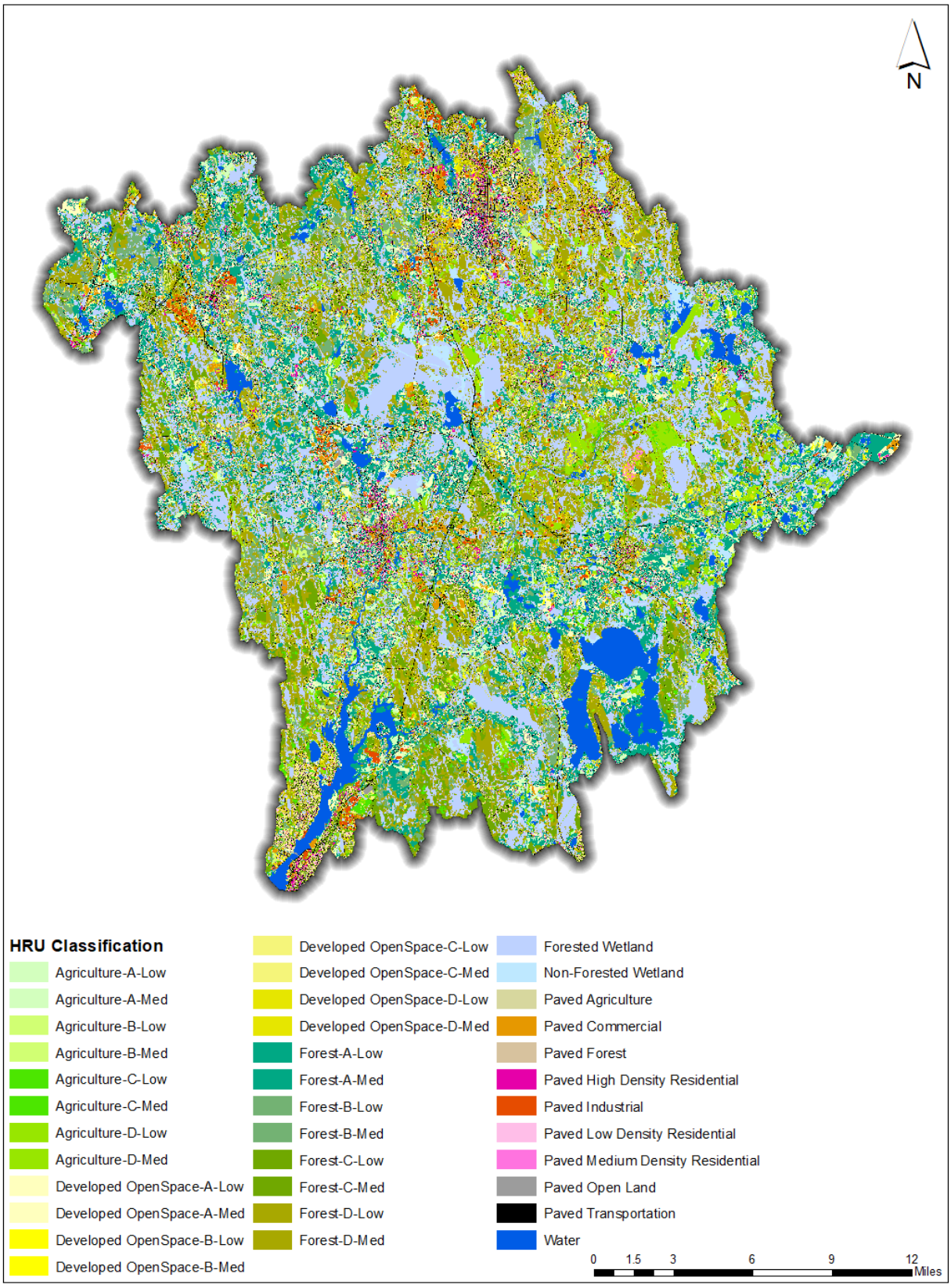

Figure 63. Mapped HRUs for the Taunton basin.

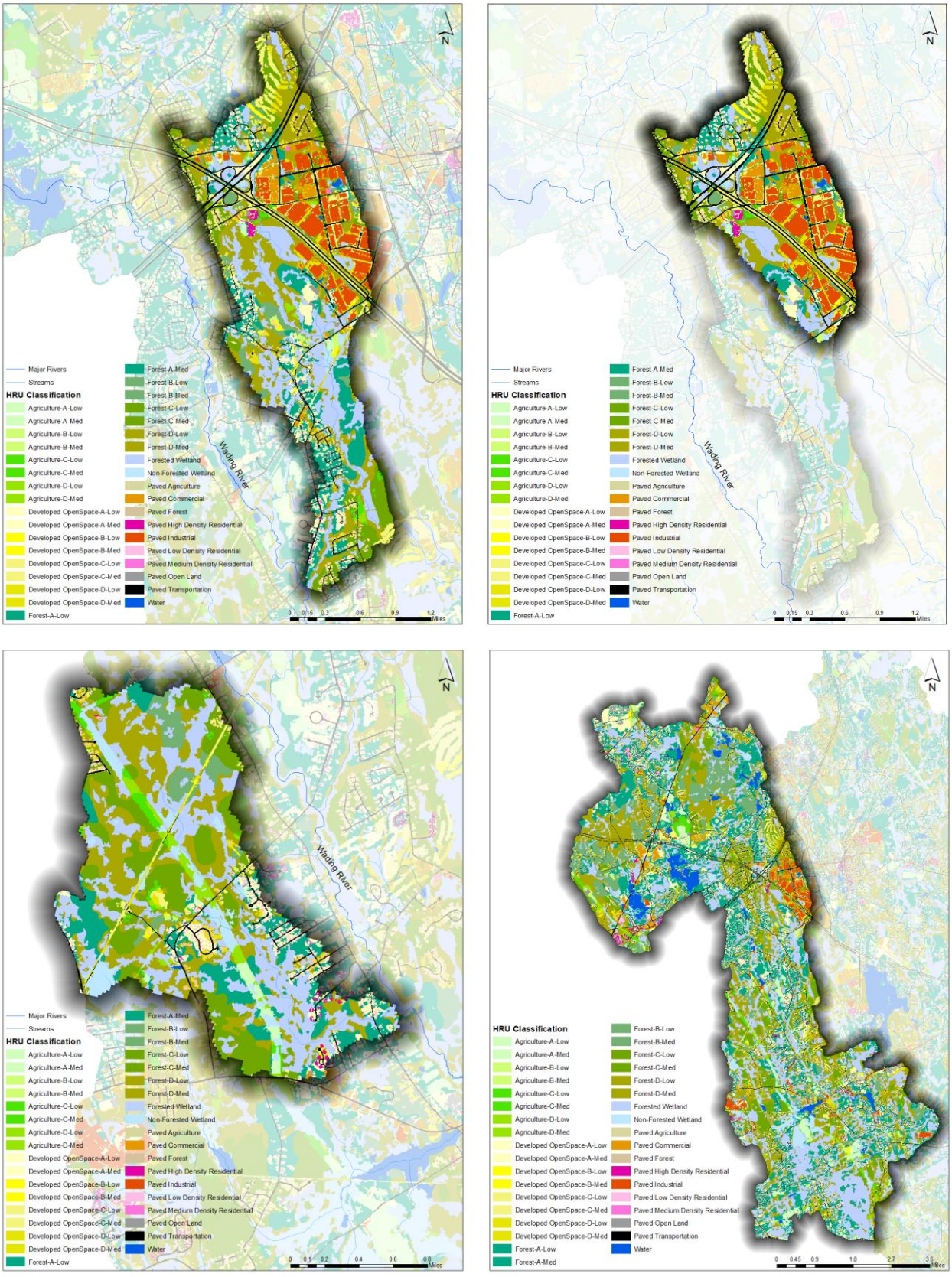

Figure 64. Mapped HRUs for Lower Hodges Brook (top left), Upper Hodges Brook (top right), Pilot Tributary (bottom left), and Wading River (bottom right).

4.1.5 *Directly Connected Impervious Area*

Mapped impervious area (MIA) represents the mapped portion of impervious cover over the landscape, as represented by available spatial layers. However, the Effective Impervious Area (EIA) is the portion of the MIA that contributes to runoff, or which is directly connected to the conveyance network within the LSPC model. Estimates of Directly Connected Impervious Area (DCIA) are rarely available locally and, thus, empirical algorithms are typically used to convert MIA to DCIA for input to LSPC (Said, 2014).

EIA is derived as a function of DCIA, with other adjustments as needed to account for other structural and non-structural management practices in the flow network. Figure 65 illustrates the transitional sequence from MIA to DCIA. Runoff from impervious areas that are not connected to the drainage network may flow onto pervious surfaces, infiltrate, and become part of pervious subsurface and overland flow. Because segments are modeled as being parallel to one another in LSPC, this process can be approximated using a conversion of a portion of impervious land to pervious land. On the open landscape, runoff from disconnected impervious surfaces can overwhelm the infiltration capacity of adjacent pervious surfaces during large rainfall/runoff events creating sheet flow over the landscape—therefore, the MIA-EIA translation is not a direct linear conversion. Finding the right balance between MIA and EIA can be an important part of the hydrology calibration effort.

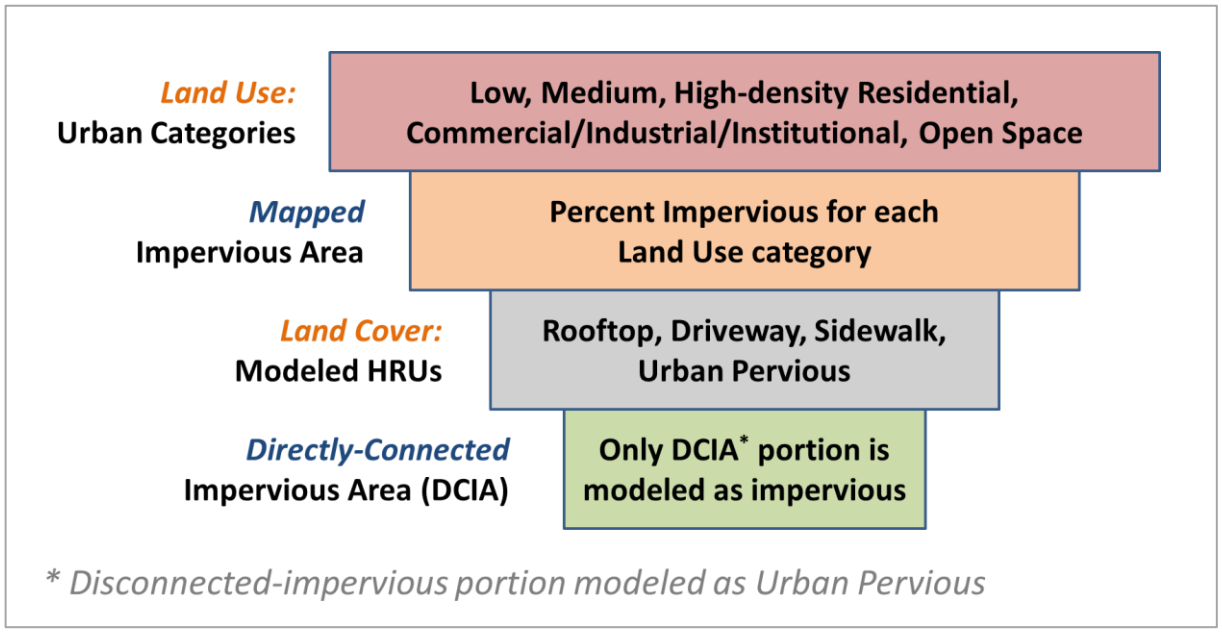

Figure 65. Translation sequence from MIA to DCIA.

The Sutherland Equations were the empirical relationships used for DCIA estimates in the LSPC model. This refinement is necessary to avoid an initial overestimation of impervious surfaces contributing to runoff before initiating process-based model calibration (Sutherland, 2000). The Sutherland Equations, presented in Figure 66, show a strong correlation between the density of the developed area and DCIA. The curve for high-density developed land trends closer to the line of equal value than the curve for less developed areas. Similarly, as the density of mapped impervious areas approaches 1.0, the translation to DCIA also approaches 1.0. An estimate of EIA equal to MIA × DCIA fraction based on the Sutherland Equations was used to adjust the MIA from the MassGIS land use – land cover layer into EIA for use in the LSPC watershed model. Impervious area summary comparing the MIA and EIA in the Wading River watershed is shown in Table 26 and the EIA from this analysis was compared with the USGS published HSPF models for the Wading River watershed (Table 27). The change form mapped to modeled areas for the Wading River watershed due to shifting in DCIA from impervious to developed pervious for each HRU type is shown in Table 28.

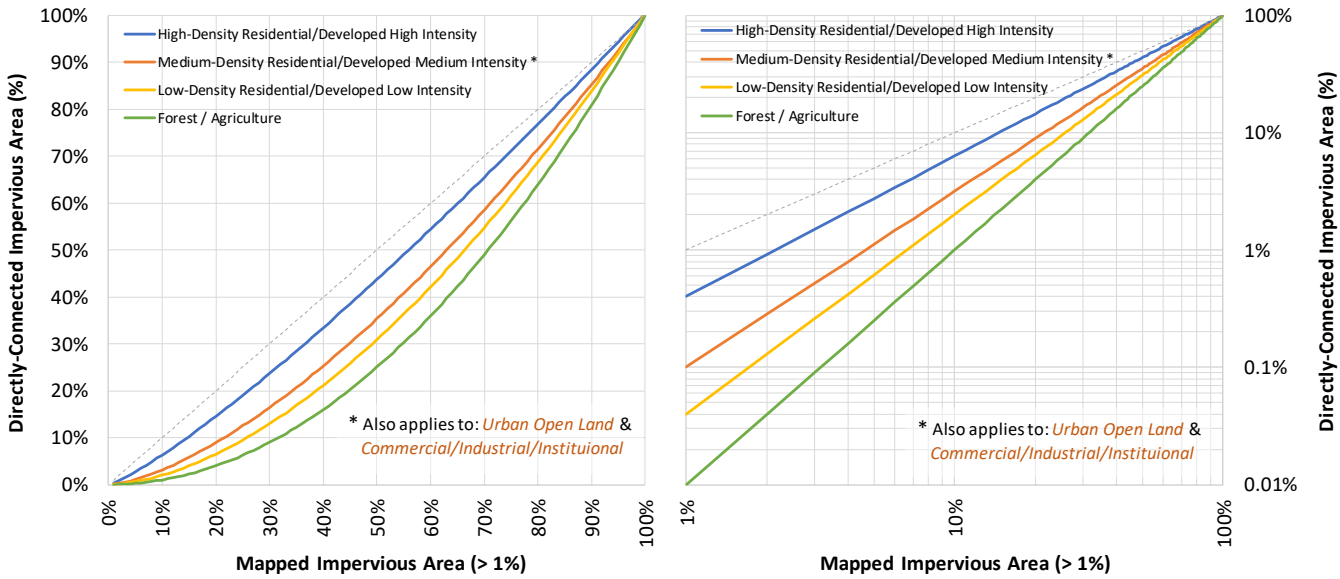

Figure 66. Relationships between Mapped and Directly Connected Impervious Area (Sutherland 2000).

Table 26. Mapped Impervious Area (MIA) and Effective Impervious Area (EIA) distribution in Wading River watershed

HRU Description	Total Impervious Area (acre)	Effective Impervious Area (acre)	EIA (%)
Paved Forest	0.3	0.0	0%
Paved Agriculture	3.4	0.0	0%
Paved Commercial	375.8	96.5	26%
Paved Industrial	366.2	103.5	28%
Paved Low Density Residential	778.4	147.4	19%
Paved Medium Density Residential	20.5	5.6	27%
Paved High Density Residential	147.4	122.3	83%
Paved Transportation	956.5	793.7	83%
Paved Open Land	245.7	61.9	25%
Total	**2,894.2**	**1,330.9**	**46%**

Table 27. HSPF and LSPC Model area comparison for Wading River watershed

Wading River Model	HSPF Model* (acre)	LSPC Model (acre)	Difference (%)
Total Impervious Area	1,367.2	1,330.9	-2.65%
Total Pervious Area	26,231.4	26,270.3	0.15%
Total	**27,598.6**	**27,601.2**	**0.01%**

* USGS published HSPF models for the Taunton basin (Barbaro and Sorenson, 2013)

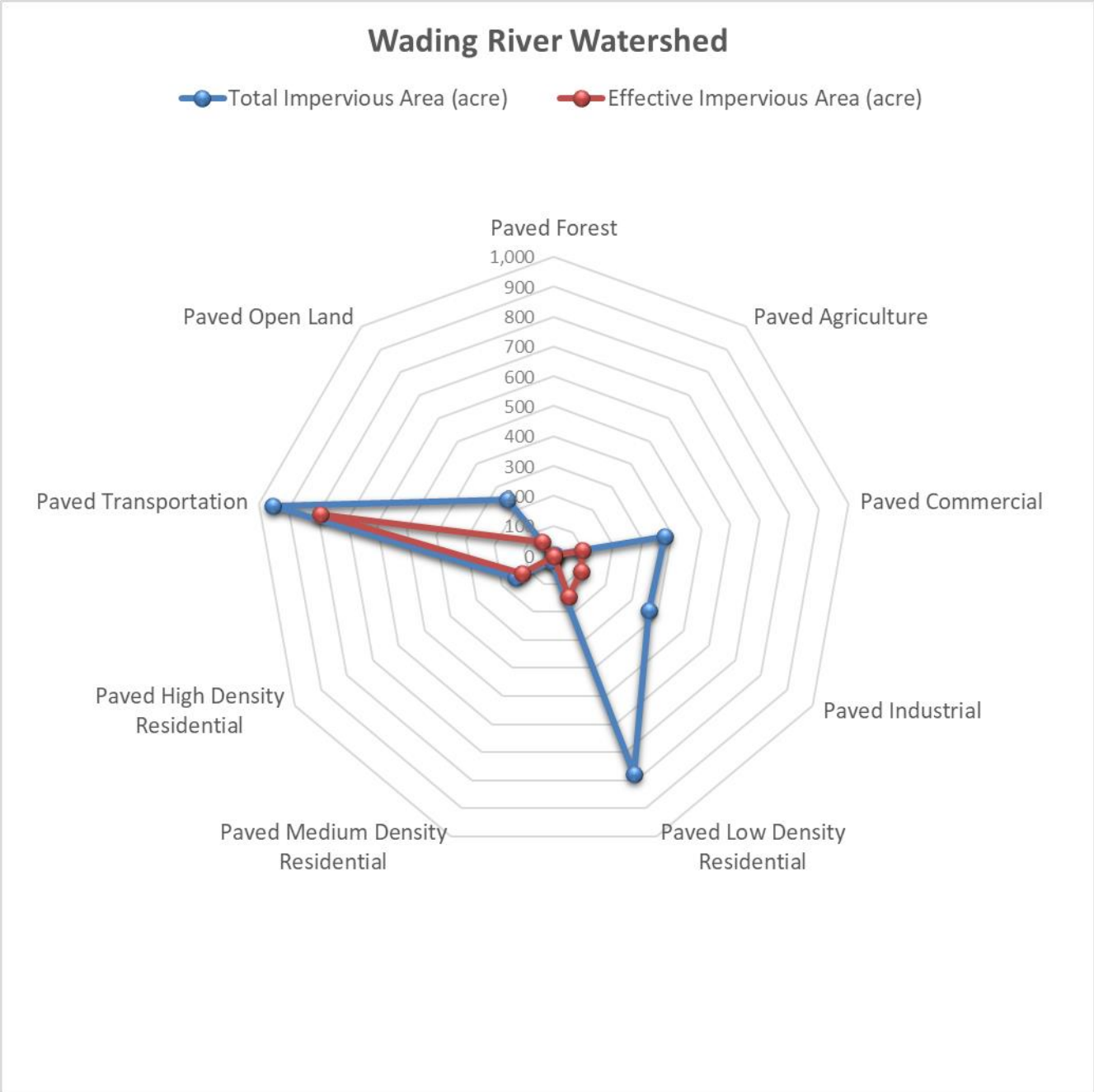

Figure 67. Mapped Impervious Area and Effective Impervious Areas distribution in Wading River watershed.

Table 28. Mapped (MIA) and Modeled (EIA) HRU area distribution in Wading River watershed

HRU Code	HRU Description	Mapped Acres	Modeled Acres	Percent Change
1001	Paved Forest	0.3	0.0	-100.0%
2001	Paved Agriculture	3.4	0.0	-100.0%
3001	Paved Commercial	375.8	96.5	-74.3%
4001	Paved Industrial	366.2	103.5	-71.8%
5001	Paved Low Density Residential	778.4	147.4	-81.1%
6001	Paved Medium Density Residential	20.5	5.6	-72.8%

HRU Code	HRU Description	Mapped Acres	Modeled Acres	Percent Change
7001	Paved High Density Residential	147.4	122.3	-17.1%
8001	Paved Transportation	956.5	793.7	-17.0%
9001	Paved Open Land	245.7	61.9	-74.8%
10110	Developed OpenSpace-A-Low	1,572.4	2,262.1	43.9%
10120	Developed OpenSpace-A-Med	301.9	431.6	43.0%
10210	Developed OpenSpace-B-Low	203.9	301.5	47.9%
10220	Developed OpenSpace-B-Med	130.1	191.6	47.3%
10310	Developed OpenSpace-C-Low	479.1	739.0	54.2%
10320	Developed OpenSpace-C-Med	134.6	194.0	44.2%
10410	Developed OpenSpace-D-Low	446.5	677.8	51.8%
10420	Developed OpenSpace-D-Med	89.4	119.8	33.9%
11000	Forested Wetland	5,281.2	5,281.2	0.0%
12000	Non-Forested Wetland	720.0	720.0	0.0%
13110	Forest-A-Low	2,949.9	2,949.9	0.0%
13120	Forest-A-Med	2,006.5	2,006.5	0.0%
13210	Forest-B-Low	750.1	750.2	0.0%
13220	Forest-B-Med	1,535.8	1,535.8	0.0%
13310	Forest-C-Low	1,460.5	1,460.5	0.0%
13320	Forest-C-Med	564.4	564.5	0.0%
13410	Forest-D-Low	2,821.1	2,821.1	0.0%
13420	Forest-D-Med	1,447.7	1,447.7	0.0%
14110	Agriculture-A-Low	417.8	418.8	0.2%
14120	Agriculture-A-Med	203.4	203.4	0.0%
14210	Agriculture-B-Low	82.0	82.1	0.2%
14220	Agriculture-B-Med	53.6	53.6	0.0%
14310	Agriculture-C-Low	106.1	106.1	0.0%
14320	Agriculture-C-Med	70.8	70.8	0.0%
14410	Agriculture-D-Low	196.2	198.4	1.1%
14420	Agriculture-D-Med	33.1	33.1	0.1%
15000	Water	649.2	649.2	0.0%
	Total	**27,601.2**	**27,601.2**	**0.0%**

The effective impervious areas have no spatial representation in GIS. For example, a commercial parcel has mapped impervious areas with no spatial reference of directly connected impervious areas. A peppering approach was developed to assign a pervious HRU category to the disconnected impervious areas (MIA – EIA) within the same commercial parcel. The approach uses a probabilistic raster reclassification algorithm to modify an existing HRU raster and replace individual HRU cells with new ones. The result of the probabilistic reclassification is a raster that has reclassified pixels scattered throughout it. Figure 68 shows the comparison between mapped HRUs and peppered HRUs for the Upper Hodges Brook sub-watershed.

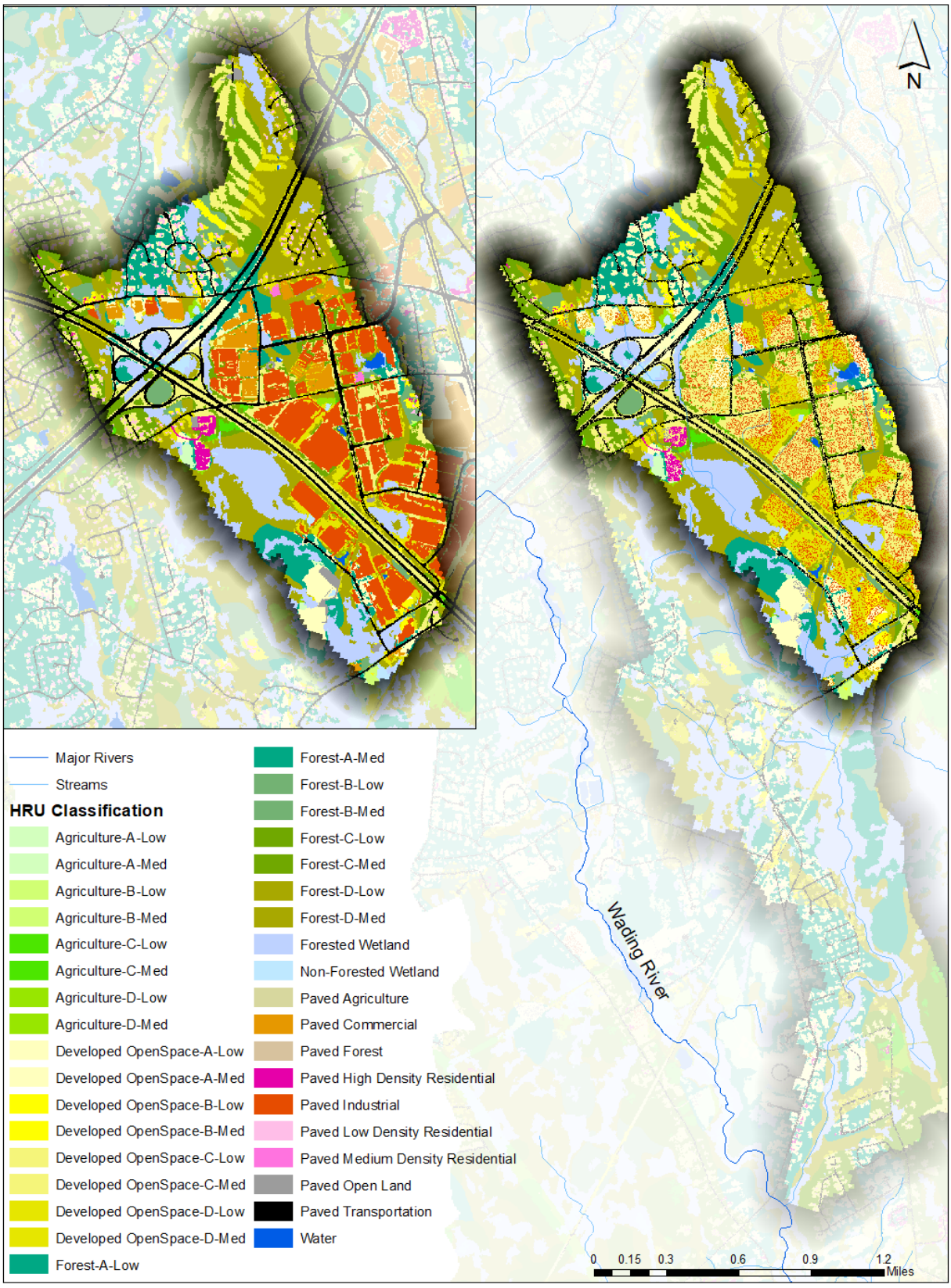

Figure 68. Peppered HRUs representing the effective impervious areas for Upper Hodges Brook (MIA on left and EIA on right).

4.2 Baseline Unit-Area HRU Time Series

The baseline time series for unit-area HRU time series will be developed under Task 6 when the LSPC model is configured and calibrated for the Wading River watershed.

4.2.1 *Water Balance and Loading Analysis*

The water balance and pollutant loading analysis will be performed under Task 6 when the LSPC model is configured and calibrated for the Wading River watershed.

4.2.2 *Factsheet Development*

The results from the baseline unit-area HRU analysis will be summarized into a factsheet under Task 6 when the LSPC model is configured and calibrated for the Wading River watershed.

5 COMPARISON OF FLOW METRICS FOR HISTORIC AND CURRENT CONDITIONS

Several flow metrics are presented below to compare the current condition time-period (water-year 2001-2019) to the historical condition (water-year 1972-1990). The analysis presented in Section 3 (Figure 61 and Table 21) identified 1972-1990 and 2001-2019 as being similar to average precipitation volume and relative distribution of rainfall days. In later Tasks, similar comparisons may be performed to investigate similarities and differences between modeled output, such as a baseline simulation and one in which next-generation stormwater management strategies have been implemented.

Figure 69 compares the FDC of streamflow in the Wading River for 2001-2019 vs. 1972-1990 and highlights the ecosurplus and ecodeficit portions of the curve. Relative to the 1972-1990 period, the current conditions have an ecosurplus of 5.8 cfs/day and an ecodeficit of 3.4 cfs/day. Table 29 presents IHA parameters for the two periods and the percent difference between them. A limitation of the analysis is that it does not currently account for natural variability and whether differences are statistically significant. Methods such as the Range of Variability Approach (RVA) may help account for variability and have been used to identify changes to IHA parameters due to dam construction (Richter et al., 1997). However, for this comparison, simple % differences are used to assess the impact that development may have had on the IHA parameters. Table 29 reinforces what the ecosurplus visualization (Figure 18) and the long-term trends (Section 2.1.5) suggested; low flows in the Wading River are getting lower. There was a 43% decrease in the average flows for August between the two periods. Although, interestingly, August flows for the 1972-1990 period had higher flows compared to July and September of that same period.

Figure 70 presents a comparison of monthly average discharge. While the patterns are similar, it is noteworthy that the historic period had substantially more discharge in august compared to the period of record and current conditions (30 cfs vs 18 cfs). Figure 71 presents boxplot comparisons of monthly flow. No significant differences existed among the monthly flow values (Alpha = 0.1, non-parametric Wilcoxon test) Figure 72 presents comparisons of 3-day minimum flow for the two periods. While the R^2 values are relatively low, there does appear to be a downward trend in the current period compared to the historical period. Figure 73 presents comparisons of the 3-day maximum flows of the two periods with bankfull and mobilizing flows shown for reference. The 2001-2019 period shows more bankfull flows than the historic period. Figure 74 presents a comparison of the Richard-Baker flashiness index for the two periods. Long-term trends in flashiness were not apparent in the full period of record (Figure 33) and there do not appear to be strong trends in the 1972-1990 or 2001-2019 period.

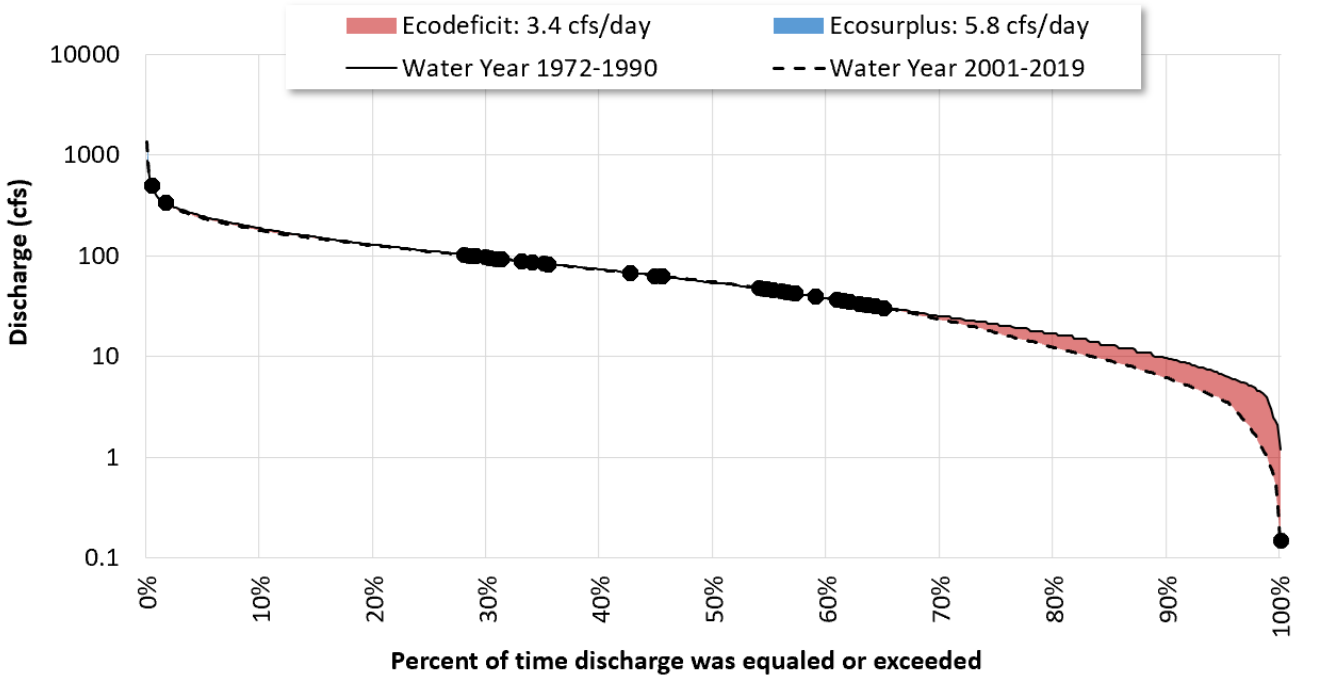

Figure 69. Ecosurplus and ecodeficit for the Wading River for 2001-2019 vs. 1972-1990. Black dots represent inflection points where the two curves change between surplus and a deficit.

Table 29. IHA parameter comparison for historical and current conditions

	1972-1990	2001-2019	% difference
Group 1. Magnitude and timing	Average (cfs)		
January	116.19	102.66	-11.65%
February	117.82	104.57	-11.25%
March	143.77	151.01	5.04%
April	140.82	147.19	4.52%
May	89.20	82.37	-7.66%
June	66.84	69.24	3.58%
July	23.91	28.51	19.22%
August	31.25	17.77	-43.15%
September	23.54	20.07	-14.77%
October	44.21	45.98	4.02%
November	75.90	74.35	-2.05%
December	107.81	105.47	-2.17%
Group 2. Magnitude and duration of annual extremes	Average (cfs)		% difference
1 day minimum	5.20	3.44	-34.0%
1 day maximum	501.32	544.25	8.6%
3 day minimum	5.98	3.54	-40.8%
3 day maximum	431.72	453.63	5.1%
7 day minimum	6.92	3.85	-44.4%
7 day maximum	351.07	361.91	3.1%
30 day minimum	11.32	7.48	-33.9%
30 day maximum	222.61	233.40	4.8%
90 day minimum	18.73	13.82	-26.2%
90 day maximum	159.32	156.19	-2.0%
Group 3. Timing of annual extremes	Average Julian Day		% difference
Julian date of annual minimum	230	249	8.30%
Julian date of annual maximum	511	529	3.51%
Group 4. Frequency and duration of high (90th percentile) and low (10th percentile) pulses	Average Count/ Average # Days		% difference
Low pulse count	453	771	70.20%
Low pulse duration (days)	7.95	12.44	56.47%
High pulse count	825	756	-8.36%
High Pulse duration (days)	6.11	5.77	-5.57%
Group 5 Rate and frequency of change	Average Count/ Average cfs		% difference
Fall rate (cfs)	4569	4826	5.62%
Fall count	22.58	22.69	0.48%
Rise rate(cfs)	1956	1982	1.33%
Rise count	4569	4826	5.62%

Table 30. Bankfull comparison for historical and current conditions

Bankfull Frequency	1972-1990	2001-2019	% difference
Average Days	9.95	9.47	-4.8%
Average Occurrences	3.53	2.89	-17.9%

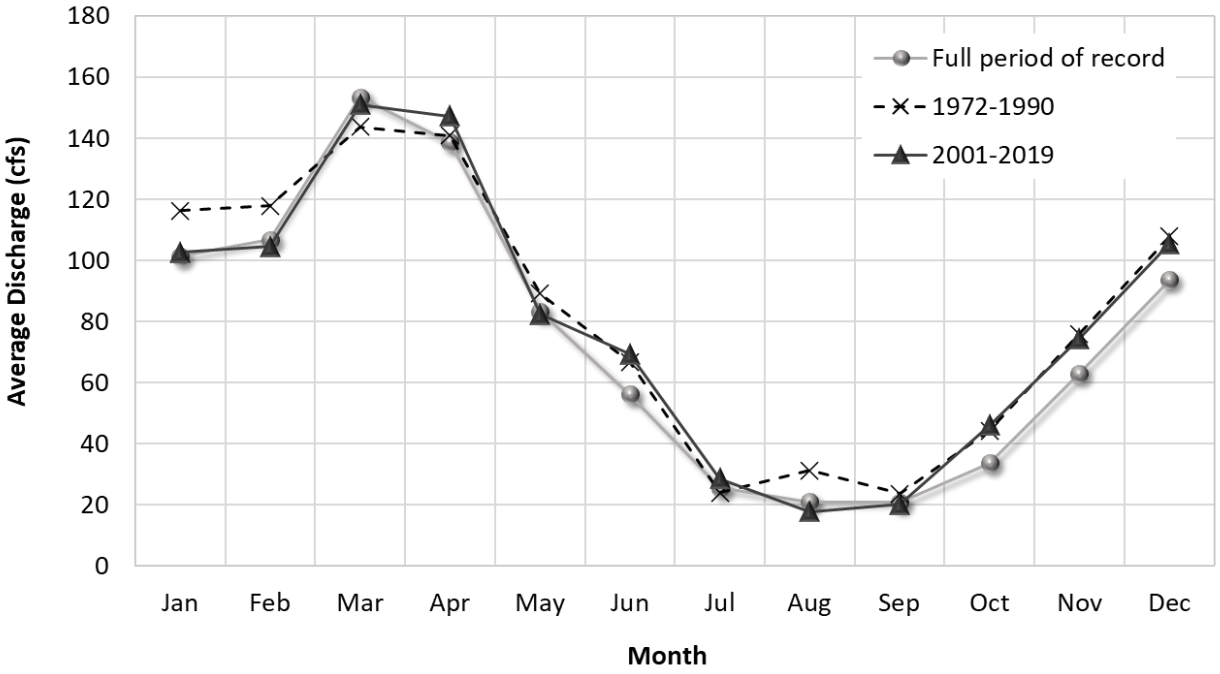

Figure 70. Monthly average discharge for the Wading River.

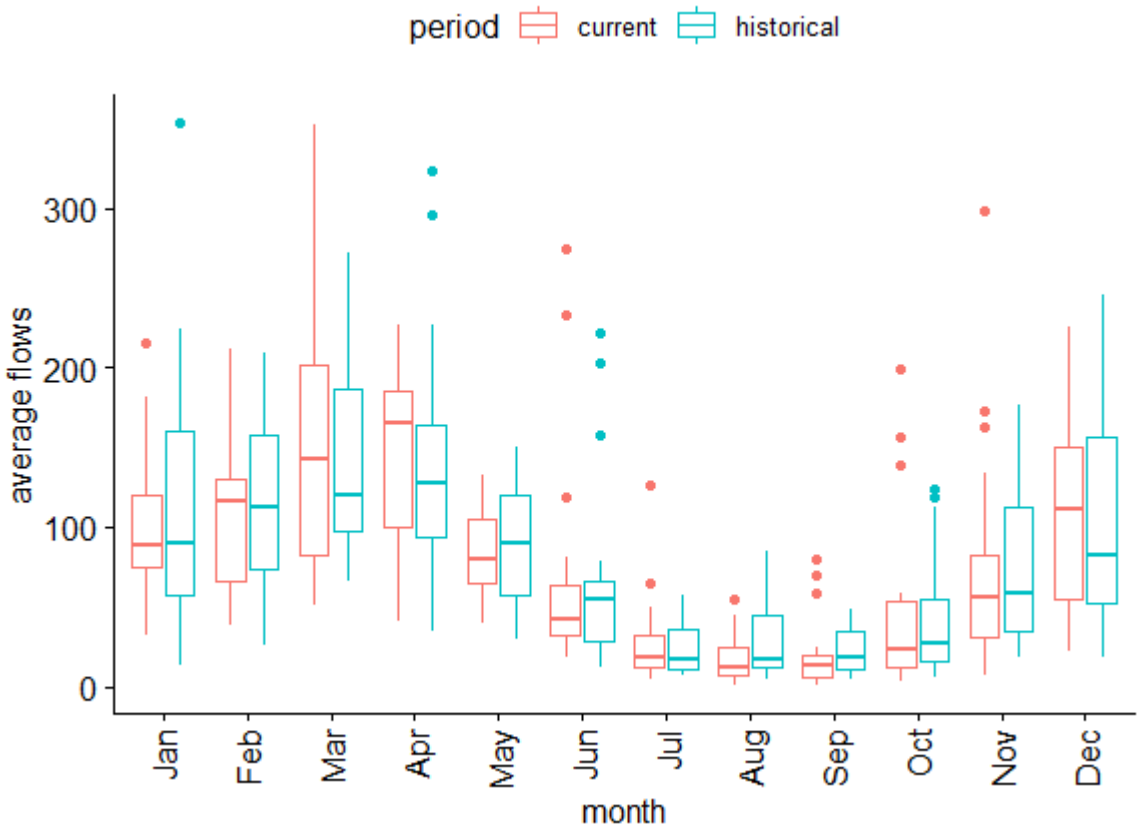

Figure 71. Box plots of monthly average discharge for the Wading River.

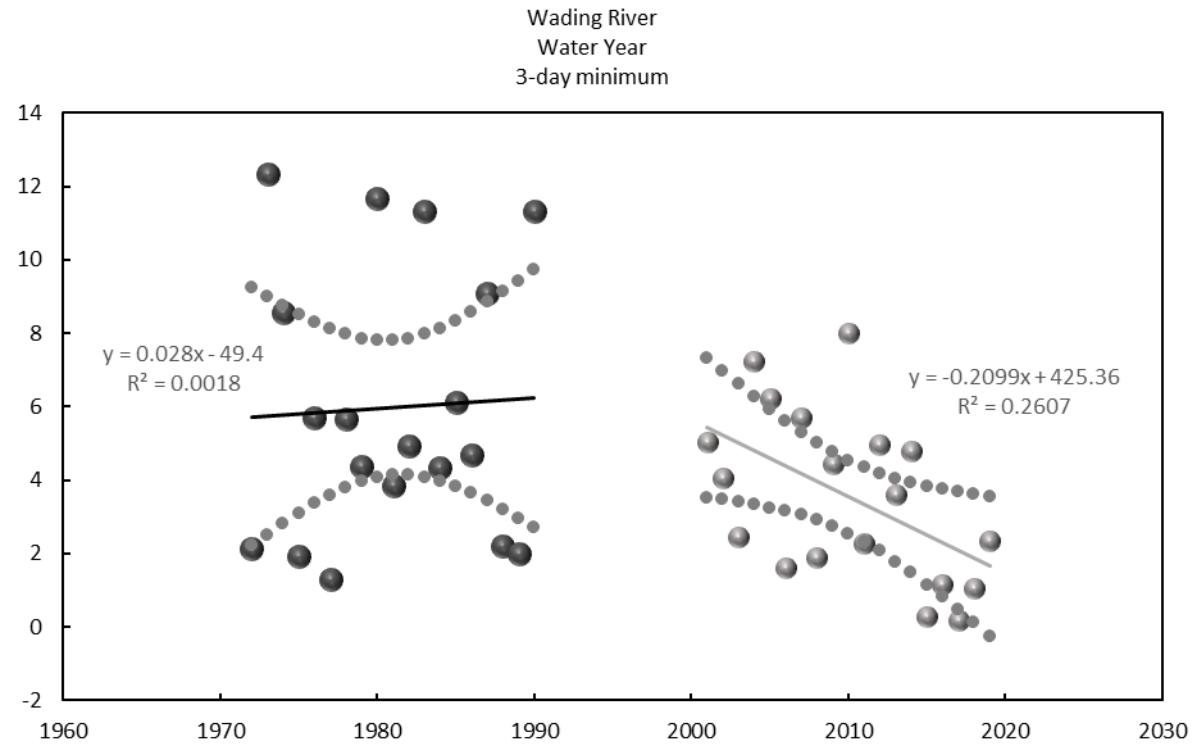

Figure 72. Comparison of 3-day minimum flows for water years 1972-1990 and 2001-2019 for the Wading River. Dotted lines show 95% confidence intervals.

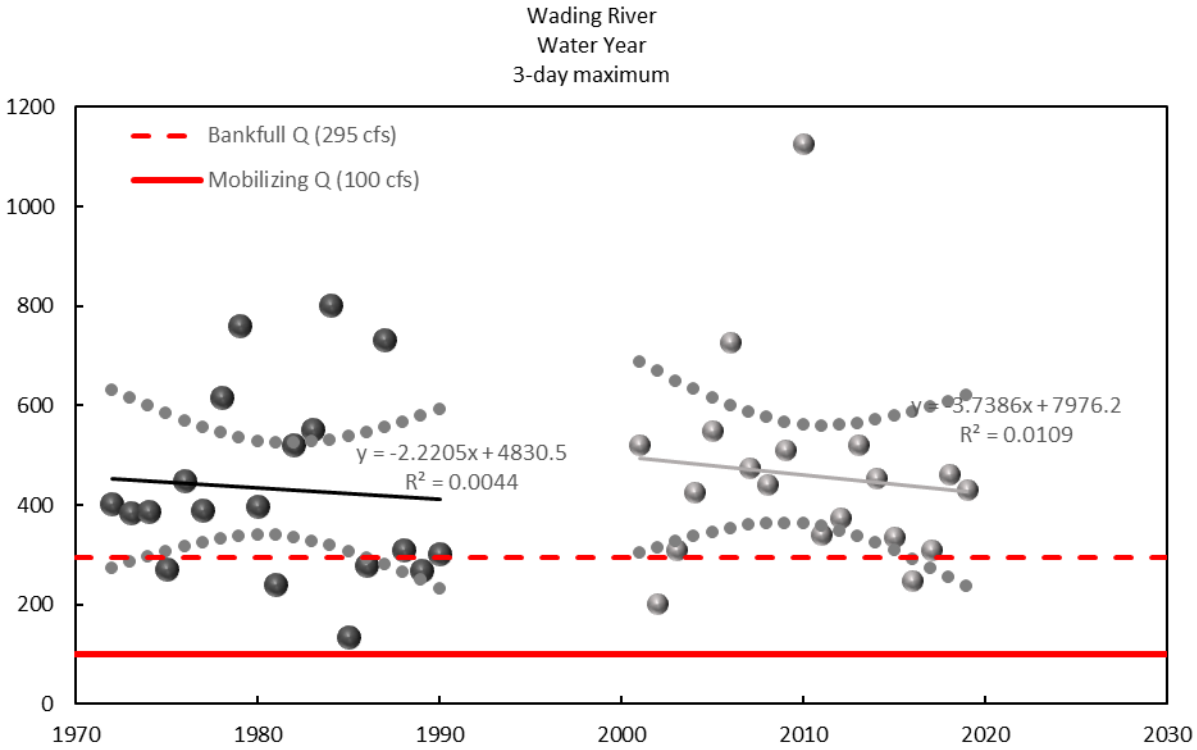

Figure 73. Comparison of 3-day maximum flows for water years 1972-1990 and 2001-2019 for the Wading River. Dotted lines show 95% confidence intervals.

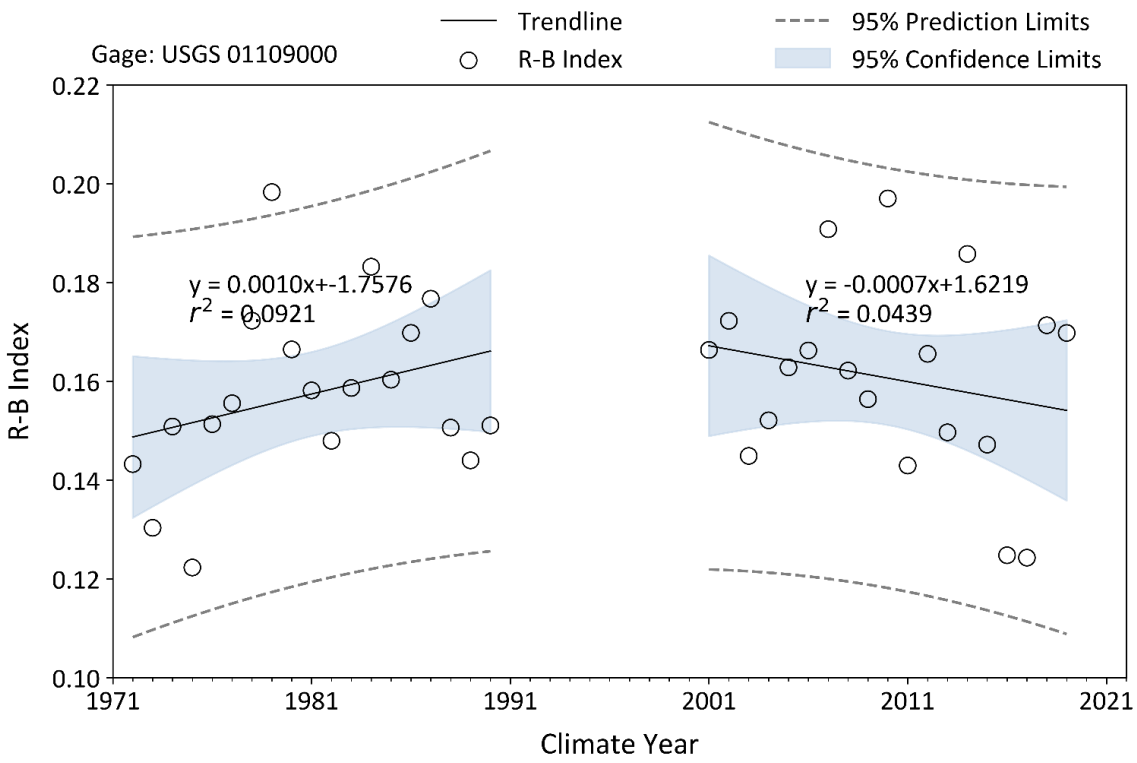

Figure 74. Comparison of Richard-baker Flashiness Index (R-B Index) for the periods 1972-1990 and 2001-2019.

Figure 75 presents quantile-Kendall plots for the full period of record and 1972-1990 and 2001-2019. Interestingly, the trend of lower flows becoming lower is not seen in the 1972-1990 period. However, 2001-2019 shows significant decreases in streamflow. The changes per year increase from ~-0.5% to ~-7.5%
There does not appear to be strong trends in the 1972-1990 or 2001-2019 period. Figure 75 presents quantile-Kendall plots for the full period of record and 1972-1990 and 2001-2019. Interestingly, the trend of lower flows becoming lower is not seen in the 1972-1990 period. However, 2001-2019 shows significant decreases in streamflow. The changes per year increase from ~-0.5% to ~-7.5%

The top graph in Figure 76 presents a graph similar to one presented in Jennings and Jarnagin (Jennings and Jarnagin, 2002), in which the authors investigated changes in discharge in a stream in Virginia due to increases in impervious surfaces in the watershed. The EPA authors present the regression lines of streamflow versus precipitation depth for different periods associated with differing amounts of impervious surfaces. Like the figure presented in Jennings and Jarnagin (2002), some care should be taken in interpreting Figure 76; a second graph is included that presents both regression lines and the data they are based on. Unsurprisingly, both periods have a rising slope indicating the increasingly direct relationship between precipitation and runoff as precipitation depths become higher. The 2001-2019 regression line suggests that streamflow response has become more closely linked to precipitation than it was in the historic 1972-1990 period. Both regression lines are second-order polynomials. While 2001-2019 data appears to dip below the historic line at lower precipitation depths, this may simply be a relic of fitting the polynomial regressions. Removing the 5 highest precipitation depths from the 1972-1990 period did not substantially alter the regression.

Overall, there appear to be some substantial differences in flow metrics over the two time periods. The analysis is based on observed data and is limited by inherent uncertainties associated with confounding impacts of both climate and impervious surfaces on streamflow. However, the comparisons are a useful and intuitive approach to understanding differences in hydrological time series. The approach should be a valuable component of synthesizing LSPC and Opti-Tool output in future tasks.

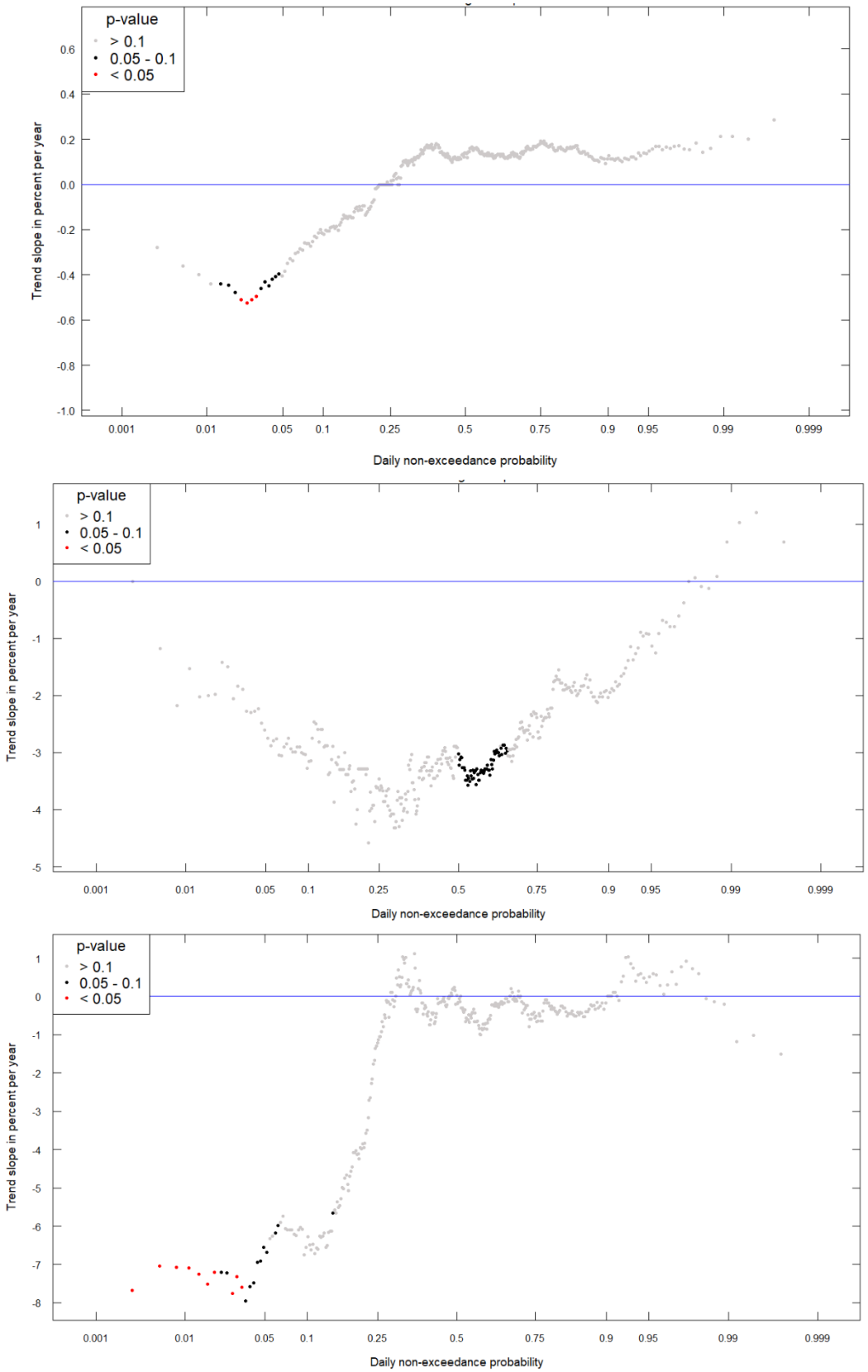

Figure 75. Quantile-Kendall plots for the entire period of record (top), 1972-1990 (middle), and 2001-2019 (bottom).

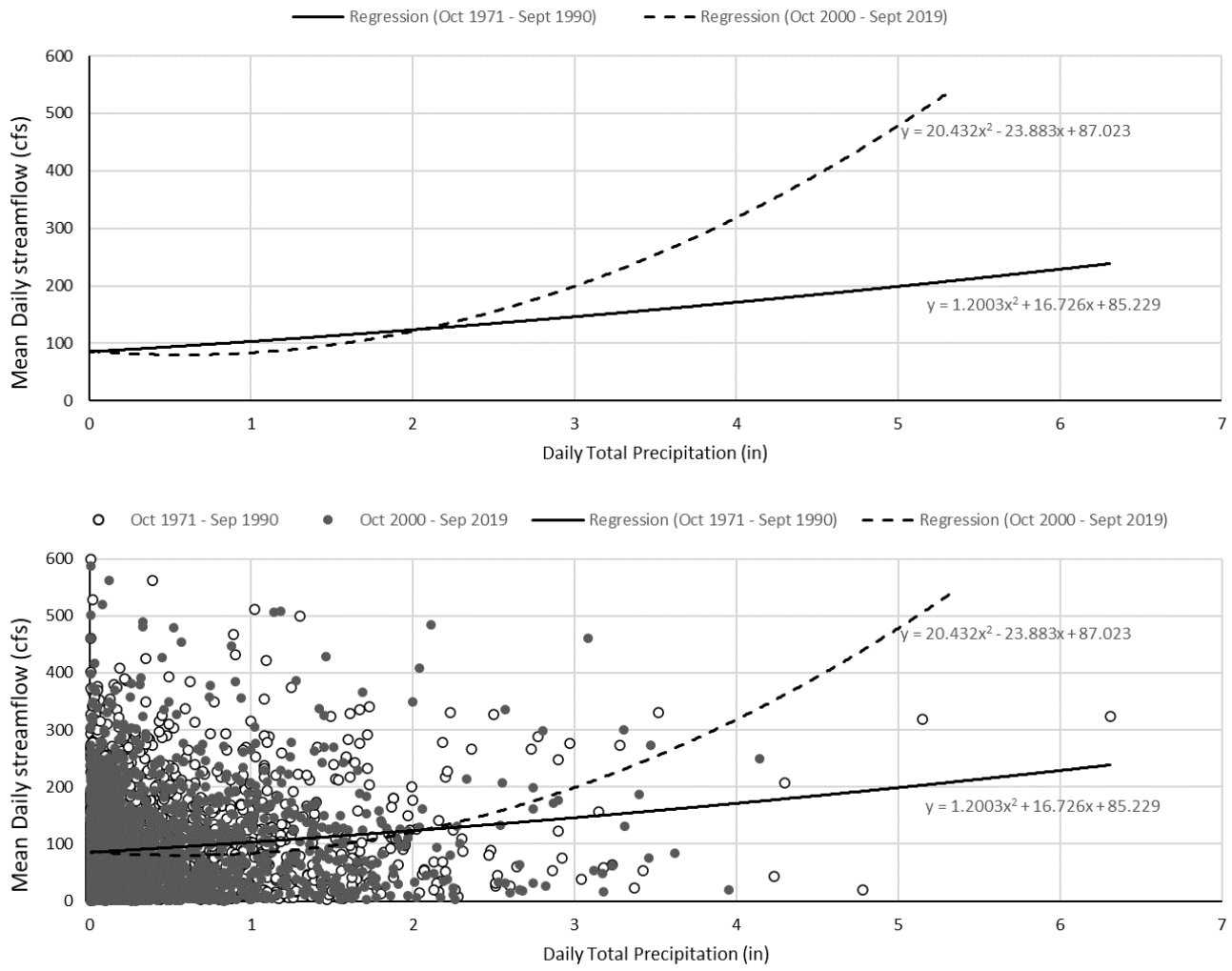

Figure 76. Streamflow versus precipitation for days with measurable precipitation. Regression only (top), regression, and data (bottom).

6 TASK 5D. DEVELOP HYDROLOGIC/STREAMFLOW AND WATER MANAGEMENT MODELING APPROACH FOR WADING RIVER WATERSHED ANALYSES

To characterize the impact of management actions on instream hydrology in the Wading River watershed, the proposed modeling approach focuses on hydrograph attenuation as quantified by a movement in the FDC from an existing impaired hydrological state toward a reference predevelopment hydrological condition. For this analysis, the proposed "predevelopment" reference condition is the FDC associated with the 1972-1990 hydrological period. A FDC modeling approach requires a coupled watershed/SCM modeling approach that accounts for the full water balance associated with precipitation, runoff, evapotranspiration, runoff, groundwater interflow, and deep groundwater recharge. This section describes the proposed watershed and SCM modeling approaches.

6.1 Watershed Modeling Approach

Our proposed modeling approach follows a top-down weight-of-evidence-based methodology. The approach leverages high-resolution HRU and meteorological data for model configuration. Figure 77 provides a schematic of the adaptive model development approach for assessing and integrating the required datasets for simulation, and how they relate to the overall model calibration and validation process. The gray arrows show the connections between the various stages of model development. The cycle can be summarized in six interrelated steps:

1. **Assess Data/Information.** Assess data to be used for land representation, source characterization, meteorological boundary conditions, etc.
2. **Define Model Domain.** Determine model segmentation and discretization needed to simulate hydrology and water quality at temporal and spatial scales appropriate for supporting decisions across the watershed.
3. **Set Boundary Conditions.** Set spatial and temporal model inputs, especially meteorological data, for establishing the conditions that drive variation in hydrology and water quality.
4. **Represent Processes.** Select the processes to be represented by the algorithms in the model based on the intended application (e.g., which pollutants to simulate).
5. **Confirm Predictions.** Adjust model rates and constants to mimic observed physical processes of the natural system, mostly through comparison to observational data.
6. **Assess Data Gaps.** Modeled responses and/or poor model performance can indicate the influence of unrepresented physical processes in the modeled system. A well-designed model can be adapted for future applications as new information about the system becomes available. Depending on the study objectives, data gaps sometimes provide a sound basis for further data collection efforts to refine the model, which cycles back to Step 1.

These steps are organized into two primary efforts: model configuration (green boxes) and model calibration and validation (blue), as described below.

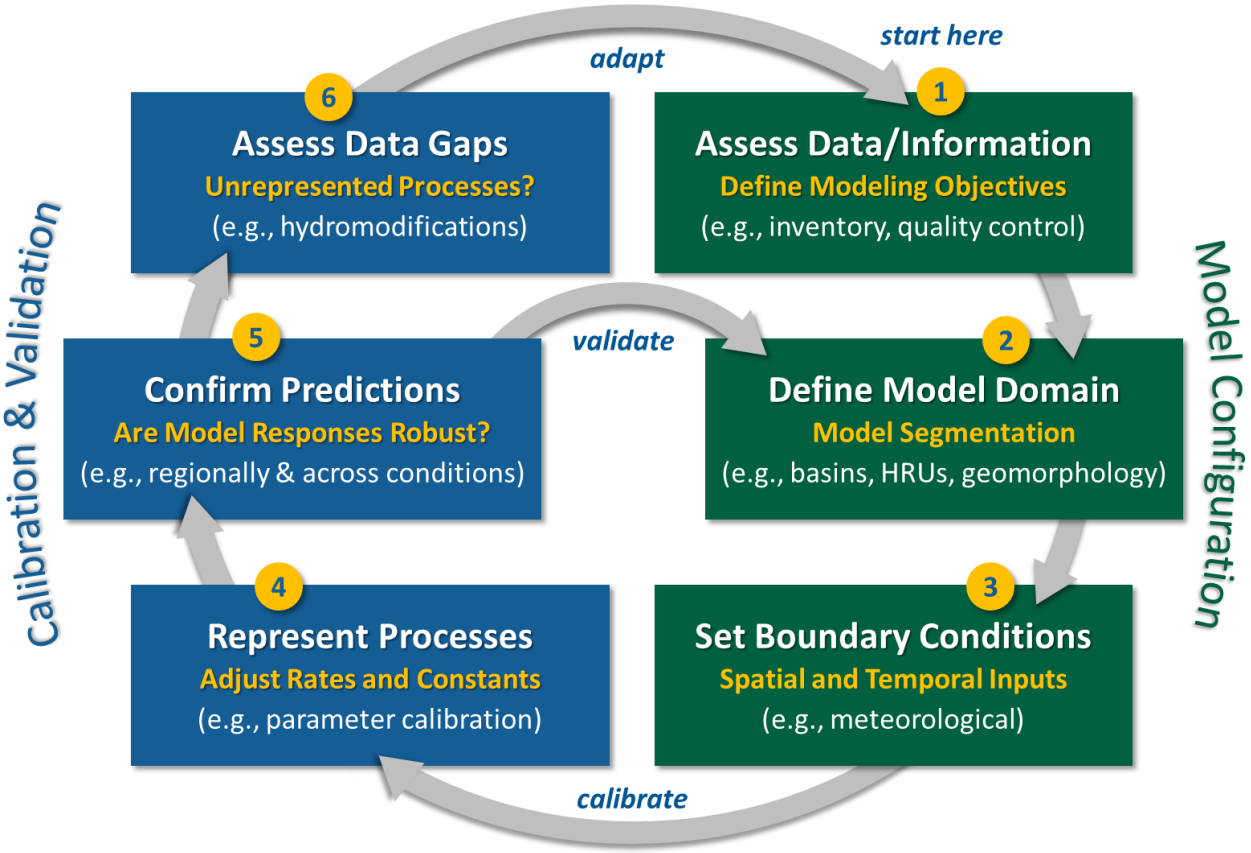

Figure 77. Conceptual representation of the LSPC model development cycle.

The proposed platform for model configuration is LSPC. LSPC model is an open-source, process-based watershed modeling system developed by the EPA for simulating watershed hydrology, sediment erosion and transport, and water quality processes from both upland contributing areas and receiving streams (EPA 2009b). The LSPC model simulates flow accumulation in stream networks and the transport of pollutants, which may be deposited or scoured from the stream bed, sorbed or transformed due to various chemical and biological processes. LSPC is capable of dynamically simulating flow, sediments, nutrients, metals, dissolved oxygen, temperature, and other pollutants for pervious and impervious lands and water bodies of varying order.

LSPC algorithms were developed from a subset of those in HSPF (Bicknell et al. 1997) but designed to overcome some of the structural attributes that limit the size, resolution, and complexity associated with HSPF model configuration (Shen et al. 2004). The hydrologic portion of HSPF is based on the Stanford Watershed Model (Crawford & Linsley 1966), one of the pioneering watershed models. LSPC is built upon a relational database platform, enabling the collation of diverse datasets to produce robust representations of natural systems. LSPC integrates GIS outputs, comprehensive data storage, and management capabilities, the original HSPF algorithms, and a data analysis/post-processing system into a PC-based Windows environment.

Figure 78 is a generalized schematic of the underlying hydrology model (Stanford Watershed Model) used in LSPC. The schematic represents land-based processes for a single land unit in the model. The schematic shows the major processes that influence hydrology in a land segment. The baseline hydrological condition will be calibrated for the most recent period using various graphical and tabular statistical assessments of model goodness of fit. Figure 79 shows an example modeled vs. observed FDC comparison.

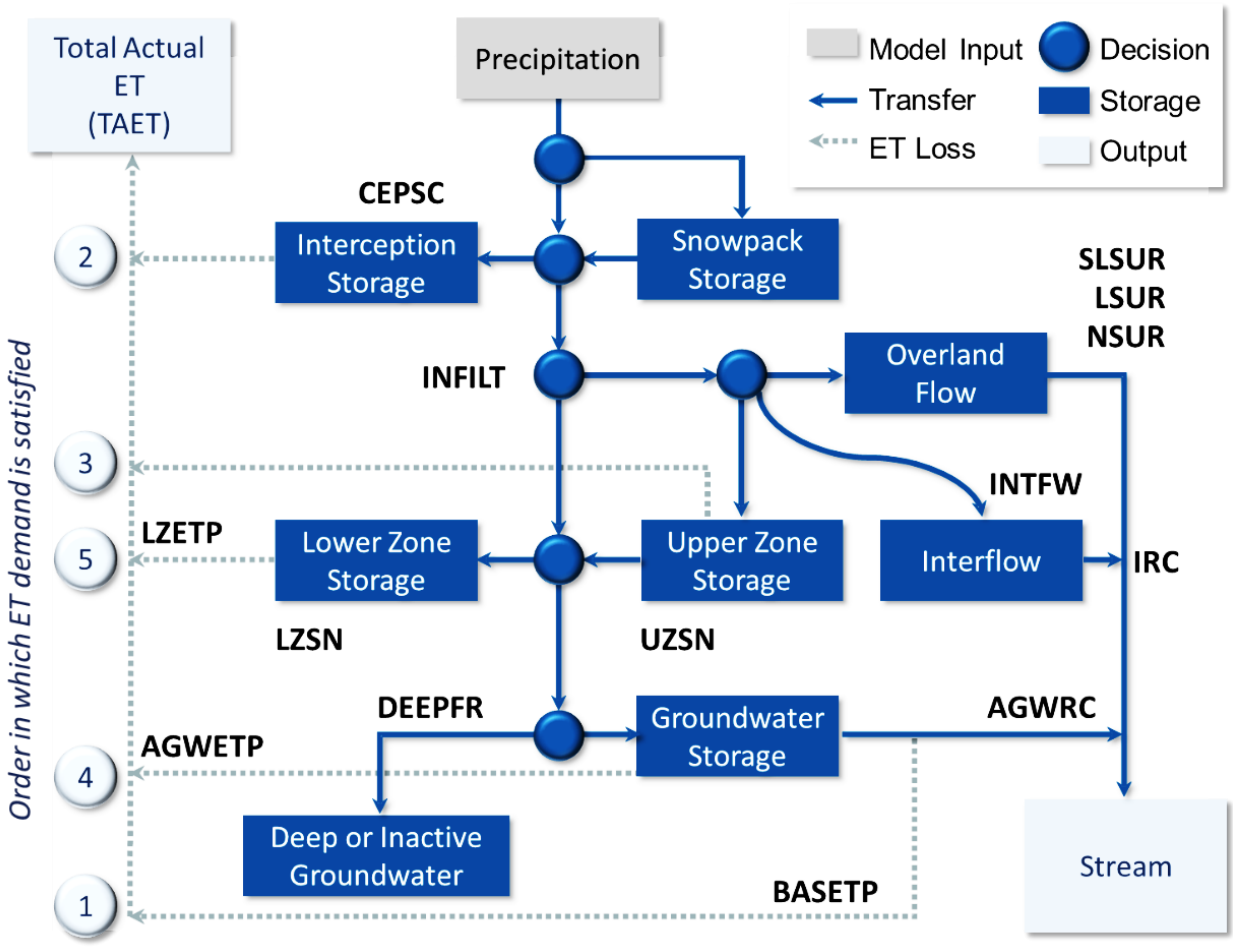

Figure 78. Hydrology model schematic for LSPC (based on Stanford Watershed Model).

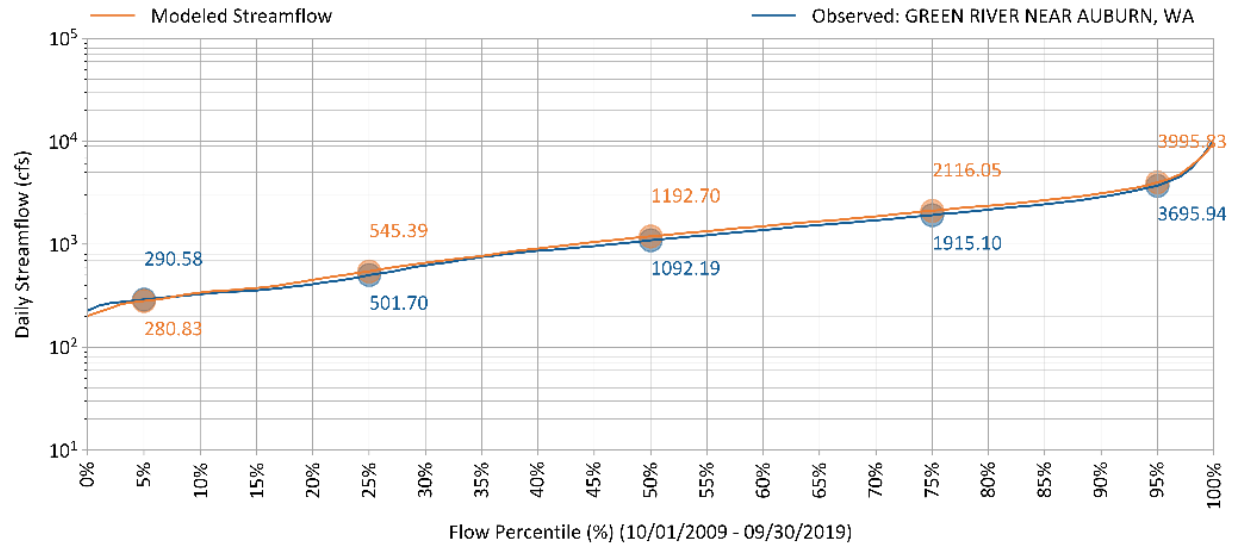

Figure 79. Example comparison of observed and predicted flow duration curves.

Figure 80 shows the performance metrics, a quantitative assessment to be performed at the selected streamflow gage to evaluate how well the model is parameterized and if the outputs are representative of observed conditions. Consistent with Moriasi et al. (2015), percent bias (PBIAS) will be the primary statistic to be used to evaluate the agreement between model-predicted and observed flows:

- **PBIAS** quantifies systematic overprediction or underprediction of observations. A bias towards underestimation is reflected in negative values of PBIAS while a bias towards overestimation is reflected in positive values. Low magnitude values of PBIAS indicate a better fit, with a value of 0.0 being optimal.

Two supplementary hydrological calibration metrics from Moriasi et al. (2015) and Donigian et al. (2000) will also be considered. They include the coefficient of determination (R^2), and Nash-Sutcliffe model efficiency (NSE):

- **R^2** describes the degree of collinearity between simulated and observed data. The correlation coefficient is an index that is used to investigate the degree of a linear relationship between observed and simulated data. R^2 describes the proportion of the variance in observed data that is explained by a model. Values for R^2 range from 0 to 1, with 1 indicating a perfect fit. Values greater than 0.70 indicate acceptable model performance (Donigian et al. 2000). The R^2 metric was calculated and presented within graphical 1-to-1 evaluation panels.
- **NSE** is a normalized statistic that determines the relative magnitude of the residual variance ("noise") compared to the measured data variance ("information"; Nash and Sutcliffe 1970). NSE indicates how well the plot of observed versus simulated data fits the 1:1 line. NSE gages how efficiently the model predicts the rising and falling of observed streamflow. Values for NSE can range between $-\infty$ and 1, with NSE = 1 indicating a perfect fit.

The use of PBIAS, R^2, and NSE as a suite of metrics provides a broad indication of model performance and additional texture to model parameterization, which ultimately guides a more incisive calibration. To provide diverse perspectives of model fitness, all calibration metrics will be assessed at varying temporal intervals and hydrologic conditions, as defined below:

- **Annual and Seasonal volume**: PBIAS of the annual volume (full data record) and seasonal (wet/dry months) will be used to quantify the magnitude of overall under- or over-prediction of the model. NSE and R^2 for annual volume (full data record) will also be evaluated to provide additional insight on model parameterization performance.
- **Highest 10% of Annual flows (Storm volume)**: The storm volume will be used to provide specific detail on wet-weather model performance. The "highest 10% of all flows" metric is a typical metric used to estimate model performance during storms. Applying the "highest 10% of flows" metric during wet months provides a more comprehensive and stable criterion for evaluating wet-weather model performance.
- **Lowest 50% of Annual flows (Low flow volume)**: A low flow metric will also be included in the model performance assessment (consistent with Donigian et al. 2000). Similar to the rationale for using the highest 10% of flows for storm volume, the lowest 50% of all flows is a more stable metric for evaluating model performance during dry weather conditions.

The performance metrics and conditions described above will provide a platform for assessing model fitness reflective of conditions in the model. These metrics will be computed using daily time series, which is a more stringent evaluation timestep than the aggregated monthly intervals that Moriasi et al. (2015) used. As a result, the "Satisfactory" level of model performance (consistent with Donigian et al. 2000 and Moriasi et al. 2015) provides a positive indication of model fitness and will be set as the model performance goal.

Hydrology Monitoring Locations	Performance Metrics (Seasonal)														
	PBIAS					R-squared					Nash-Sutcliffe E				
	All	Winter	Spring	Summer	Fall	All	Winter	Spring	Summer	Fall	All	Winter	Spring	Summer	Fall
GREEN RIVER NEAR AUBURN, WA	-	-	+	-	-										
GREEN RIVER AT 200TH STREET AT KENT, WA	-	-	-	-	-										
CEDAR RIVER BELOW DIVERSION NEAR LANDSBURG, WA	+	+	+	+	-										
CEDAR RIVER AT RENTON, WA	-	+	+	+	-										
WHITE RIVER AT R STREET NEAR AUBURN, WA	+	+	+	+	+										

Calibration Metrics	Recommended Error Criteria (PBIAS)				Reference
	Very Good	Good	Satisfactory	Unsatisfactory	
All Conditions	<5%	5% - 10%	10% - 15%	>15%	Moriasi et al. (2015)
Seasonal Flows	<10%	10% - 15%	15% - 25%	>25%	
Highest 10% of Daily Flow Rates					
Lowest 50% of Daily Flow Rates					
Days Categorized as Storm Flow					
Days Categorized as Baseflow					

Calibration Metrics	Recommended Error Criteria (R^2)				Reference
	Very Good	Good	Satisfactory	Unsatisfactory	
All Conditions	>0.85	0.75 - 0.85	0.60 - 0.75	≤0.60	Moriasi et al. (2015)
Seasonal Flows	>0.75	0.60 - 0.75	0.50 - 0.60	≤0.50	
Highest 10% of Daily Flow Rates					
Lowest 50% of Daily Flow Rates					
Days Categorized as Storm Flow					
Days Categorized as Baseflow					

Calibration Metrics	Recommended Error Criteria (E)				Reference
	Very Good	Good	Satisfactory	Unsatisfactory	
All Conditions	>0.80	0.70 - 0.80	0.50 - 0.70	≤0.50	Moriasi et al. (2015)
Seasonal Flows	>0.70	0.50 - 0.70	0.40 - 0.50	≤0.40	
Highest 10% of Daily Flow Rates					
Lowest 50% of Daily Flow Rates					
Days Categorized as Storm Flow					
Days Categorized as Baseflow					

Figure 80. Example summary of calibration evaluation metrics and evaluation criteria.

6.2 SCM Modeling Approach with FDC Attenuation Objective

A coupled watershed-SCM modeling framework provides an integrated platform for representing the impact of stormwater management on watershed-scale hydrology and water quality. LSPC is designed for direct linkage to the Opti-Tool. Conversely, Opti-Tool outflow time-series can be exported as a linkage file that in turn becomes an input to LSPC. Figure 81 shows how the two models will be linked. The baseline watershed model routes surface, interflow, and groundwater outflow directly to the stream network. When LSPC is linked to Opti-Tool, overland flow (SURO) from managed areas is intercepted and routed to SCMs, where it is either treated, bypassed, or overflows when inflow exceeds treatment capacity. Infiltrated water from

SCMs is stored in an aquifer segment for attenuated routing back to the LSPC reach-network. For the managed areas, the stormwater outflow from Opti-Tool replaces the baseline SURO from LSPC, while other components of the water balance, along with unmanaged areas, are routed directly to the reach network. Unless they are part of the modeled management strategy (e.g., channel modifications, stream restoration, and the like), all hydromodifications and special features within the LSPC network are unchanged between baseline and managed scenarios.

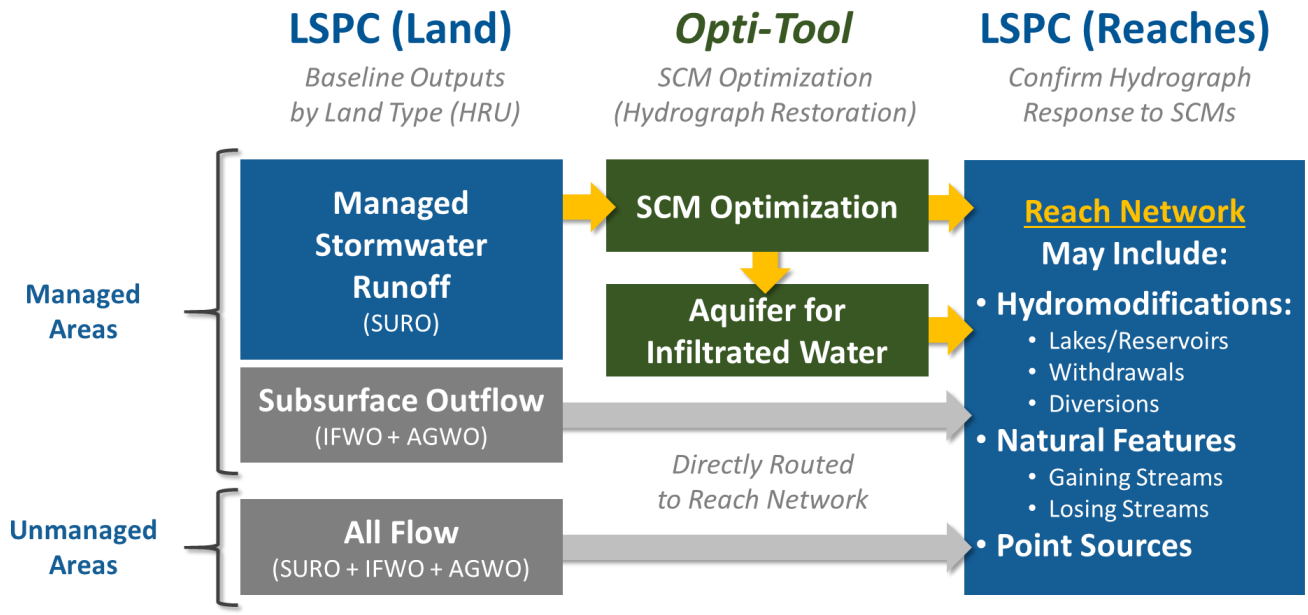

Figure 81. LSPC and Opti-Tool linkage schematic for integrated watershed-SCM hydrology modeling.

To simulate hydrograph attenuation, a conceptual model must bend the FDC to reduce stormwater runoff. As a result, the collection of SCMs in the system needs to work on both sides of the FDC, high flow and low flows, simultaneously. Some SCMs that are effective for managing small storms are less effective for managing larger storms. Conversely, SCMs that are effective for managing flood conditions often provide little benefit toward increasing baseflow. Some practices that are cost-effective for one objective are less cost-effective for others. Table 31 presents a summary of high-level competing management questions to be addressed through this effort. This section provides background information and describes the proposed modeling approach for implementing a FDC attenuation objective using the Opti-Tool.

Table 31. Management questions to be addressed through SCM optimization modeling

Competing Management Questions	
Who?	Which agencies need to cooperate to address hydrology and water quality impairment?
What?	What types of and how many SCMs are needed to restore an impaired hydrograph?
When?	How should agencies prioritize, sequence, and build SCMs in a watershed of interest?
Where?	Where in the system do SCMs yield the most benefit toward management objectives?
Why?	What is the most cost-effective strategy that also has the highest likelihood of successful adoption and implementation?
How?	A multi-objective inclusive solution technique (MOIST) can help address competing management objectives

6.2.1 *Background and Precedence*

There is precedence for the proposed hydrograph attenuation approach, which is being called the Multi-Objective Inclusive Solution Technique (MOIST). MOIST is a culmination of project insights gained from applying EPA's System for Urban Stormwater Treatment and Analysis IntegratioN (SUSTAIN), the underlying simulation model behind the Opti-Tool, for cost-benefit optimization modeling in several systems for different management objectives. The Little Bear Creek Basin Plan water quality study in Snohomish County, WA (Snohomish County Public Works, 2017) is the closest analog to the Taunton River basin study. In Snohomish County, a prototype of this approach was derived to optimize SCMs in a watershed to achieve a hydrograph attenuation objective. A series of three progressively increasing storms were each used to build optimization curves. Afterward, data from those curves were merged to create a composite curve that retained optimized solutions from all three curves. Figure 82 shows the representative 72-hour hyetal distribution derived from local literature and design standards. The 72-hour hyetal distribution included a small "soaking storm" to establish antecedent moisture content (AMC), followed by the main rainfall event. Table 32 presents the rainfall magnitudes that were multiplied against the hyetal distribution shown in Figure 82.

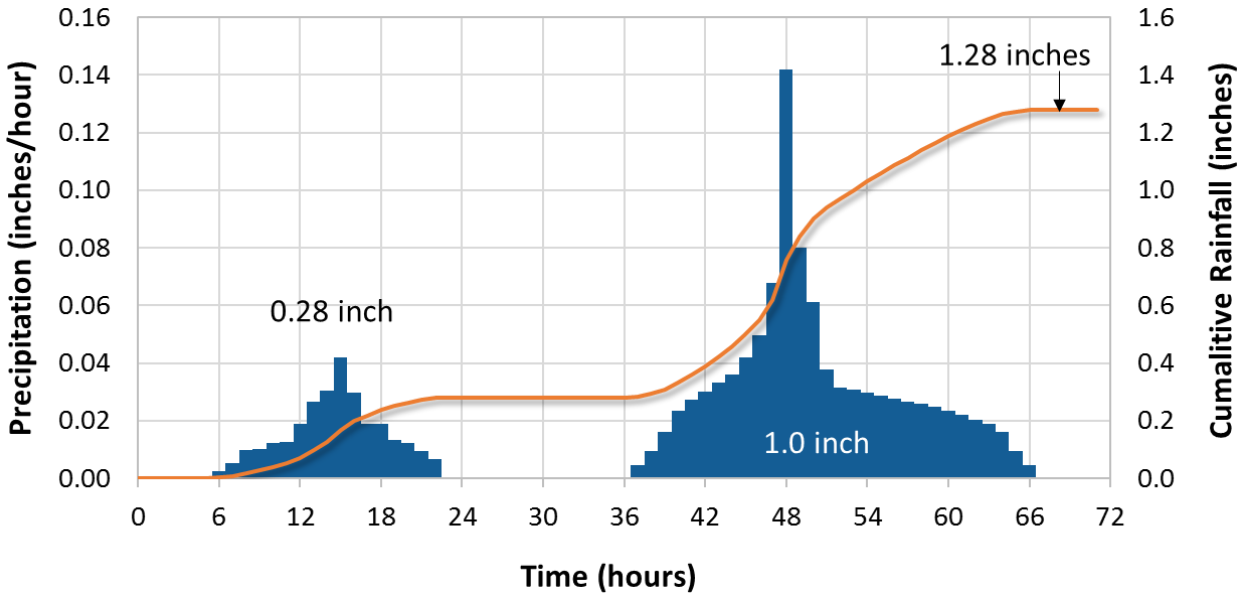

Figure 82. 72-hour storm hyetal distribution from Little Bear Creek Basin Plan (Snohomish County Public Works, 2017).

Table 32. Progressively increasing storm sequence used to build a MOIST curve (Snohomish County Public Works, 2017)

Storm Description		72-hour Rainfall Volume	72-hour Runoff Volume
1	"Average" Storm[1]	2 inches	1.25 inches
2	"Extreme" Condition[1]	6.5 nches	6.0 inches
3	"Flood" Scenario[2]	40 inches	39.5 inches

1: The "Average" and "Extreme" conditions were derived from analysis of 61-year rainfall time series
2: The "Flood" Scenario, though unrealistic, was used to flesh out the remaining SCM opportunity during optimization.

Each of the storms was used to optimize the same SCM opportunities in the Little Bear Creek watershed. Figure 83, adapted from the LBCBP (Snohomish County Public Works, 2017) presents an analysis of outputs from those runs. By default, each cost-effective solution along the curve is independent of every other solution and represents the most cost-effective way to achieve *that* specific target, regardless of what was cost-effective to achieve a nearby target. Adjacent solutions may be similar, but solutions farther away can diverge in SCM composition. A post-processing step can be applied to force higher solutions to be inclusive of lower solutions. The relative amount of distributed LID vs. regionalized detention also changed with storm size. LID was preferred for smaller storms, while detention was preferred for larger storms. For the largest "Flood" scenario, LID was the SCM of last resort.

	Storm Description	72-hour Rainfall Volume	72-hour Runoff Volume
1	"Average" Storm	2 inches	1.25 inches
2	"Extreme" Condition	6.5 nches	6.0 inches
3	"Flood" Scenario	40 inches	39.5 inches

"Average" Storm

"Extreme" and "Flood" Storms

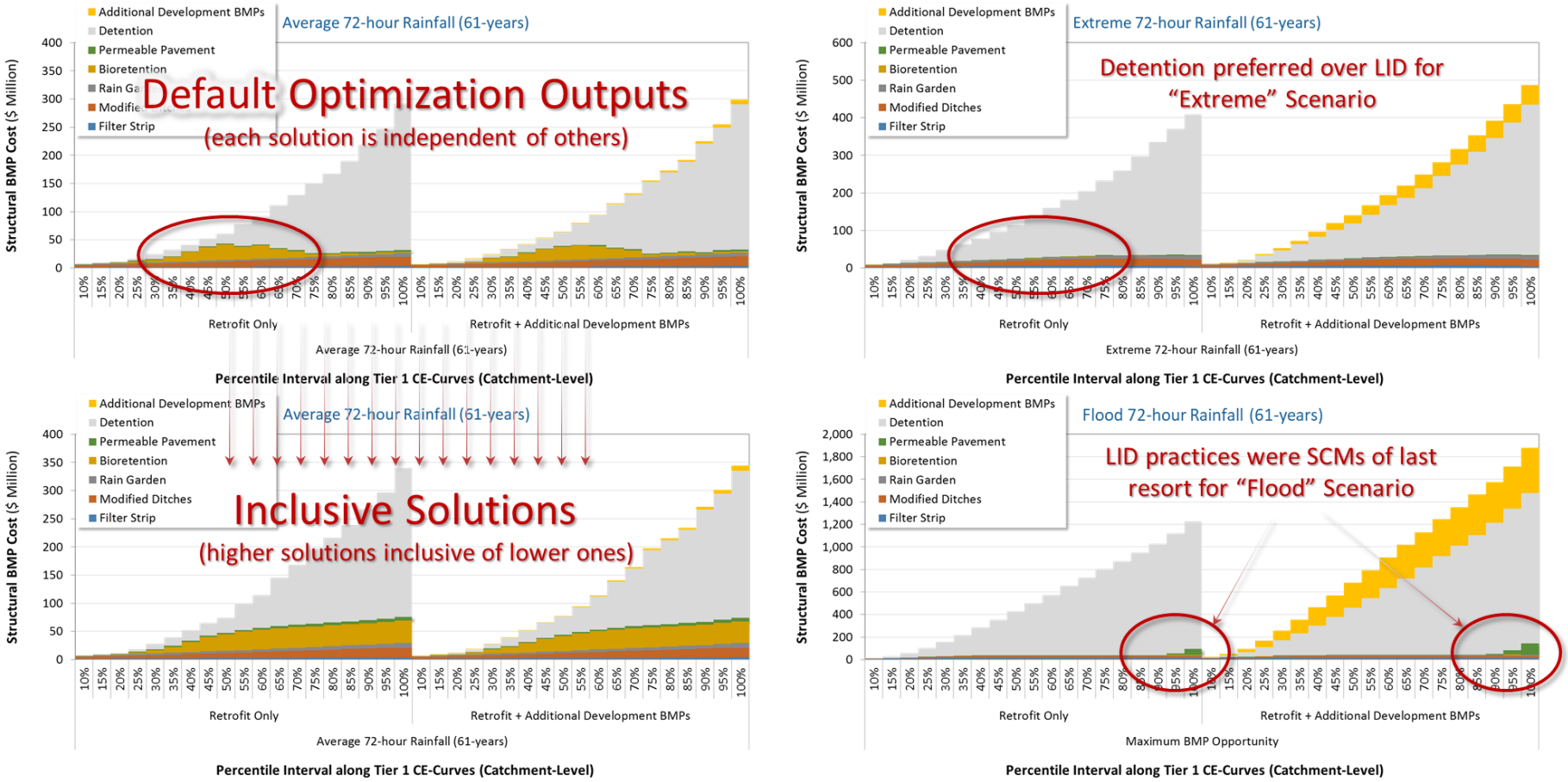

Figure 83. Analysis of "Average," "Extreme" and "Flood" scenario outputs for three optimization runs in Snohomish County (Snohomish County Public Works, 2017).

As shown in Figure 84, adapted from the LBCBP (Snohomish County Public Works, 2017) results from the three curves were combined to form a composite solution set that was both inclusive *within* each storm curve (i.e., *each* objective), and *across* all storm curves (i.e., *all* objectives). This framework comprises the multi-objective inclusive solution technique (MOIST) proposed for the three selected pilot sub-watersheds within the Wading River watershed and Opti-Tool enhancements to address FDC/hydrograph attenuation optimization. The Little Bear Creek Basin Plan study demonstrated that this approach produced more cost-effective solutions at the watershed scale for hydrograph attenuation because lower-cost LID solutions, which provided FDC recharge opportunity and treatment, are working most of the time because smaller storms have a higher frequency of occurrence than larger storms. Furthermore, whenever larger SCMs were needed to mitigate larger events, the required sizes for those SCMs were partially offset by having smaller SCMs present in the modeling network.

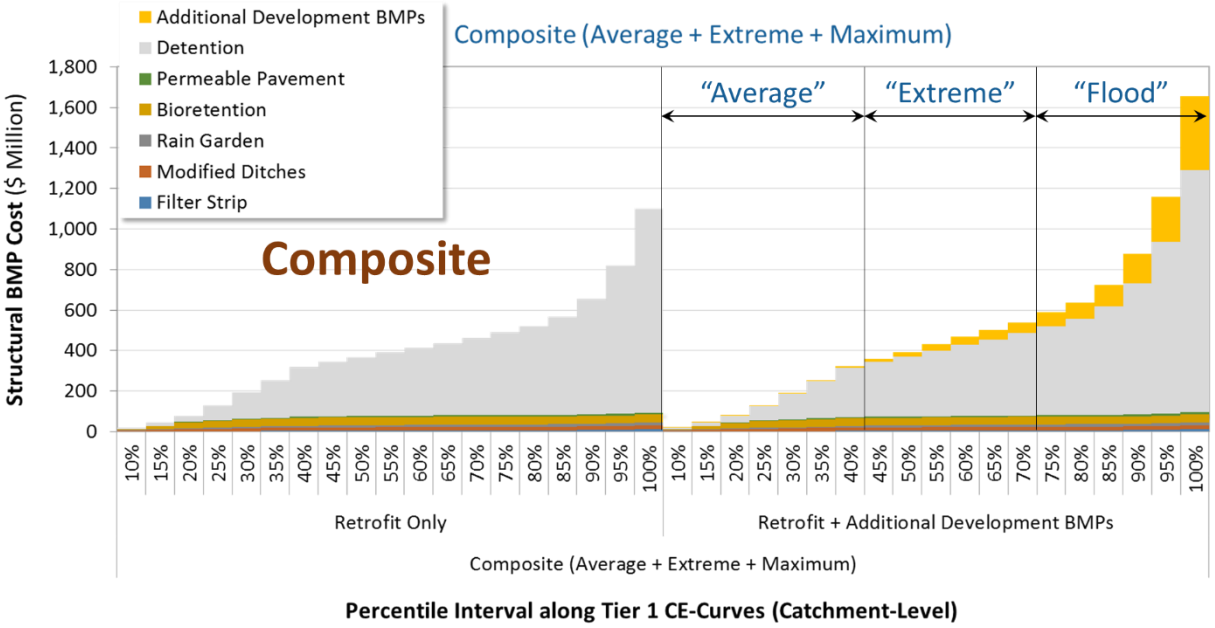

Figure 84. Composite SCM solution matrix from the Little Bear Creek Basin Plan (Snohomish County Public Works, 2017).

6.2.2 *MOIST Adaptation for Opti-Tool Integration*

Using local rainfall data and design guidance, the MOIST approach can be adapted for application in the Opti-Tool for the Wading River watershed. A series of progressively increasing storms will be used to build a composite solution matrix like the prototype application described in the Little Bear Creek Basin Plan. Figure 82 presents the NRCS Type III 24-hour Distribution, which is typical for Massachusetts (Mass DEP, 2002). Table 32 presents 24-hour rainfall depths at T.F. Green Airport for "small," "medium," and "large" storms. After completing the baseline watershed model build, associated runoff boundary conditions will be generated as inputs for Opti-Tool optimization runs.

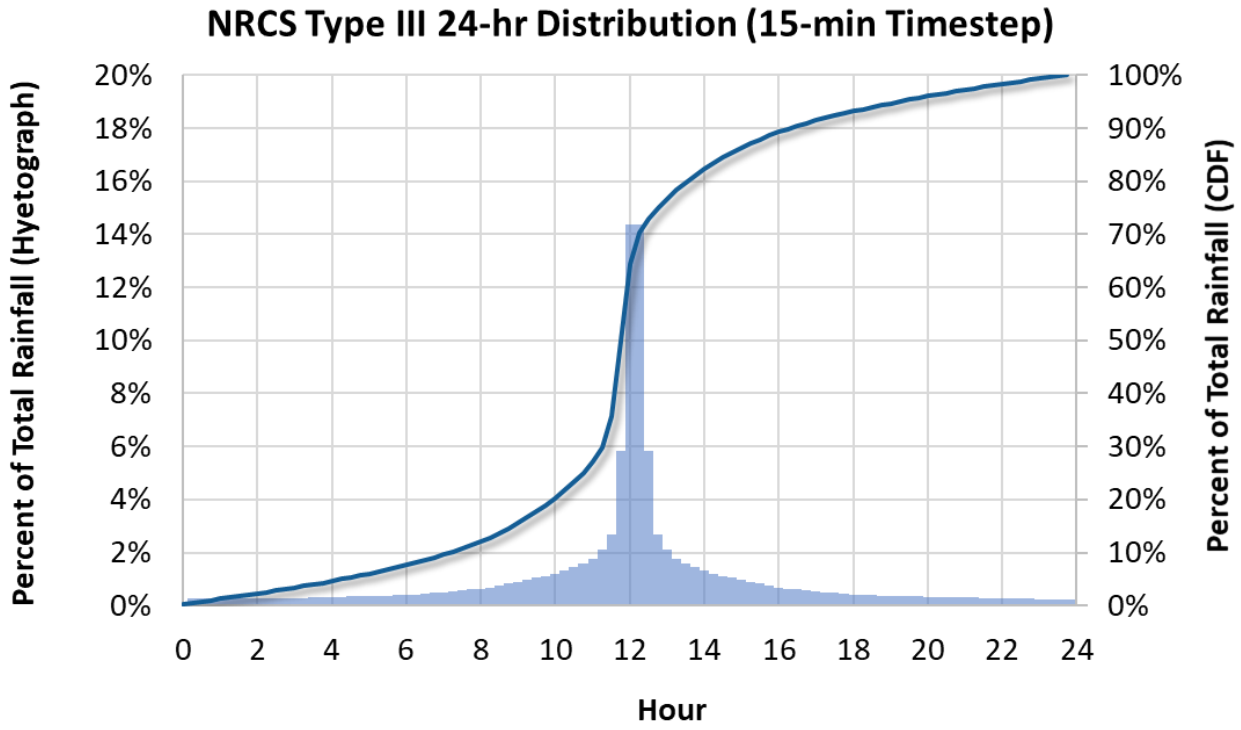

Figure 85. Massachusetts design-storm hyetograph for generating cost-effectiveness curves (NRCS).

Table 33. Progressively increasing storm sequence used to build Tier 1 solution matrix

Description [1]		Return Period	24-hour Rainfall Volume	24-hour Runoff Volume [2]
1	Small	1-yr	2.1	*placeholder*
2		2-yr	2.8	*placeholder*
3	Medium	5-yr	3.3	*placeholder*
4		10-yr	3.9	*placeholder*
5	Large	25-yr	5.1	*placeholder*
6		50-yr	6.5	*placeholder*

1: Managing storms with return periods between 1-yr and 50-yr will provide more recharge potential than extreme events (i.e., 100-yr and 500-yr storms)
2: Under Task 6, typical runoff estimates will be derived from the baseline model as inputs for optimization.

6.3 Future Climate Change Scenarios

An advantage of having time series of downscaled future climate change is the flexibility it provides for deriving useful modeling statistics such as return period storm intervals similar to those presented in Table 33. Table 34 is a summary table of average 6-hour storm return intervals for 10 different GCMs in San Mateo County, CA for RCP scenarios 4.5 and 8.5. An alternative set of future storms can be used to stress test system resiliency of both the baseline model and optimized management plans. Other features such as extreme wet and drought periods can also be mined from the time series and used for staging and testing model scenarios. Future climate time series can also be pushed through the optimized SCM footprints to assess the resiliency of the proposed plans toward mitigating future climate change impacts. Because the optimization outputs are cost-effectiveness curves if a solution that meets a management objective for the historical period is tested against future climate change and is shown to underperform the management

objective, a different point with a more aggressive collection of SCMs to address the future climate condition can be identified that provides the same benefit as historical climate condition.

Table 34. Example summary of return periods statistics derived from LOCA downscaled time series of future climate change scenarios relative to historical (Source: San Mateo County)

Climate Change		6-hour Storm Size (in.)					
Scenario	Model	2-yr	5-yr	10-yr	25-yr	50-yr	100-yr
Current (Historical)		1.91	2.38	2.77	3.31	3.74	4.18
All	Median (All)	2.07	2.65	3.13	3.84	4.49	5.16
	Mean (All)	2.11	2.72	3.25	4.01	4.65	5.35
RCP 4.5	Median (4.5)	2.05	2.59	3.04	3.71	4.27	4.89
	Mean (4.5)	2.08	2.66	3.16	3.88	4.48	5.13
	ACCESS1-0	2.07	2.59	3.05	3.76	4.36	5.03
	CanESM2	2.20	2.93	3.54	4.42	5.15	5.95
	CCSM4	2.02	2.58	3.00	3.53	3.91	4.28
	CESM1-BGC	2.18	2.75	3.31	4.20	5.02	5.97
	CMCC-CMS	2.16	2.72	3.12	3.61	3.95	4.27
	CNRM-CM5	2.49	3.38	4.14	5.24	6.16	7.17
	GFDL-CM3	1.98	2.41	2.78	3.31	3.73	4.18
	HadGEM2-CC	1.88	2.49	3.00	3.72	4.31	4.93
	HadGEM2-ES	1.92	2.38	2.85	3.61	4.29	5.10
	MIROC5	1.87	2.41	2.84	3.45	3.92	4.42
RCP 8.5	Median (8.5)	2.12	2.73	3.31	4.22	4.97	5.79
	Mean (8.5)	2.16	2.81	3.38	4.21	4.91	5.68
	ACCESS1-0	2.04	2.59	3.12	3.99	4.78	5.71
	CanESM2	2.41	3.31	4.07	5.18	6.11	7.12
	CCSM4	2.08	2.64	3.09	3.69	4.14	4.60
	CESM1-BGC	2.27	2.88	3.47	4.40	5.23	6.19
	CMCC-CMS	2.30	3.09	3.69	4.47	5.05	5.64
	CNRM-CM5	2.54	3.48	4.30	5.52	6.57	7.75
	GFDL-CM3	1.97	2.46	2.85	3.37	3.77	4.16
	HadGEM2-CC	2.04	2.72	3.34	4.28	5.10	6.04
	HadGEM2-ES	2.14	2.71	3.28	4.20	5.04	6.03
	MIROC5	1.76	2.22	2.56	2.99	3.30	3.60

Yellow highlighted are instances where the return period storm exceeds the historical 100-yr storm.

7 REFERENCES

Archfield, S.A., Vogel, R.M., Steeves, P.M., Brandt, S.L., Weiskel, P.W., Garabedian, S.P., 2009. The Massachusetts Sustainable-Yield Estimator: A decision-support tool to assess water availability at ungaged stream. USGS Scientific Investigations Report 2009–5227.

Baker, D.B., Richards, R.P., Loftus, T.T., Kramer, J.W., 2004. A new flashiness index: Characteristics and applications to midwestern rivers and streams. JAWRA J. Am. Water Resour. Assoc. 40, 503–522. https://doi.org/https://doi.org/10.1111/j.1752-1688.2004.tb01046.x

Barbaro, J.R., Sorenson, J.R., 2013. Nutrient and sediment concentrations, yields, and loads in impaired streams and rivers in the Taunton River Basin, Massachusetts, 1997–2008: U.S. Geological Survey Scientific Investigations Report 2012–5277.

Barlow, P.M., 2000. Documentation of computer program STRMDEPL—A program to calculate streamflow depletion by wells using analytical solutions, in Zarriello, P.J., and Ries, K.G., III, 2000, A precipitation runoff model for the analysis of the effects of water withdrawals on.

Bent, G.C., Waite, A.M., 2013. Equations for Estimating Bankfull Channel Geometry and Discharge for Streams in Massachusetts. USGS Scientific Investigations Report 2013–5155.

Brill, G., Shiao, T., Kammeyer, C., Diringer, S., Vigerstol, K., Ofosu-Amaah, N., Matosich, M., Müller-Zantop, C., Larson, W., Dekker, T., 2021. Benefit Accounting of Nature-Based Solutions for Watersheds: Guide. Oakland, CA.

Detenbeck, N., Weaver, C., 2018. ScenCompare. WMOST Climate Scenario Viewer and Comparison Post Processor. Narragansett, RI.

Donigian, A.S. Jr. 2000. *HSPF Training Workshop Handbook. Lecture #15. Watershed Model Calibration and Verification: Issues and Procedures*. Prepared for U.S. Environmental Protection Agency, Office of Water, Office of Science and Technology, Washington, DC.

EPA, 2020. Basins Framework and Features [WWW Document]. URL https://www.epa.gov/ceam/basins-framework-and-features

EPA, 2016. What climate change means for Massachusetts. EPA 430-F-16-023.

Friends of Lake Mirimichi, 2020. Historical information about our Lake [WWW Document]. URL http://lakemirimichi.org/History.html

Hayhoe, C.P., Wake, T.G., Huntington, L., Luo, M.D., Schrawtz, J., Sheffield, E., Wood, E., Anderson, B., Bradbury, A., Degaetano, T.J., Wolfe, D., 2006. Past and Future Changes in Climate and Hydrological Indicators in the U.S. Northeast. Clim. Dyn. 28, 381–707. https://doi.org/10.1007

Hirsch, R.M., De Cicco, L.A., 2015. User Guide to Exploration and Graphics for RivEr Trends (EGRET) and dataRetrieval: R Packages for Hydrologic Data (version 2.0, February 2015): U.S. Geological Survey Techniques and Methods book 4, chap. A10. US Department of Interior. US Geological Survey. https://doi.org/http://dx.doi.org/10.3133/tm4A10.

Huang, J., Zhan, J., Yan, H., Wu, F., Deng, X., 2013. Evaluation of the Impacts of Land Use on Water Quality. Sci. World Journal.

Jennings, D.B., Jarnagin, S.T., 2002. Changes in anthropogenic impervious surfaces, precipitation and daily streamflow discharge: A historical perspective in a mid-Atlantic subwatershed. Landsc. Ecol. 17, 471–489. https://doi.org/10.1023/A:1021211114125

Kavehei, E., Jenkins, G.A., Adame, M.F., Lemckert, C., 2018. Carbon sequestration potential for mitigating the carbon footprint of green stormwater infrastructure. Renew. Sustain. Energy Rev. 94, 1179–1191. https://doi.org/10.1016/j.rser.2018.07.002

MA EOEE, 2011. Climate Change Adaptation Report.

Marasco, D.E., Hunter, B.N., Culligan, P.J., Gaffin, S.R., McGillis, W.R., 2014. Quantifying evapotranspiration from urban green roofs: A comparison of chamber measurements with commonly used predictive methods. Environ. Sci. Technol. 48, 10273–10281. https://doi.org/10.1021/es501699h

Mass DEP, 2002. Hydrology Handbook for Conservation Commissioners. Division of Watershed

Management Wetlands and Waterways Program.
Moore, T.L.C., Hunt, W.F., 2013. Predicting the carbon footprint of urban stormwater infrastructure. Ecol. Eng. 58, 44–51. https://doi.org/10.1016/j.ecoleng.2013.06.021
Moriasi, D.N., Gitau, M.W., Pai, N. Daggaupati, P. 2015. Hydrologic and Water Quality Models: Performance Measures and Evaluation Criteria. Transactions in American Society of Agricultural and Biological Engineers, Volume 58(6): 1763 – 1785.
Nash, J.E., and Sutcliffe, J.V.. 1970. River flow forecasting through conceptual models: Part 1. A discussion of principles. J. Hydrol. 10: 282–290. doi: https://doi.org/10.1016/0022-1694(70)90255-6.
Natural Capital Project, 2021. InVest Sample Dataset [WWW Document]. URL http://releases.naturalcapitalproject.org/?prefix=invest/3.9.0/data/
Northeast Climate Adaptation Science Center, 2018. Massachusetts Climate Change Projections - Statewide and for Major Drainage Basins Temperature, Precipitation, and Sea Level Rise Projections.
Norton Conservation Commission, 2010. Norton's Lakes and Ponds. Norton, MA.
Reichold, L., Zechman, E.M., Brill, E.D., Holmes, H., 2010. Simulation-Optimization Framework to Support Sustainable Watershed Development by Mimicking the Predevelopment Flow Regime. J. Water Resour. Plan. Manag. 136, 366–375. https://doi.org/10.1061/(asce)wr.1943-5452.0000040
Resilient Massachusetts Action Team, 2020. Climate Resilience Design Standards and Guidelines (DRAFT).
Richter, B.D., Baumgartner, J. V, Powell, J., David, P., Richter, B.D., Baumgartner, J. V, Powell, J., Braunt, D.P., 1996. A Method for Assessing Hydrologic Alteration within Ecosystems Published by Wiley for Society for Conservation Biology All use subject to https://about.jstor.org/terms A Method for Assessing Hydrologic Alteration within Ecosystems 10, 1163–1174.
Richter, B.D., Baumgartner, J. V, Wigington, R., Braun, David, P., 1997. How much water does a river need. Freshw. Biol. 37.
Said, A., 2014. Generalized Method for Estimating Variability in Directly Connected Impervious Areas. Glob. J. Eng. Sci. Res. Manag. 1.
Snohomish County Public Works, 2017. Little Bear Creek Basin Plan. A Final Watershed-Scale Stormwater Plan Prepared in Fulfillment of Special Condition S5.C.5.c.vi of the Phase I Municipal Stormwater Permit.
Sutherland, R., 2000. Methods for Estimating the Effective Impervious Area of Urban Watersheds. In: The Practice of Watershed Protection. Technical Note 58. Center for Watershed Protection, Ellicott City, MD.
Swanson, S., 2002. Indicators of Hydrologic Alteration. Resource Notes No 58.
Tong, S., Chen, W., 2002. Modeling the relationship between land use and surface water quality. J. Environ. Manage. 66, 377–393.
Tunsaker, C., Levine, D., 1995. Hierarchical Approaches to the Study of Water Quality in Rivers. Bioscience 45, 193–203.
USDA, 2019. SSURGO2 (Soil Survey Geographic Database).
USDA, 2003. National Soil Survey Handbook.
USGS, 2002. NED (National Elevation Dataset). [WWW Document]. URL https://catalog.data.gov/dataset/usgs-national-elevation-dataset-ned
Vogel, R.M., Sieber, J., Archfield, S.A., Smith, M.P., Apse, C.D., Huber-Lee, A., 2007. Relations among storage, yield, and instream flow. Water Resour. Res. 43, 1–12. https://doi.org/10.1029/2006WR005226
Wang, K., Dickinson, R.E., 2012. A review of global terrestrial evapotranspiration: Observation, modeling, climatology, and climatic variability. Rev. Geophys. 50. https://doi.org/10.1029/2011RG000373
Wilson, C., 2015. Land use/land cover water quality nexus: quantifying anthropogenic influences on surface water quality. Environ. Monit. Assess. 187.